Wolf-Rayet Stars

(Abstract)

WR stars are characterized by their immense, broad emission lines emanating from a dense, rapidly-expanding hot wind. Most of them are the He-burning descendents of the most massive stars (the O-type stars), and will likely explode as type Ib/c supernovae and leave behind a black hole. They are important for many reasons, some of which include: they have the strongest winds for any known stable star, they energize and enrich the ISM (with both ions and in some cases dust), they allow us to see nuclear-fused products at the surface of a star, they permit age-dating of young starbursts. However, many mysteries remain to be solved, such as: why are their mass-loss rates so high; what is the detailed structure of their winds; what is the role of rotation and binarity in their properties; how does dust form in some cases in such an apparently hostile environment? As with many astronomical phenomena, (ultra) high resolution interferometry is playing, and will continue to play, a key role in unravelling these puzzles.

Bibliography:

Wolf-Rayet Stars, J.D. Hillier, 2001, Encyclopedia of Astronomy & Astrophysics, IOP Publishing, UK

Wolf-Rayet Phenomena in Massive Stars and Starburst Galaxies, eds. K.A. van der Hucht, G. Koenigsberger, P.R.J. Eenens, 1999, IAU Symp. 193, ASP

Wolf-Rayet Central Stars of Planetary Nebulae, R. Tylenda, 1996, ASPCS 96, eds. C.S. Jeffery & U. Heber

Wolf-Rayet Stars in the Framework of Stellar Evolution, Proc. 33rd Liege Int'l Ap. Coll., 1996, eds. J.M. Vreux, A. Detal, D. Fraipont-Caro, E. Gosset, G. Rauw, Univ. de Liege.

Introduction to Stellar Winds, H.J.G.L.M Lamres, J.P. Cassinelli, 1999, CUP

The VIIth catalogue of galactic Wolf-Rayet stars, K.A. van der Hucht, 2000, New Astronomy Reviews.

WOLF-RAYET STARS

- Prelude, discovery
- Phenomenology, statistics
- Stellar Evolution and WR stars
- Spectral analysis, wind properties
- Wind interactions
  - intra
  - + CSM / ISM
  - binaries
- Conclusions
- Outstanding Problems

Number of grains of sand on Earth's beaches:

$$\frac{\text{Total volume}}{\text{Vol. of a grain}} \approx \frac{10^5\,\text{km} \times 1\,\text{km} \times 5\,\text{m}}{\frac{4}{3}\pi\,(0.25\,\text{mm})^3}$$

$$\sim \frac{5 \times 10^{11}\,\text{m}^3}{6 \times 10^{-11}\,\text{m}^3} \sim 10^{22}$$

Number of stars in the visible Universe:

$$\text{No. galaxies} \times \frac{\text{No. stars}}{\text{galaxy}} \approx \frac{4\pi \times \left(\frac{180}{\pi} \times 60^2\right)^2 \square''}{2'' \times 2''} \times 10^{11}$$

$$\sim 10^{11} \times 10^{11} \sim 10^{22}$$

1867 (134 years ago)

— a good year —

- WR stars discovered
  by Charles Wolf & Georges Rayet
  (1867 Comptes Rendus Acad. Sci. Paris 65, 292)
  in Paris, using a visual spectroscope on a small telescope

WR 134 = HD 191765	WN6
WR 135 = HD 192103	WC 8
WR 137 = HD 192641	WC7pd + OB

- Canada was born
  (Sir John A. Macdonald ....)

WR stars

in 2 ionization sequences:

(1) WN He, N, (H), ... population I

(2) WC, WO He, C, O, ... population I

[WC] CSPN (15%)

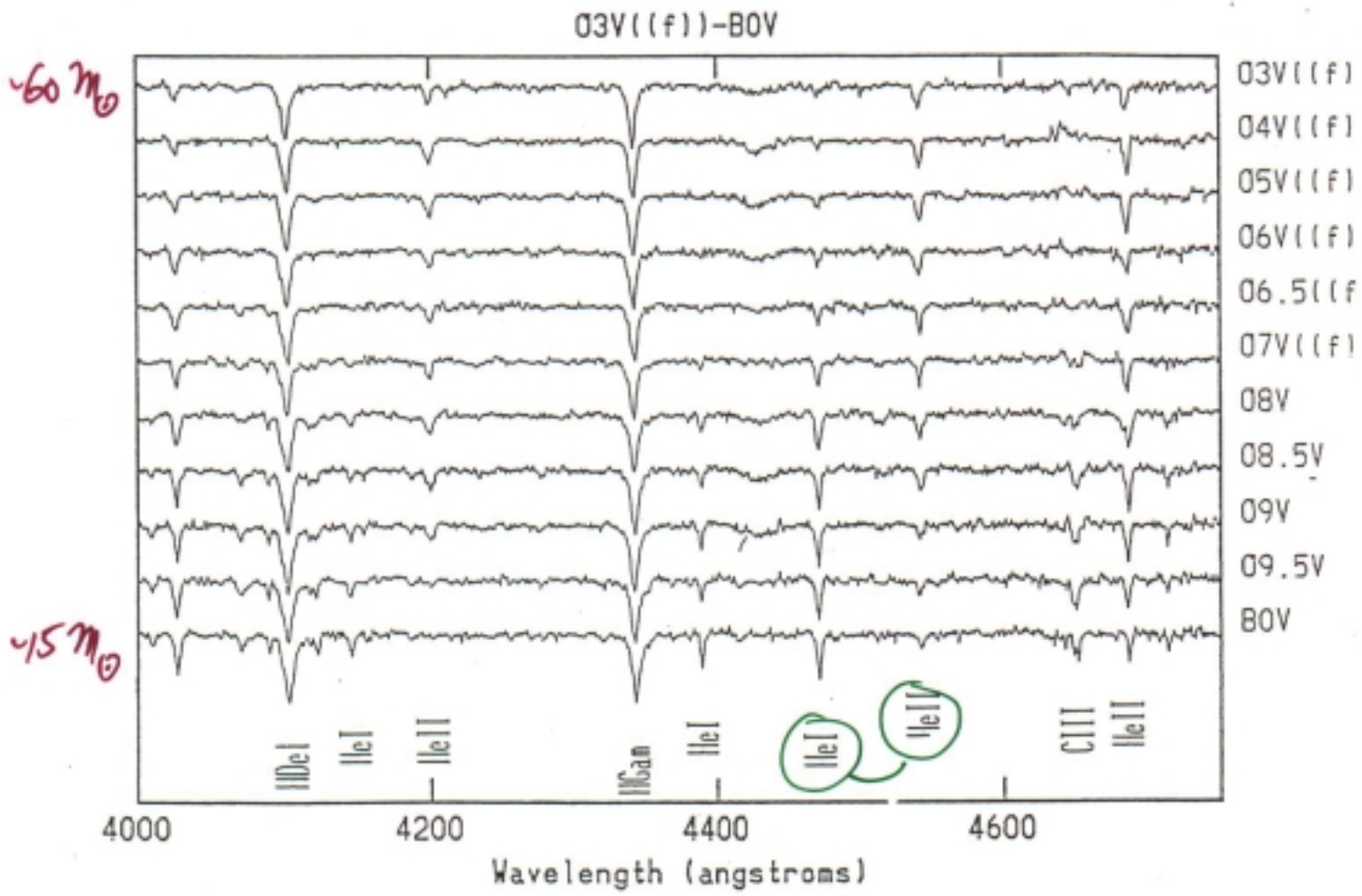
O3V((f))-B0V
~60 M⊙
~15 M⊙
O3V((f)
O4V((f)
O5V((f)
O6V((f)
O6.5((f
O7V((f)
O8V
O8.5V
O9V
O9.5V
B0V
HeI
HeI
HeII
HGam
HeI
HeI
HeII
CIII
HeII
4000
4200
4400
4600
Wavelength (angstroms)

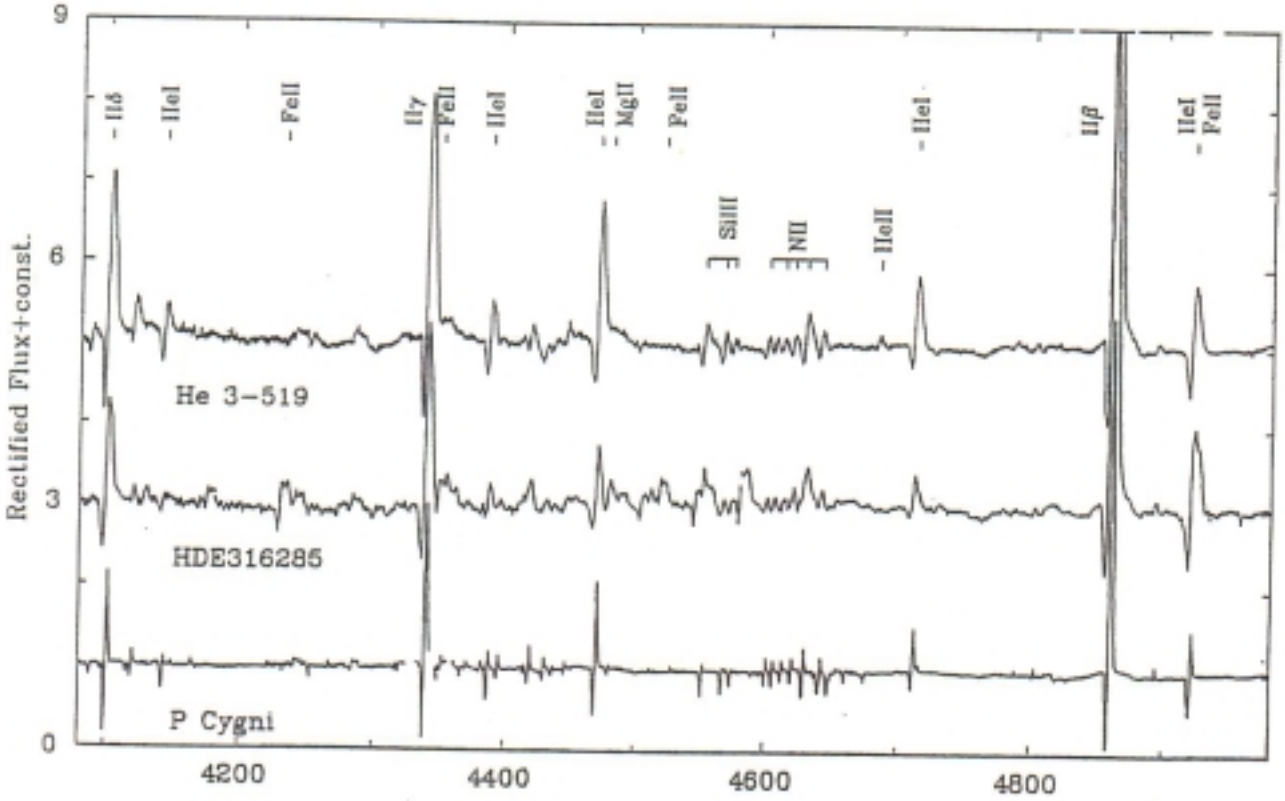
Rectified Flux+const.
9
6
3
0
Hδ
HeI
FeII
Hγ
FeII
HeI
HeI
MgII
FeII
SiIII
NII
HeII
HeI
Hβ
HeI
FeII
He 3-519
HDE316285
P Cygni
4200
4400
4600
4800

Massey

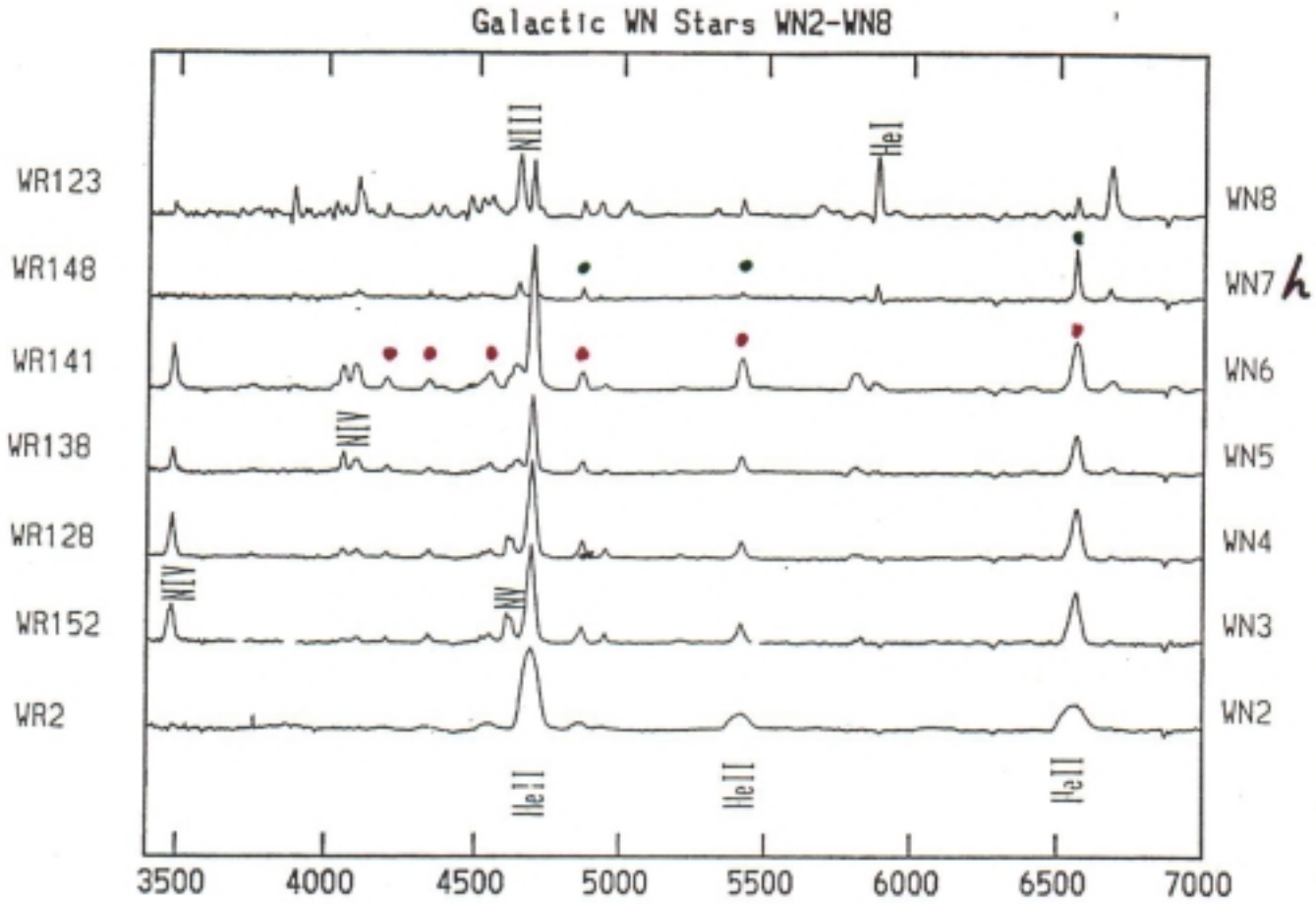
Galactic WN Stars WN2-WN8
WR123
WR148
WR141
WR138
WR128
WR152
WR2
WN8
WN7
WN6
WN5
WN4
WN3
WN2
NIII
HeI
NIV
NV
HeII
3500
4000
4500
5000
5500
6000
6500
7000

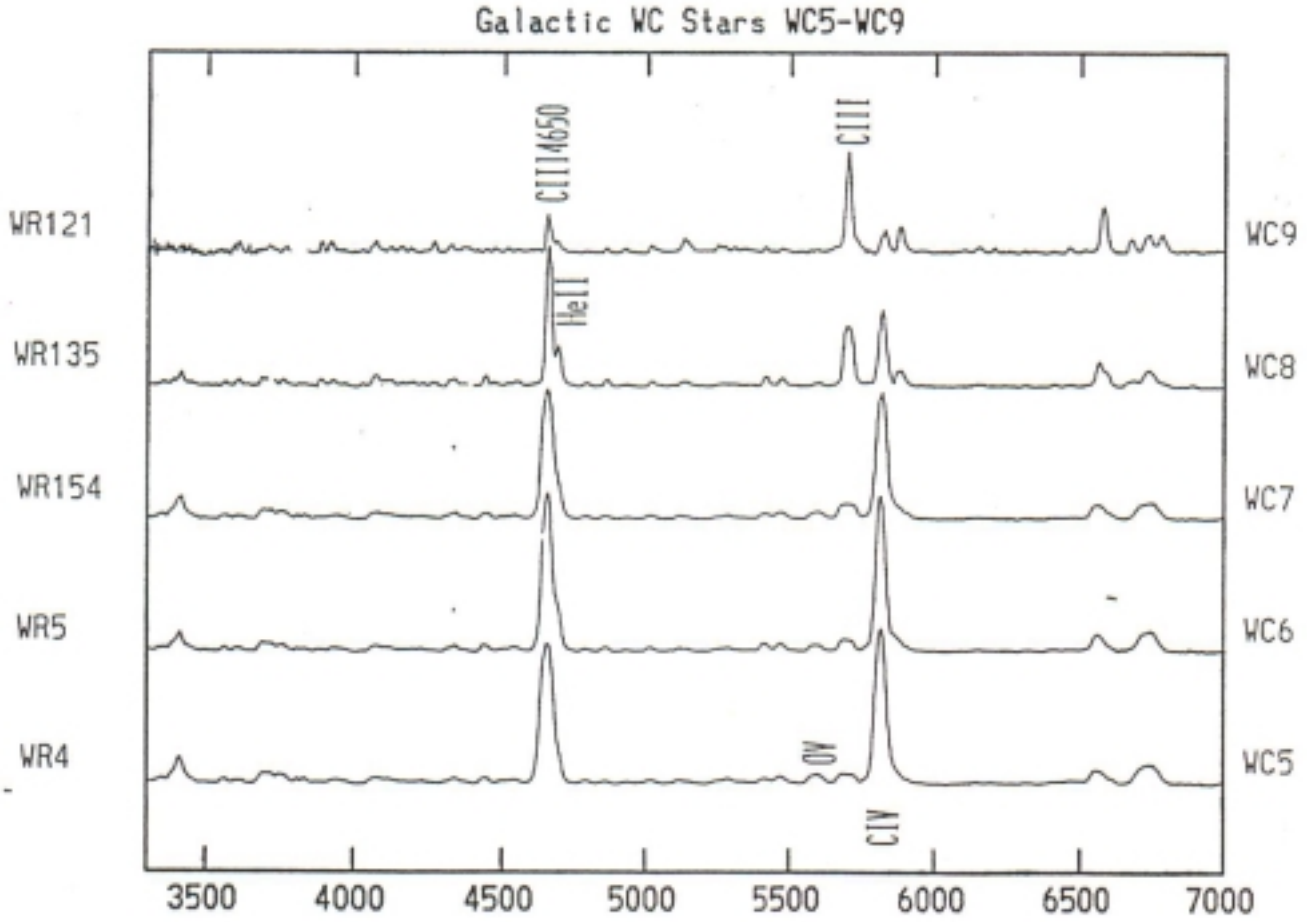
Galactic WC Stars WC5-WC9
WR121
WR135
WR154
WR5
WR4
WC9
WC8
WC7
WC6
WC5
CIII4650
CIII
HeII
OV
CIV
3500
4000
4500
5000
5500
6000
6500
7000

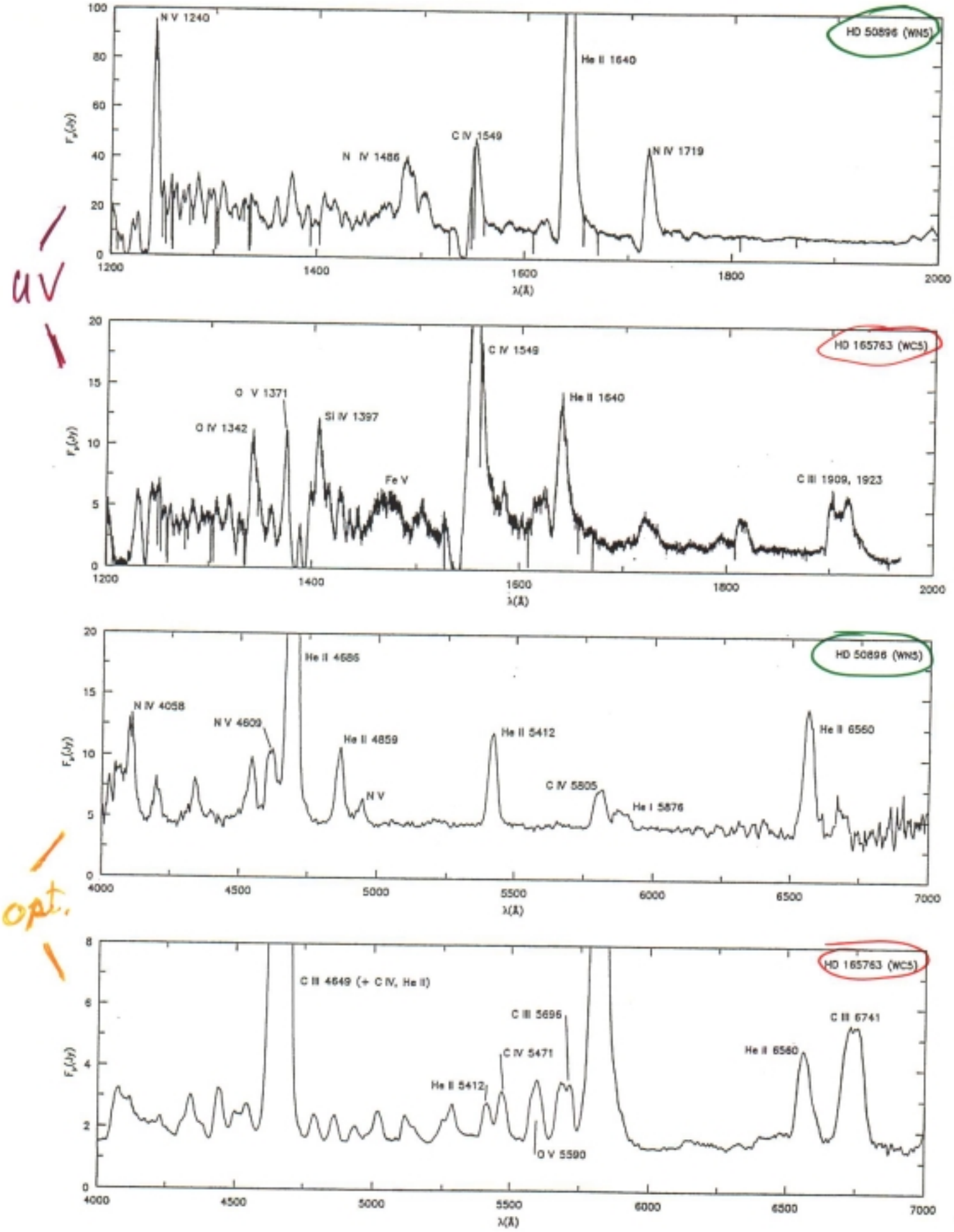

Hillier (1999)

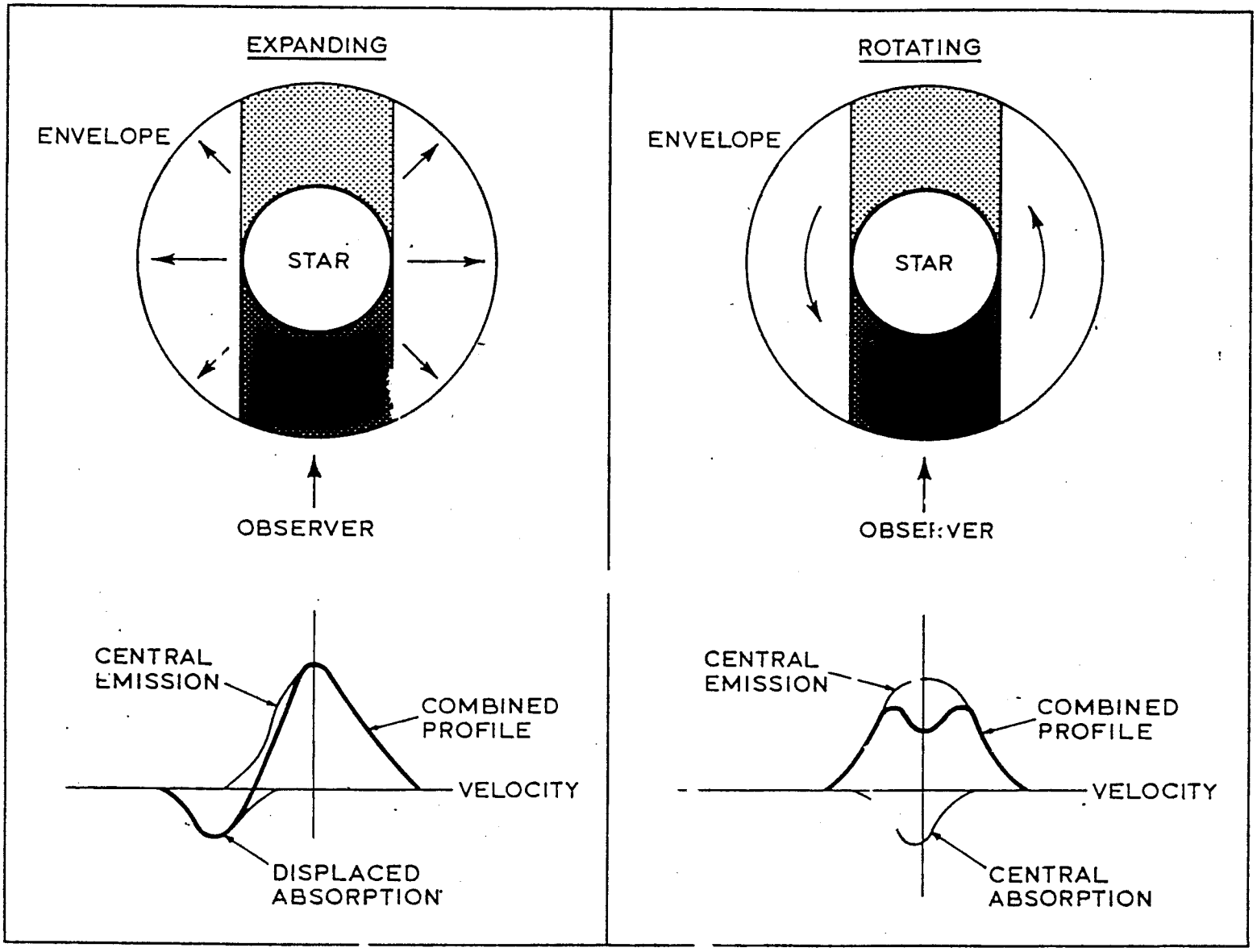
EXPANDING
ENVELOPE
STAR
OBSERVER
CENTRAL EMISSION
COMBINED PROFILE
VELOCITY
DISPLACED ABSORPTION
ROTATING
ENVELOPE
STAR
OBSERVER
CENTRAL EMISSION
COMBINED PROFILE
VELOCITY
CENTRAL ABSORPTION

Accelerating or decelerating atmosphere?

Kuhi (1973)

Observations

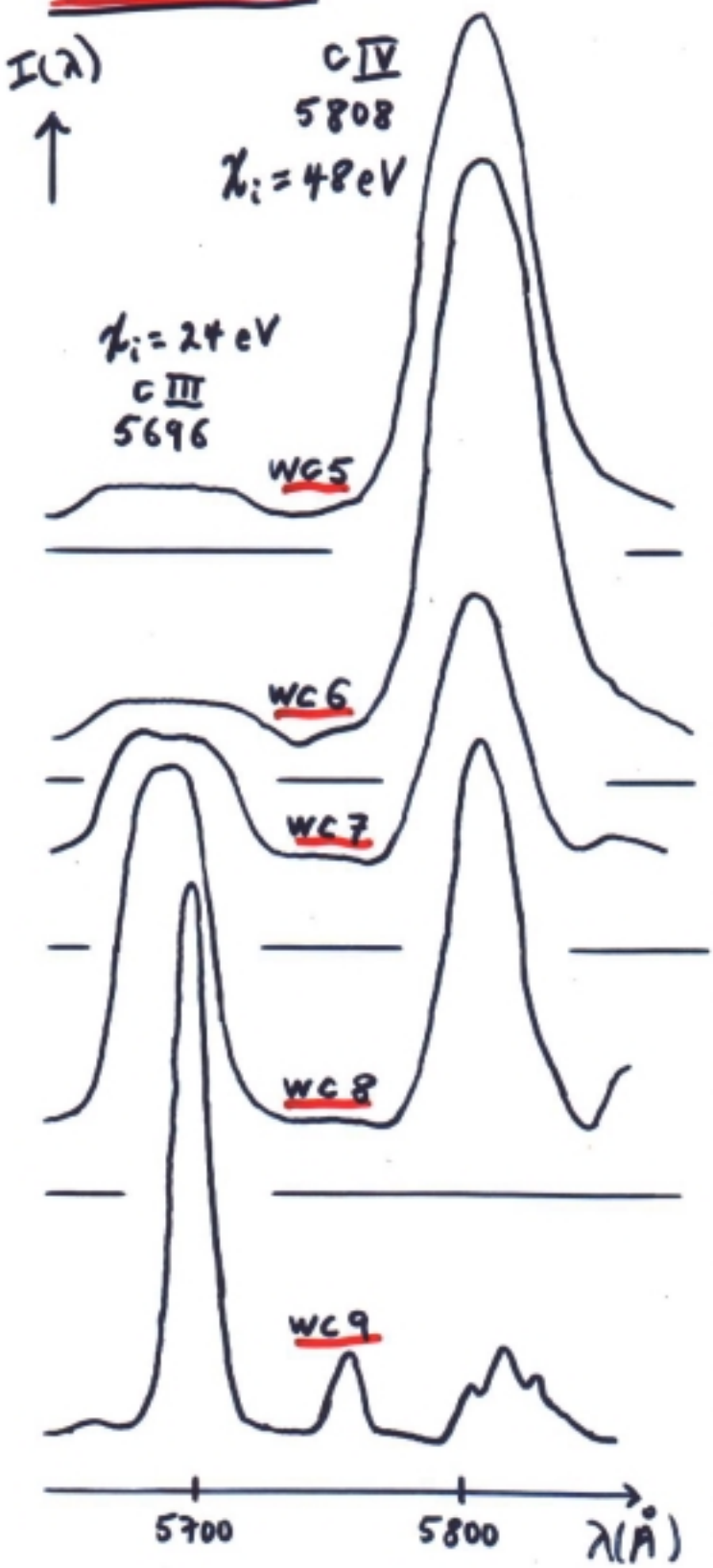

$$\ddot{r} = \frac{\text{const}}{r^2}$$

Model: radiation pressure

$$v^2 = v_0^2 + (v_\infty^2 - v_0^2)\left(1 - \frac{R_0}{r}\right)$$

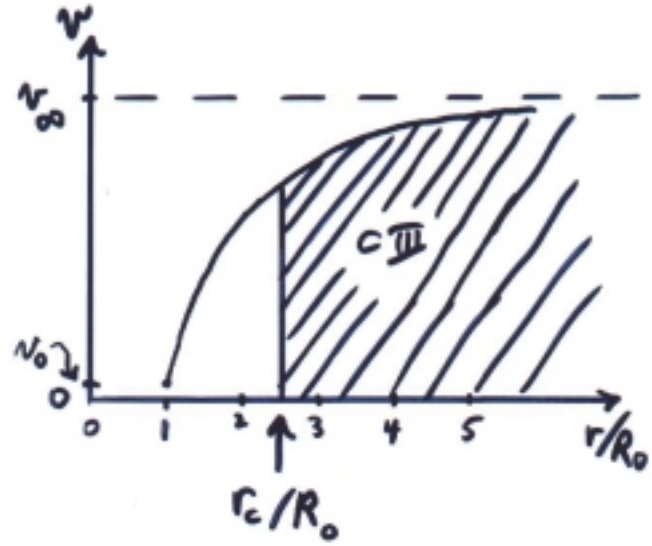

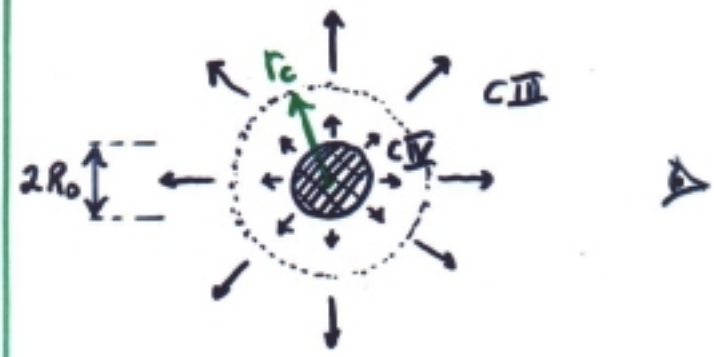

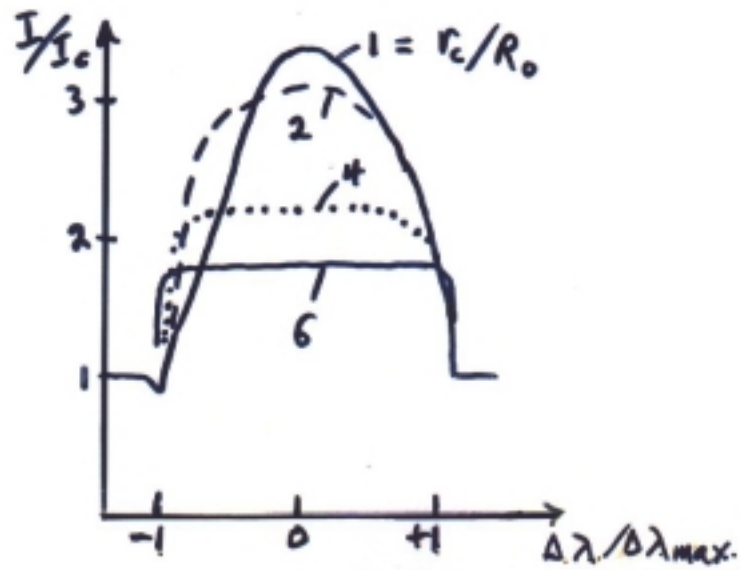

WR Statistics (pop. I)

	known	expected
Galaxy	227	1000 - 2000
LMC	134	✓
SMC	11	✓
M31, M33, other LG...	~200	$> 10^3$?
> LG	"a few"	many !!

"WR galaxies" many, unresolved

- Spatial distribution like O stars
- WR/O $\approx 10\%$ $= f_1(Z)$
- WN/WC $= f_2(Z)$

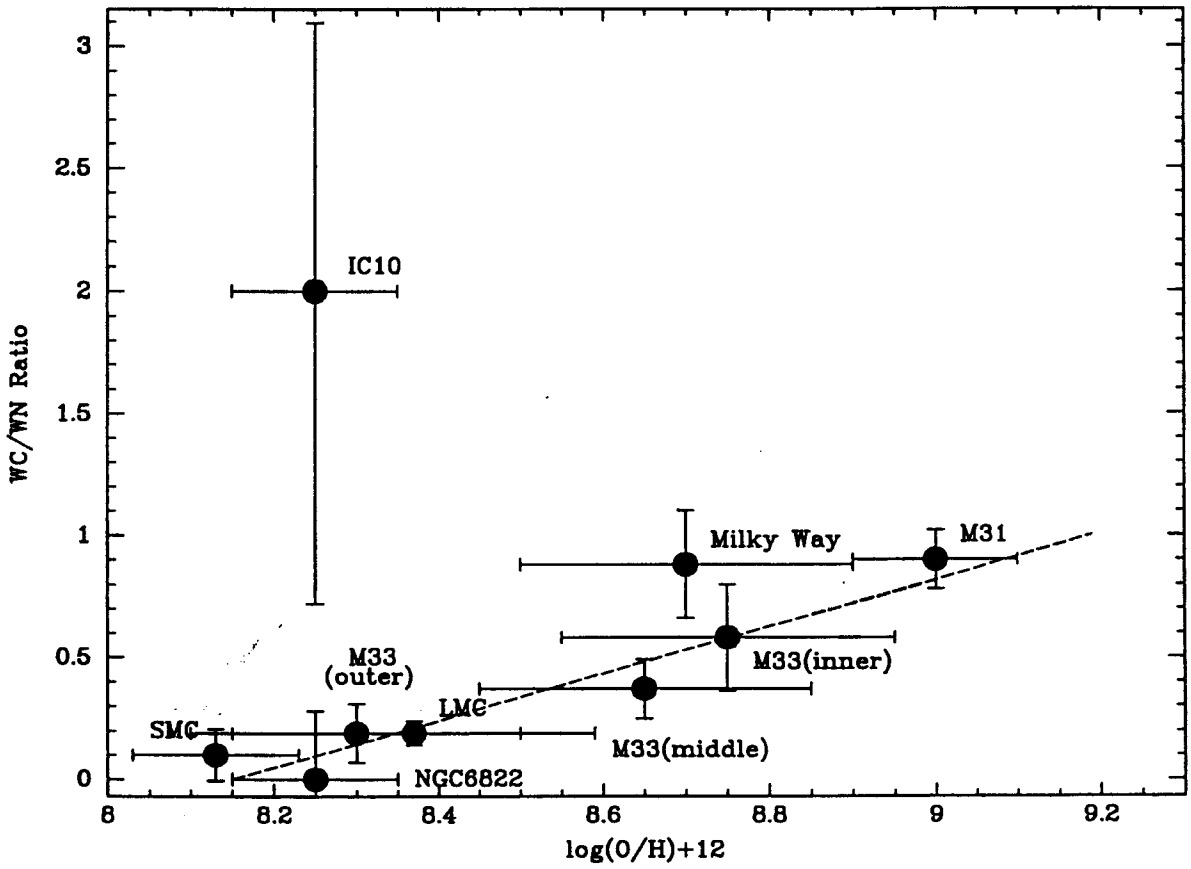
WC/WN Ratio
log(O/H)+12
IC10
Milky Way
M31
M33
(outer)
M33(inner)
LMC
SMC
M33(middle)
NGC6822
0
0.5
1
1.5
2
2.5
3
8
8.2
8.4
8.6
8.8
9
9.2

Massey 1999

STELLAR EVOLUTION

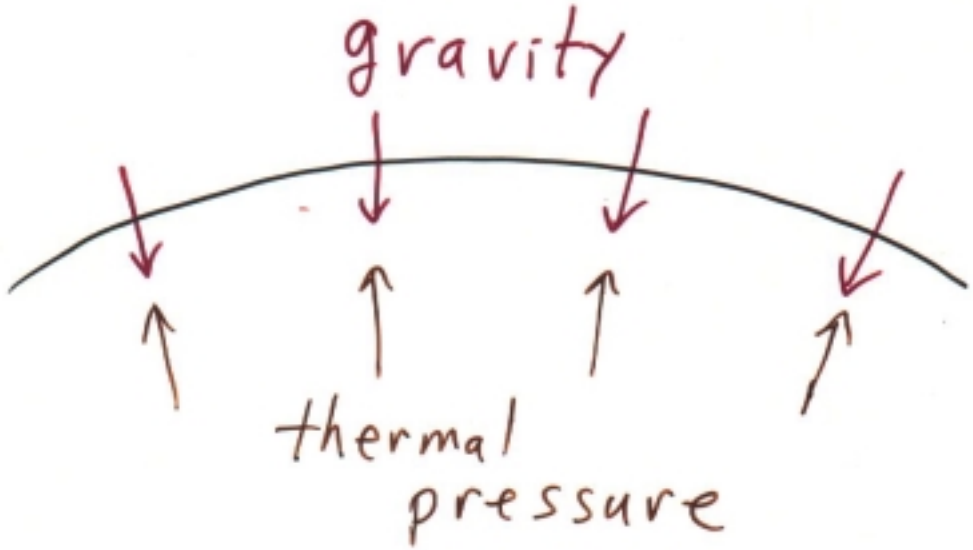

$m_i < 8\, m_\odot$ → degenerate

$\boxed{m_i > 8\, m_\odot}$ → supernova

massive

The Victor:

gravity → $\boxed{\text{Black Hole}}$

~ none → $\boxed{\text{NS}}$, WD, BD

thermal → Nothing

$$L = 4\pi R^2 \sigma T_e^4$$

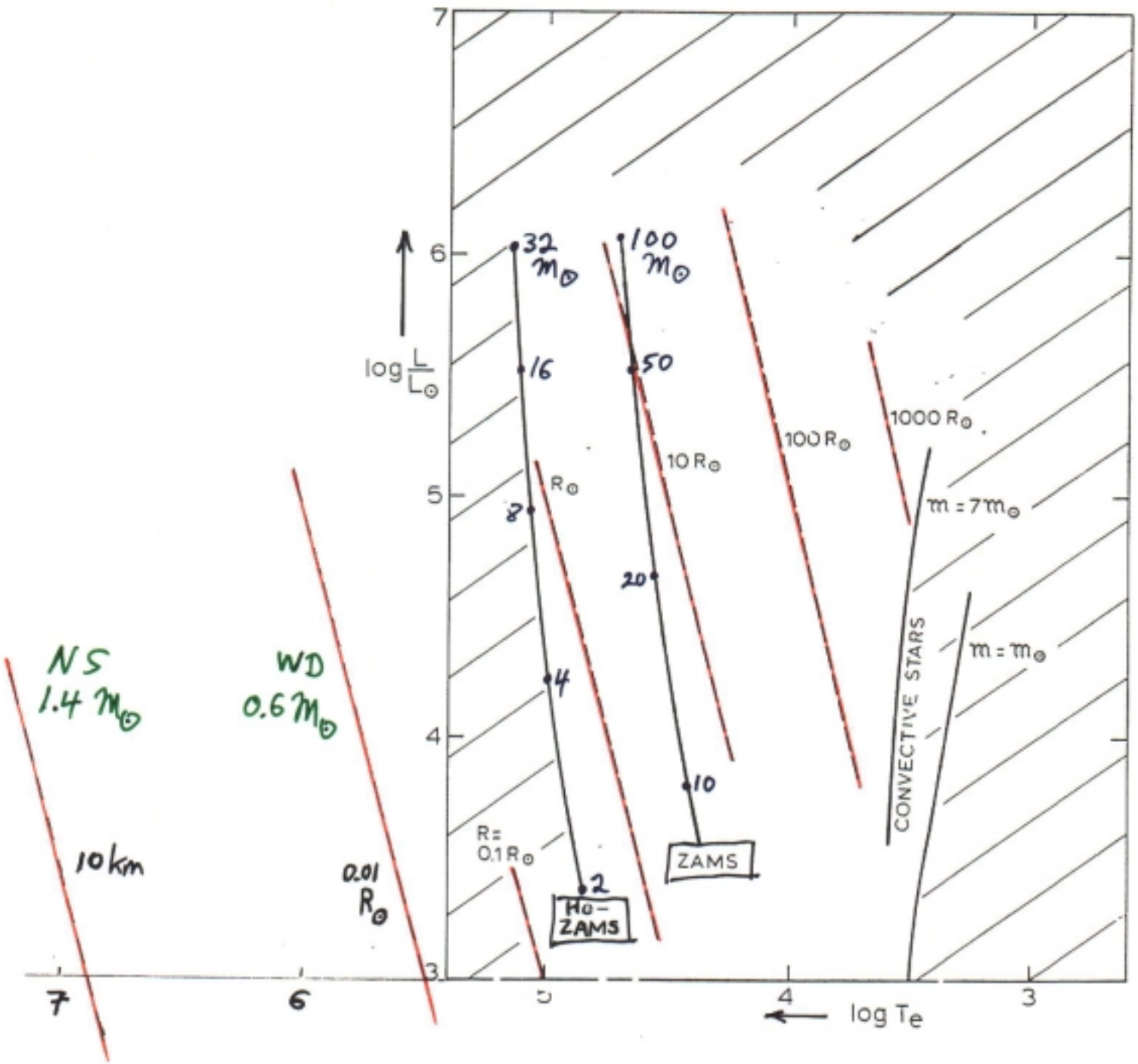

$R_\odot = 7 \times 10^5$ km

de Jager 1986

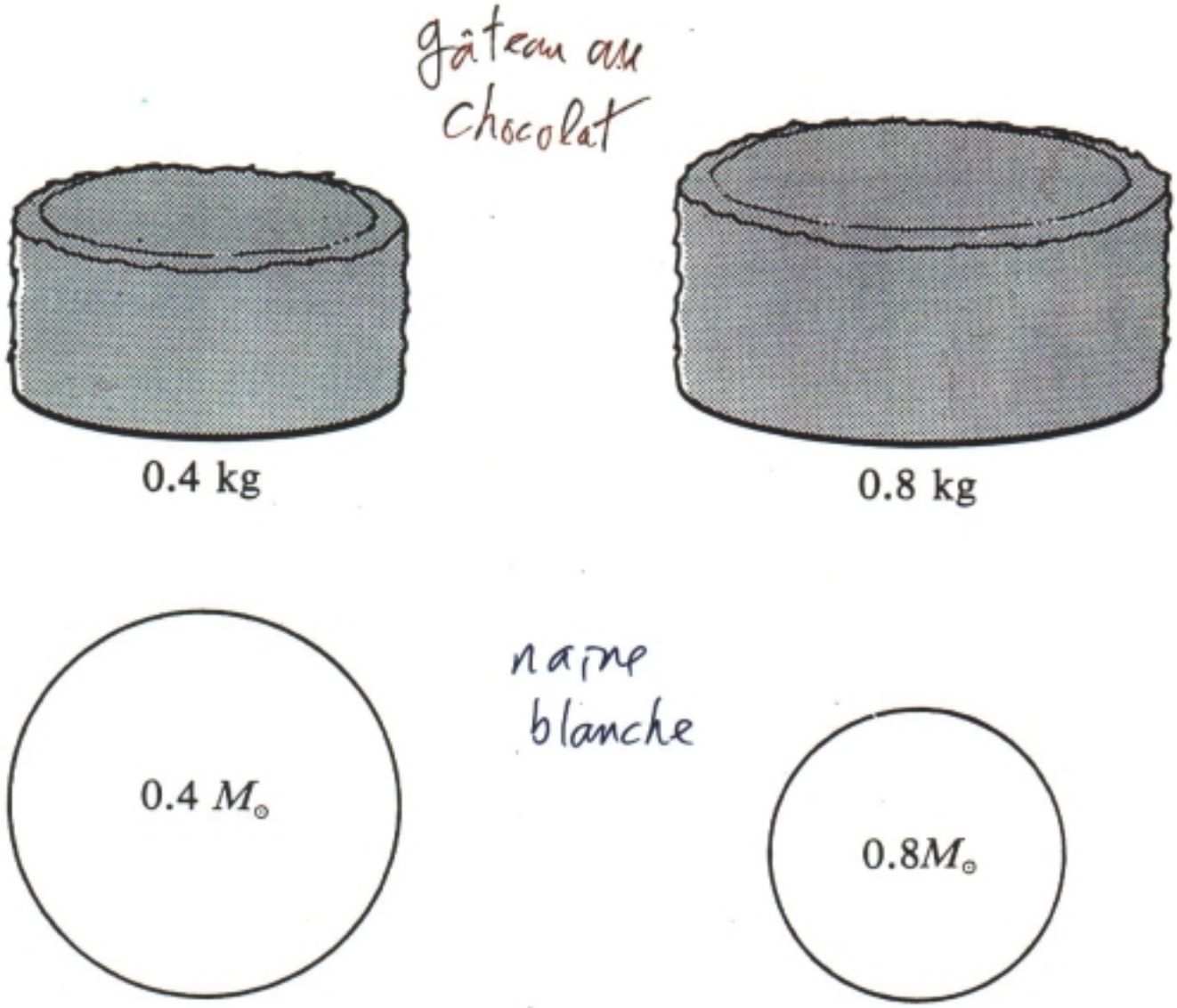

Figure 7.1. The difference between chocolate cakes and white dwarfs. A chocolate cake of 0.8 kilogram which is twice as massive as a chocolate cake of 0.4 kilogram would have twice the volume. A white dwarf of $0.8M_\odot$ which is twice as massive as a white dwarf of $0.4M_\odot$ would have only half the volume.

F. Shu 1982

$m_i = 3\ m_\odot$

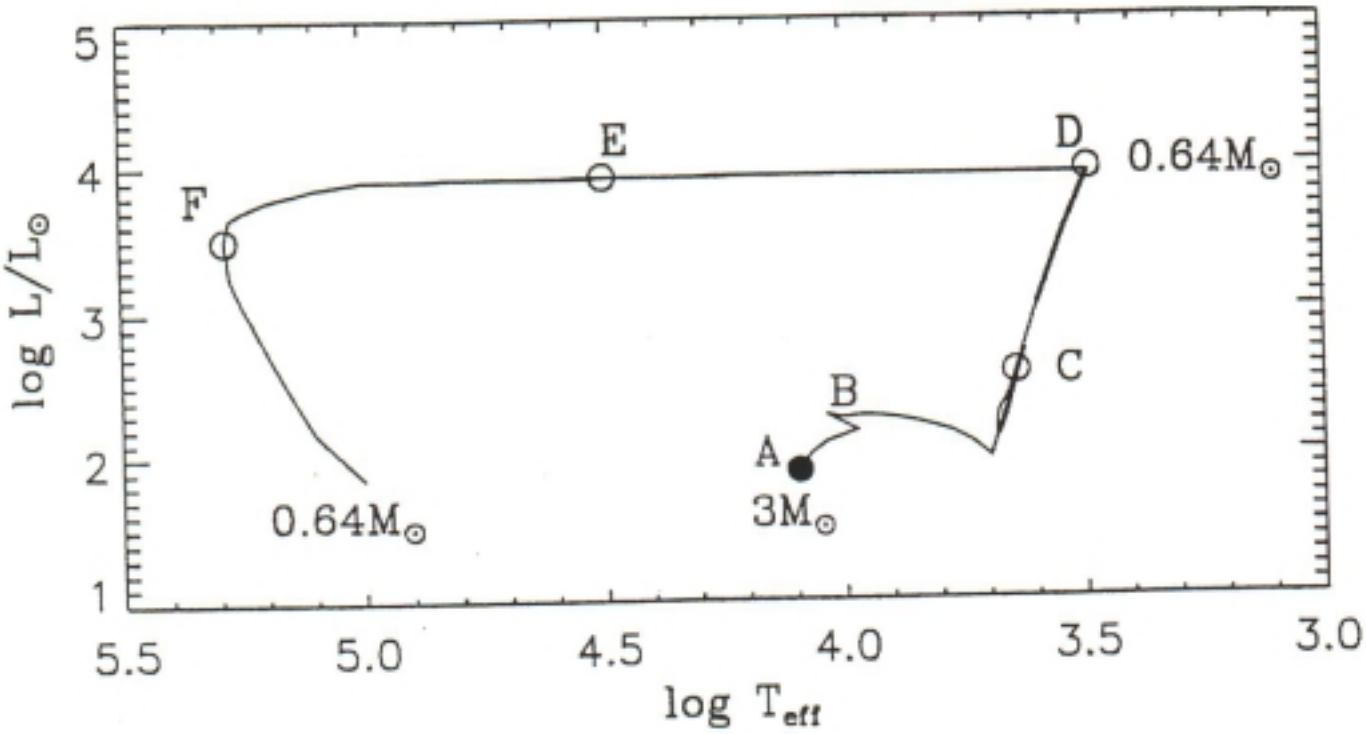
log L/L⊙
log T_eff
A
B
C
D
E
F
3M⊙
0.64M⊙
0.64M⊙

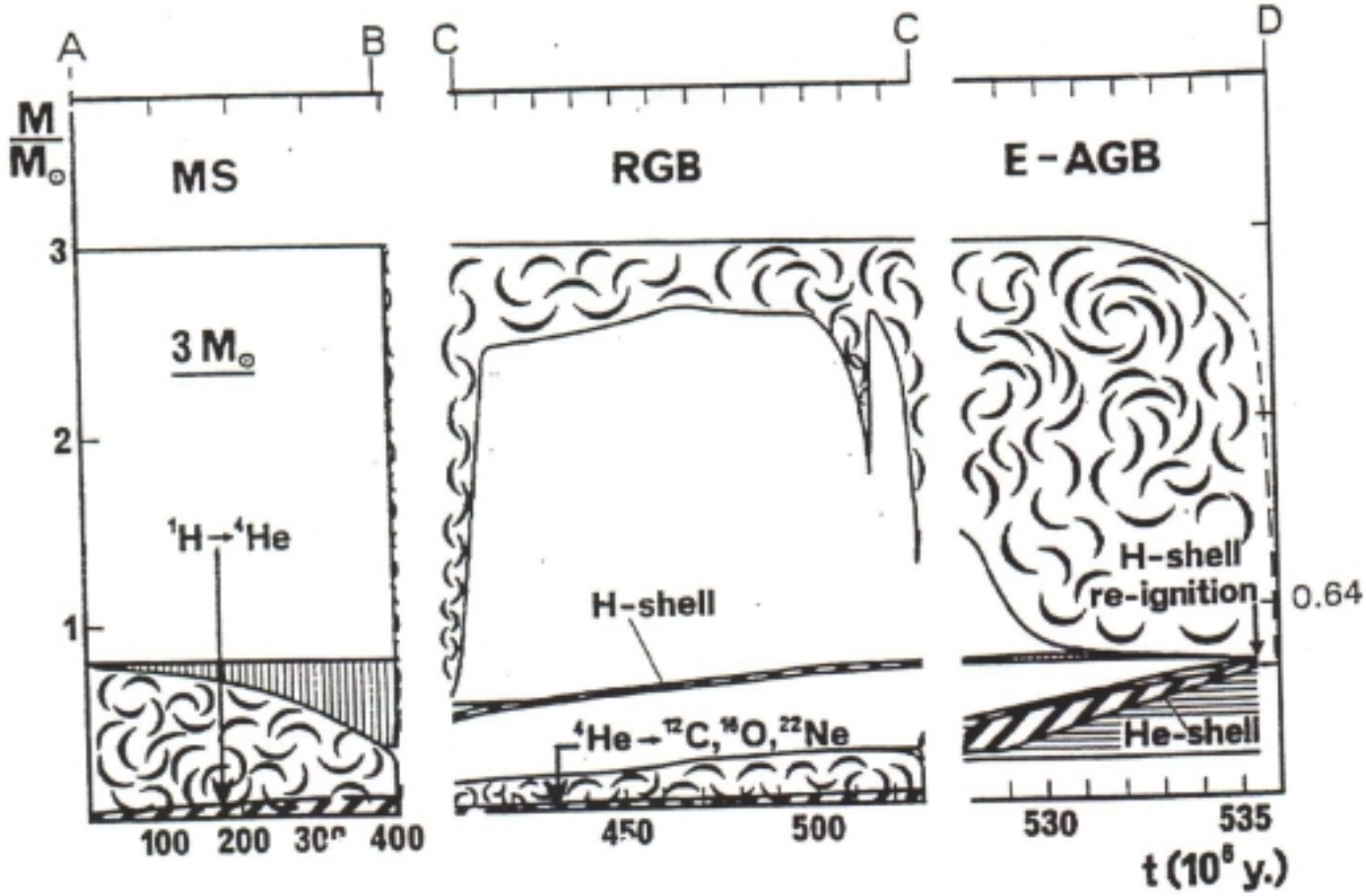
M/M⊙
MS
RGB
E-AGB
3 M⊙
¹H→⁴He
H-shell
⁴He→¹²C,¹⁶O,²²Ne
H-shell re-ignition
He-shell
0.64
t (10⁶ y.)

$m_i = 60\ m_\odot$

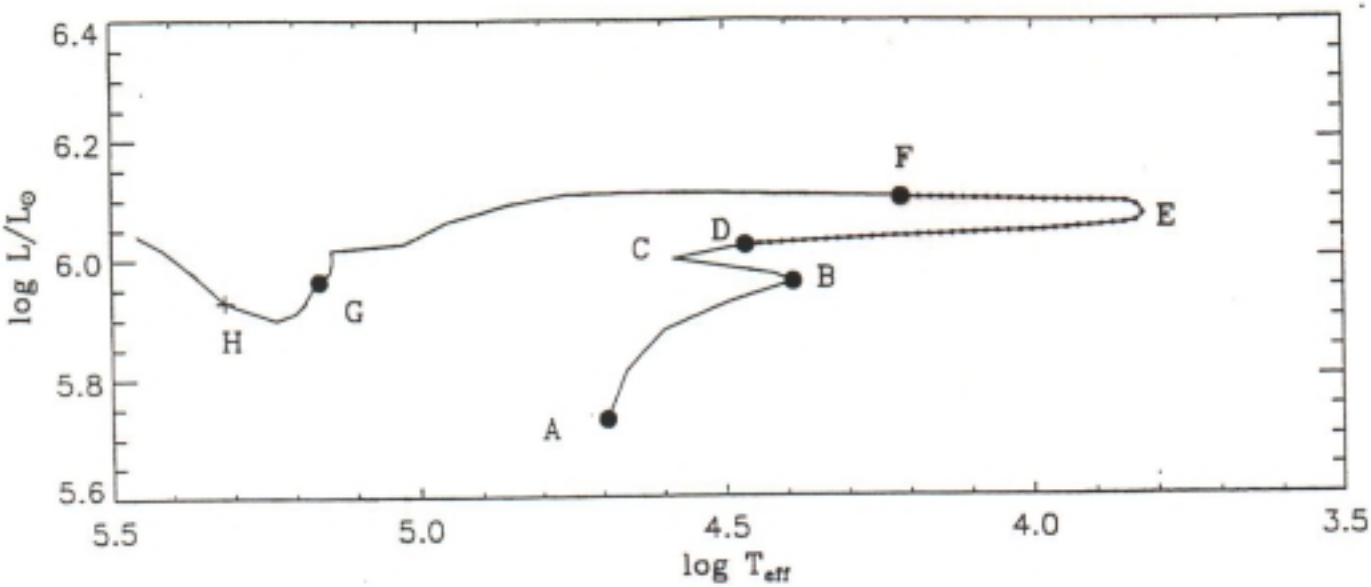

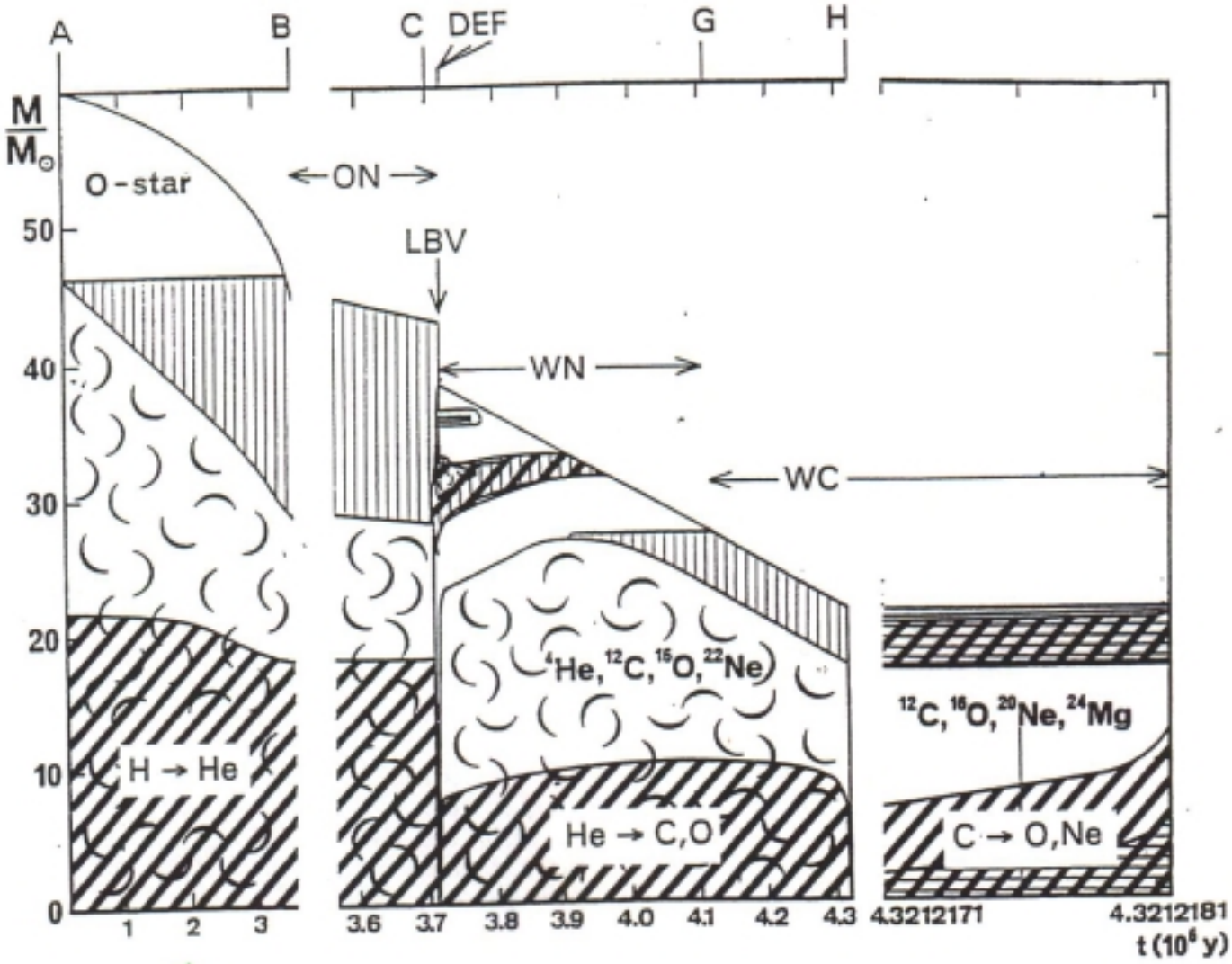

M an

0.7 M an

1 an

$$\mathcal{M}_i = 60\ \mathcal{M}_\odot$$

Core	Time		
$H \rightarrow He$	3.7 Myrs	$\longleftrightarrow$	37 min.
$He \rightarrow C, O$	0.6 Myrs	$\longleftrightarrow$	6 min.
$C \rightarrow O, Ne$	10^{-6} Myr $= 1$ yr	$\longleftrightarrow$	10^{-5} min $= 0.6$ msec
Total:	4.3 Myr	$\longleftrightarrow$	43 min

i.e. 1 min $\longleftrightarrow$ 10^5 yrs

1 sec $\longleftrightarrow$ 1700 yrs

$m_i = 60\ m_\odot$

abondances à la surface

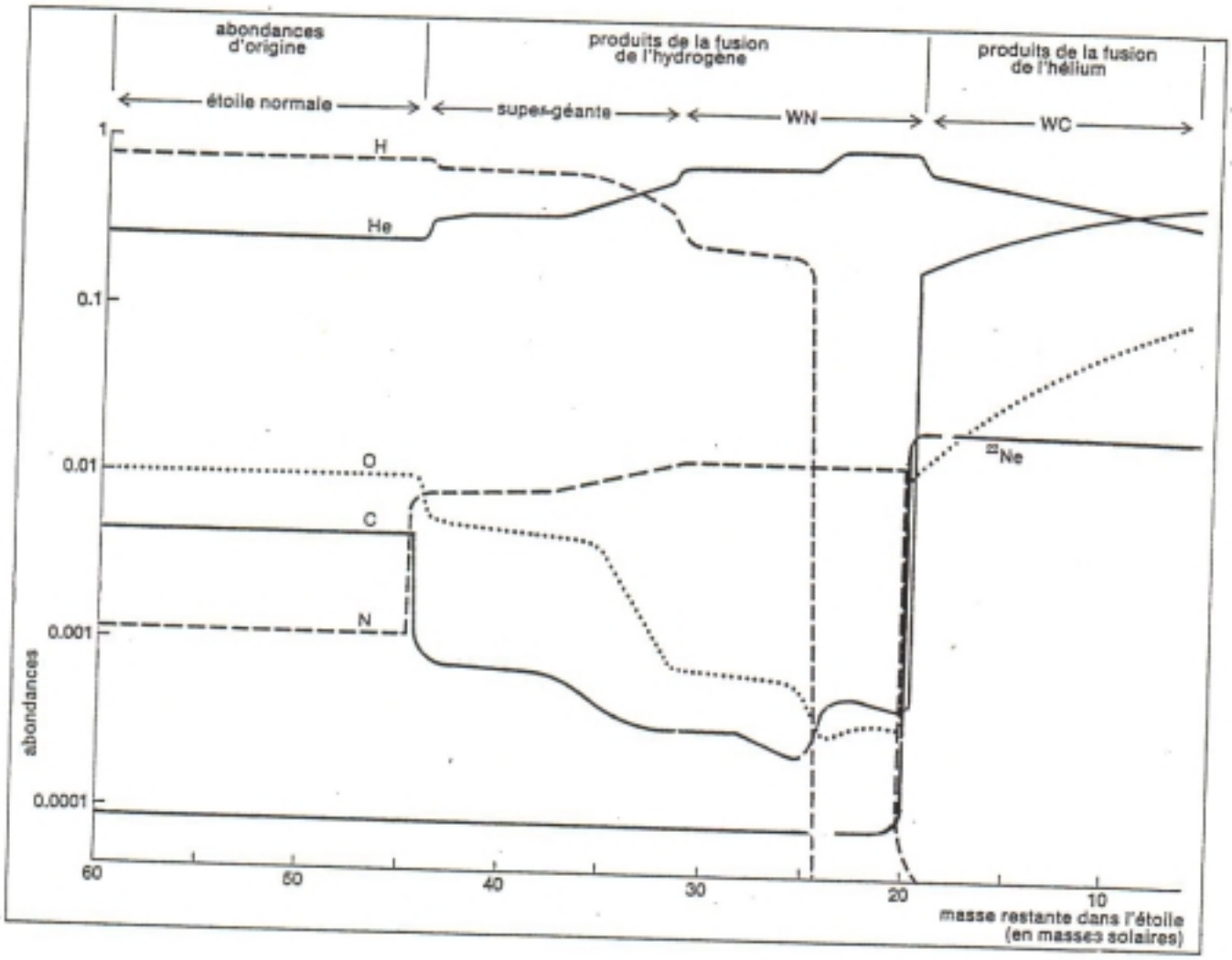

cf. Winds of Normal Stars

$\sim m^3$ $\quad$ $\sim 10^{-14}\, M_\odot/a$ $\quad$ $\sim 500\,km/s$ $\quad$ $\frac{1}{2}\dot{m} v_\infty^2$

$m/m_\odot$	Sp	$L/L_\odot$	$R/R_\odot$	$\dot{m}/\dot{m}_\odot$	$v_\infty/v_{\infty\odot}$	$\frac{\dot{m} v_\infty}{(\dot{m} v_\infty)_\odot}$	$\frac{L_w}{L_{w\odot}}$	$\frac{L_w/L}{(L_w/L)_\odot}$
1	G2 V	1	1	1	1	1	1	1
10	B2 V	10^3	5	10^5	2	$2 \cdot 10^5$	$4 \cdot 10^5$	$4 \cdot 10^2$
100	O3 V	10^6	15	10^8	6	$6 \cdot 10^8$	$4 \cdot 10^9$	$4 \cdot 10^3$

!

[WR: 10^9]

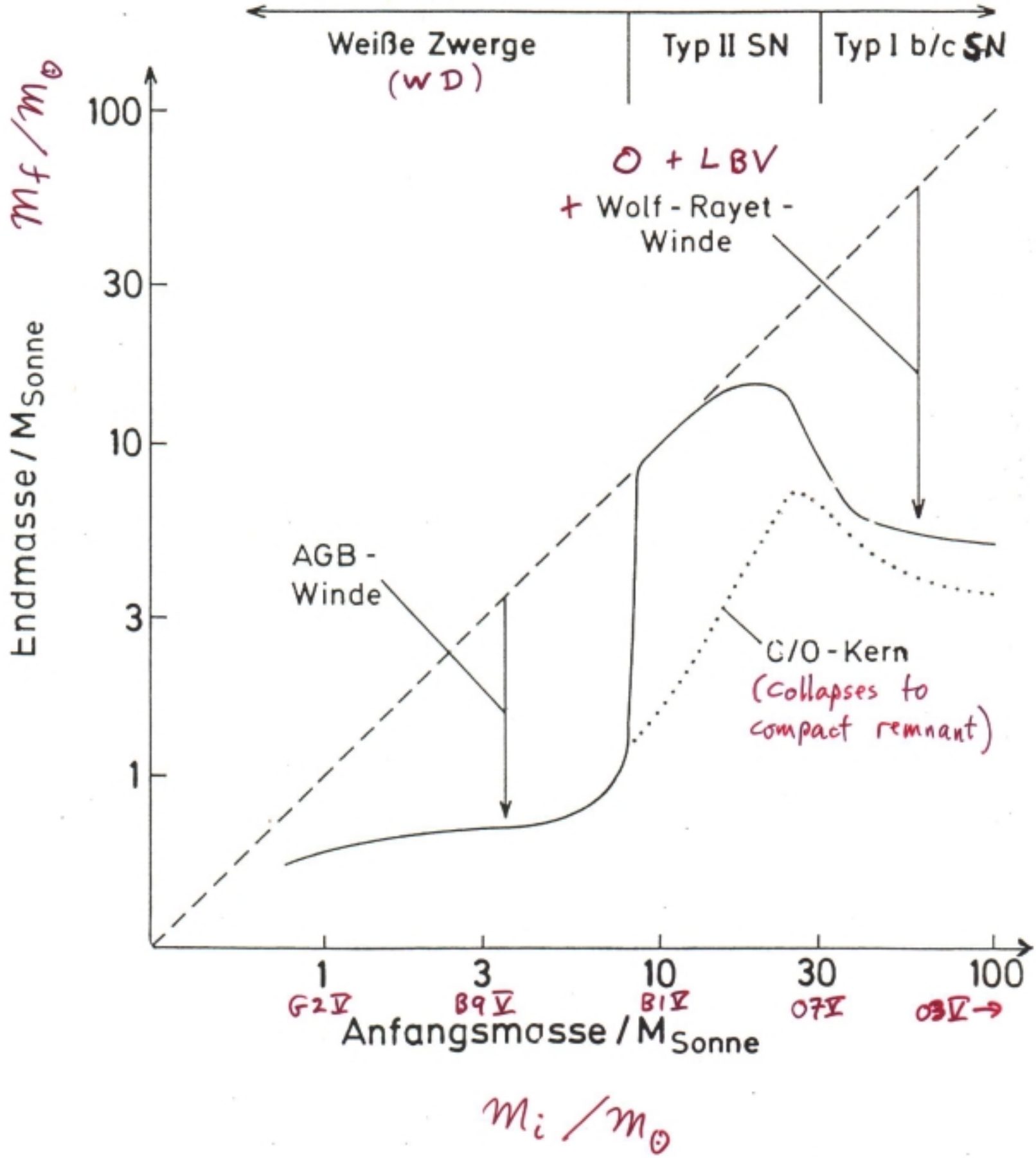
Weiße Zwerge
(WD)
Typ II SN
Typ I b/c SN
$m_f / m_\odot$
Endmasse / M_{Sonne}
100
30
10
3
1
O + LBV
+ Wolf - Rayet - Winde
AGB - Winde
C/O - Kern
(Collapses to compact remnant)
1
3
10
30
100
G2V
B9V
B1V
O7V
O3V →
Anfangsmasse / M_{Sonne}
$m_i / m_\odot$

m_f versus m_i (Langer 2000)

(for single stars)

- if $\dot{m} \equiv 0 \Rightarrow m_f \equiv m_i$

  (and we'd be doing something else now)

- for $m_i \lesssim 8\ m_\odot$
  - mass-loss all at end, generated by pulsational instabilities as AGB
  - PN = fast wind driving into slow debris, excited by hot CS
  - final WD: $m \sim 0.6\ m_\odot$, ~indep. of m_i

- for $m_i \simeq 8 \ldots 25\ m_\odot$ (early B, late O)
  - $\dot{m}$ relatively low
  - explode as H-rich (at surface) SN II with low KE & L_{SN}
  - remnant = NS

- for $m_i \approx 25 \ldots 100: m_\odot$ (O stars)
  - $\dot{m}$ high during all pre-SN stages
  - explode as H-poor, He-rich (at surface) SN Ib/c
  - remnant (prob.) BH

LMC

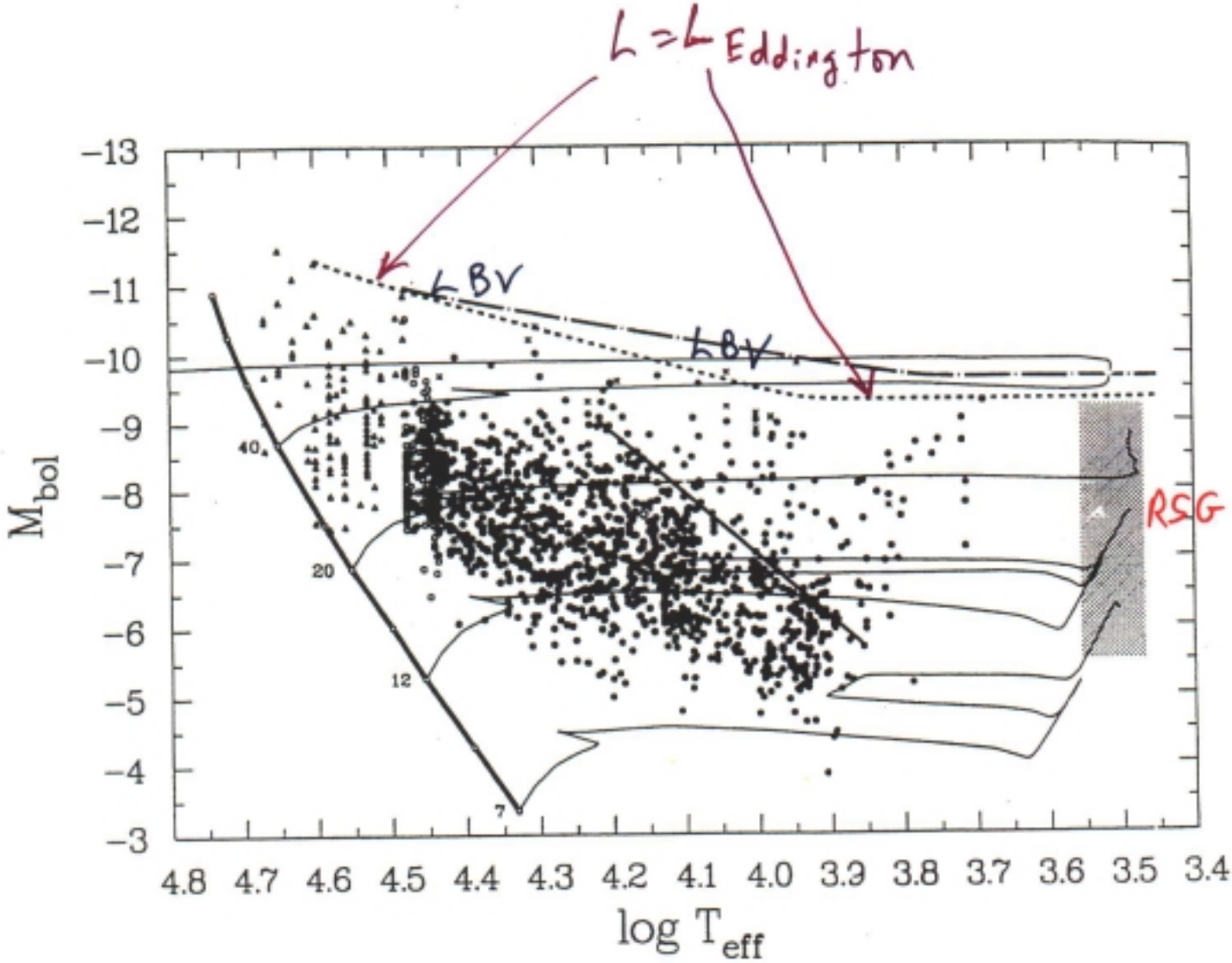

stable: $$\frac{Gm}{R^2} > \kappa \frac{L/c}{4\pi R^2}$$

unstable: $$\frac{Gm}{R^2} = \kappa \frac{L_{Edd}/c}{4\pi R^2}$$

$$\Rightarrow L_{Edd} = \left(\frac{4\pi c G}{\kappa}\right) m$$

20

Moffat, Drissen + Robert
1989 IAU Coll. 113, p. 229

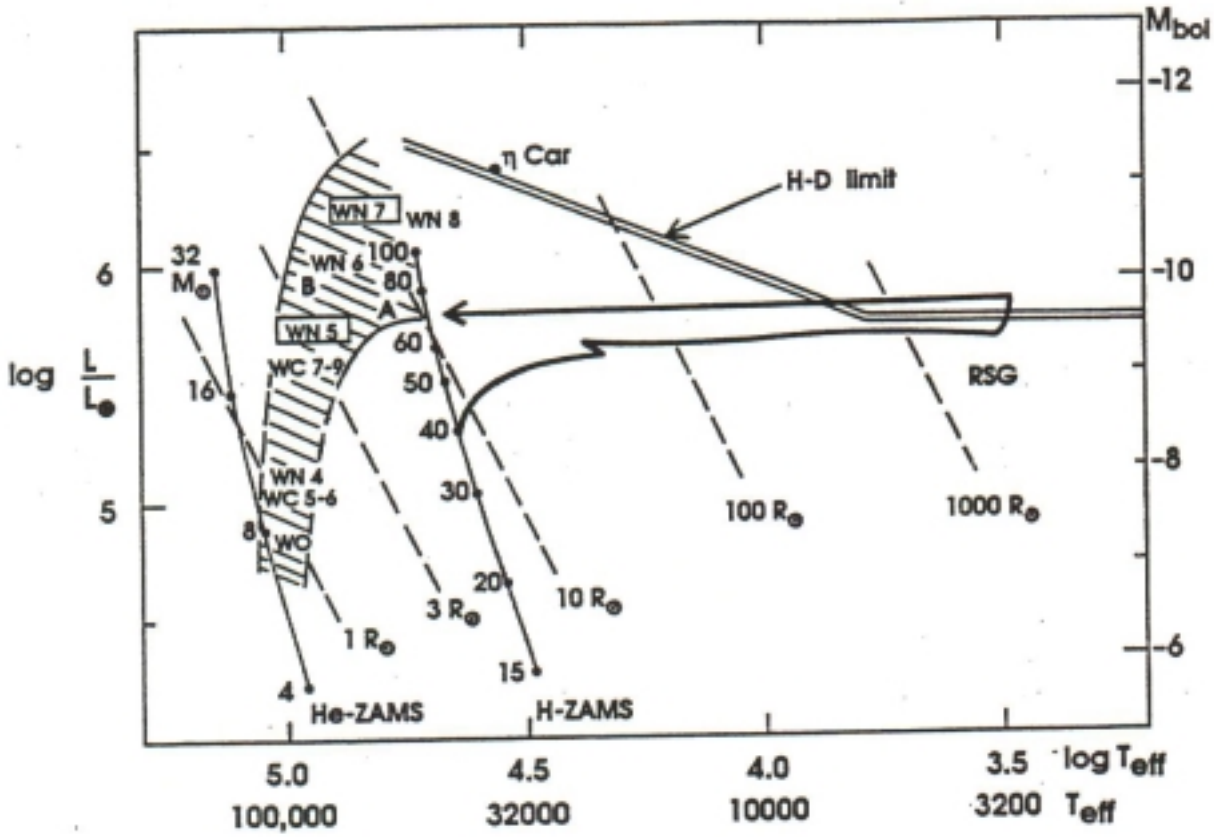

Figure 3. Average positions of W-R stars of different subclass in the HR diagram. The positions of the framed subtypes are constrained by direct eclipse observations of stars of the corresponding type. The hatched, funnel-shaped region allows for the observed spread in M_{bol}. The evolutionary track of a $40M_\odot$ ZAMS star from Maeder and Meynet (1987) is shown for comparison.

~ Consensus (at $Z_\odot$)

$m_i \gtrsim 50\, m_\odot$

O → OIf → BSG → LBV → WN → WC → SN

only difference

$m_i \simeq 35 \ldots 50\, m_\odot$

O → BSG → YSG → RSG → YSG → WN → WC → SN

.... and possibly

WNL → WNE → WCE $\ll Z_\odot$

WNL → WCL → WCE $\gtrsim Z_\odot$

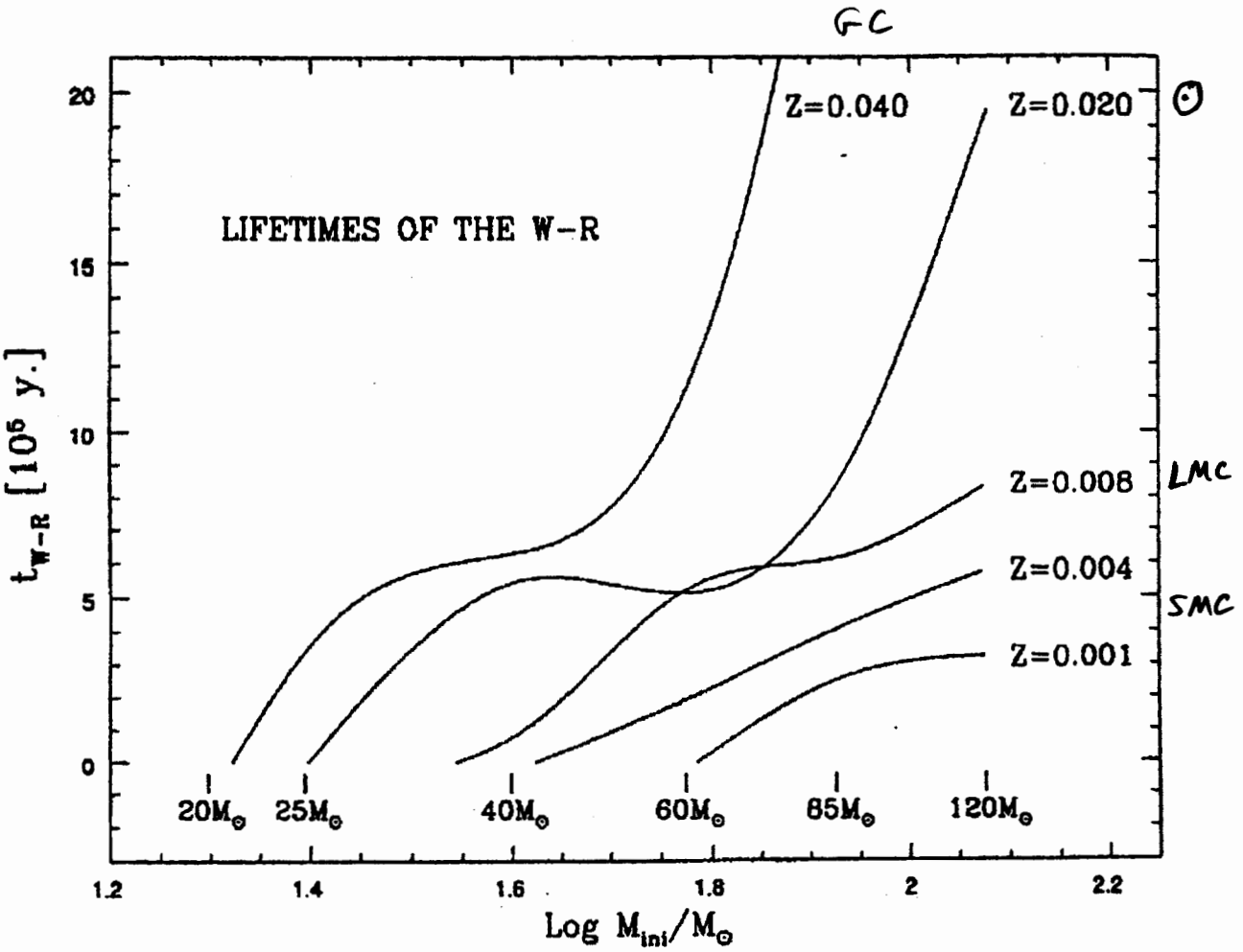

Figure 5: WR lifetimes as a function of M and Z.

2 viewgraphs !

Best way to study stellar evolution w.r.t WR stars is in young star clusters. An excellent example is NGC 3603 at $d = 7$ kpc in the Carina arm.

It contains $\gtrsim 50$ O-stars, many of the earliest, most-luminous (∴ massive) types: O3. At its core, within ~2" (~0.2 ly), are located 3 WR stars, all the brightest stars in the entire cluster. Actually, they exhibit strong emission lines yet have only slightly reduced H-abundances compared to solar.

① Show IR image :- see Brandl et al. 1999 A+A 352, L69 or HST image : Brandner et al. 2000 A+A ---

② A beautiful montage of optical spectra taken with HST is shown in Drissen et al. (1995 AJ 110, 2235); as the luminosity increases, absorption lines change into emission, as the wind strengthens. Presumably it is the mass that is increasing with L, so that in this case, it is the WR stars that show emission lines here, not as is often the case because of their evolved status, but rather they are H-burning main sequence stars.

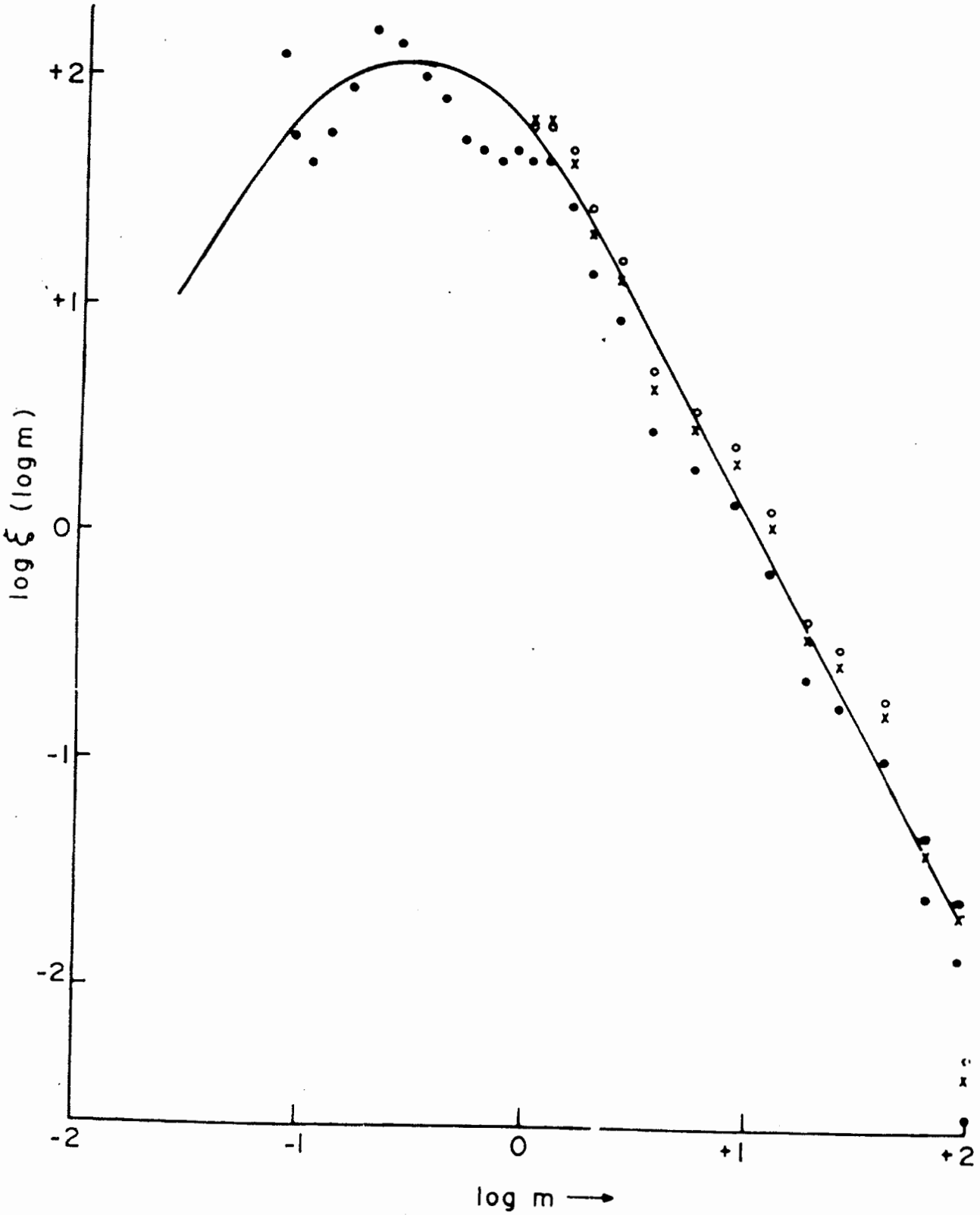

"F I M"

Salpeter IMF

range of mass	number of stars	$\frac{m_{tot}}{m_\odot}$	$\frac{L_{tot}}{L_\odot}$
80-40 $M_\odot$	10	600	2,000,000
40-20 $M_\odot$ ↓ 1/2	30 ↓ 3x	900	800,000
20-10 $M_\odot$	100	1,500	300,000
10-5 $M_\odot$	300	2,200	130,000
5-2.5 $M_\odot$	1,000	4,000	50,000
2.5-1.2 $M_\odot$	3,000	6,000	20,000
1.2-0.6 $M_\odot$	10,000	9,000	7,000
0.6-0.3 $M_\odot$	30,000	14,000	3,000
0.3-0.15 $M_\odot$	100,000	22,000	1,000
0.15-0.075 $M_\odot$	300,000	34,000	400

$(L \sim m^3)$

Zinnecker (1996)

Lamers & Cassinelli 1999

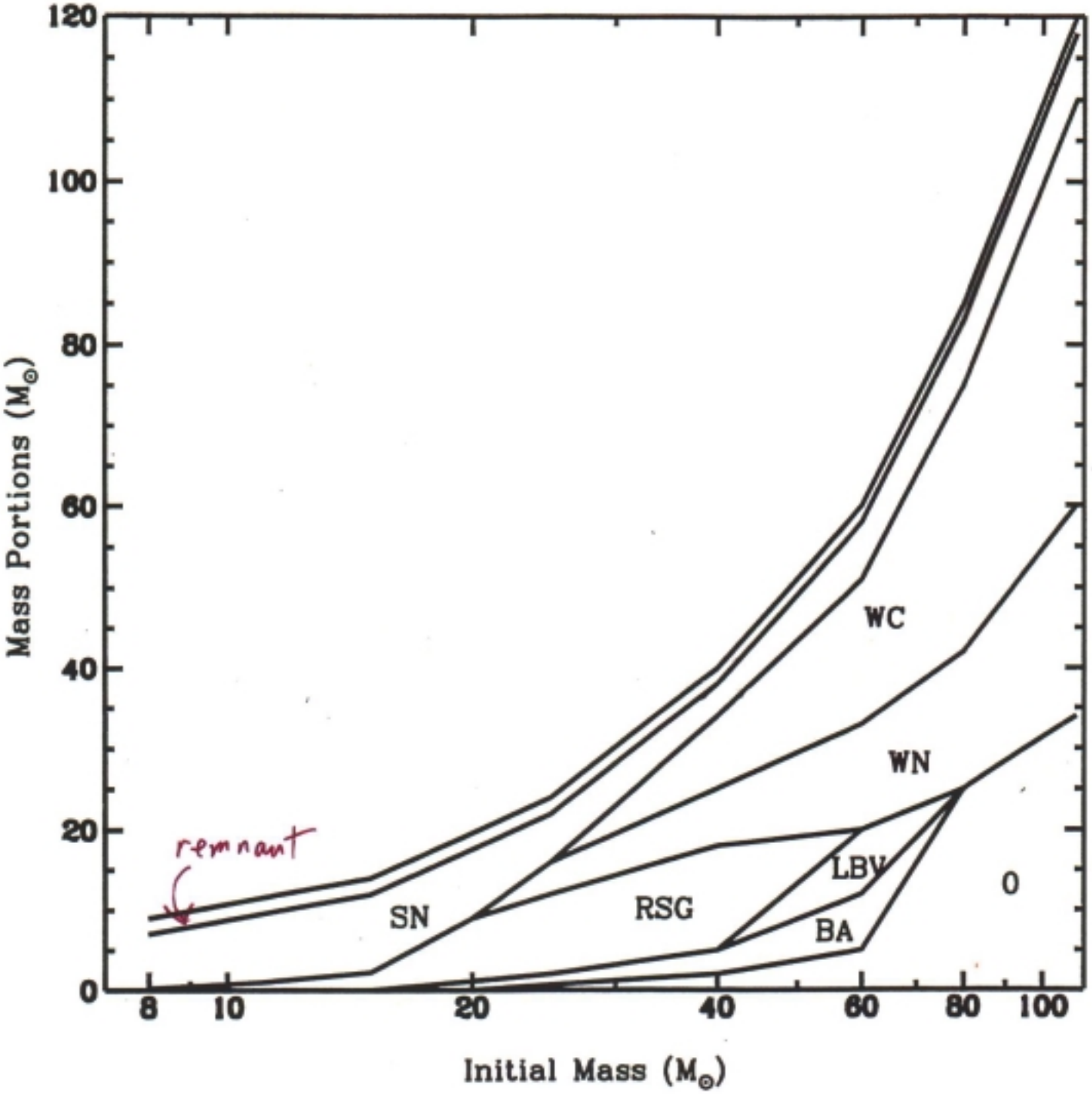

.... after IMF

Lamers + Cassinelli 1999

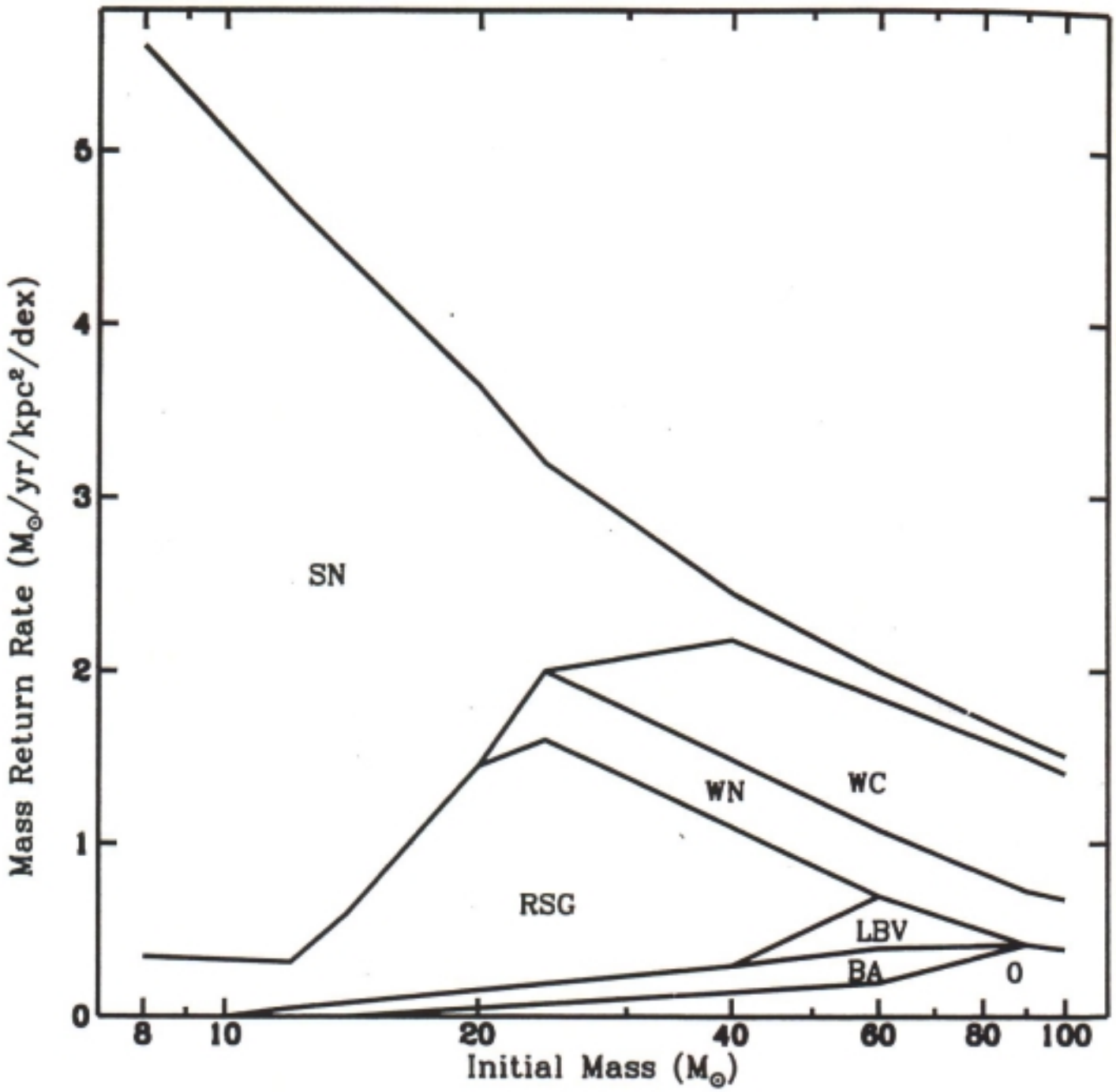

Chandra Cas A

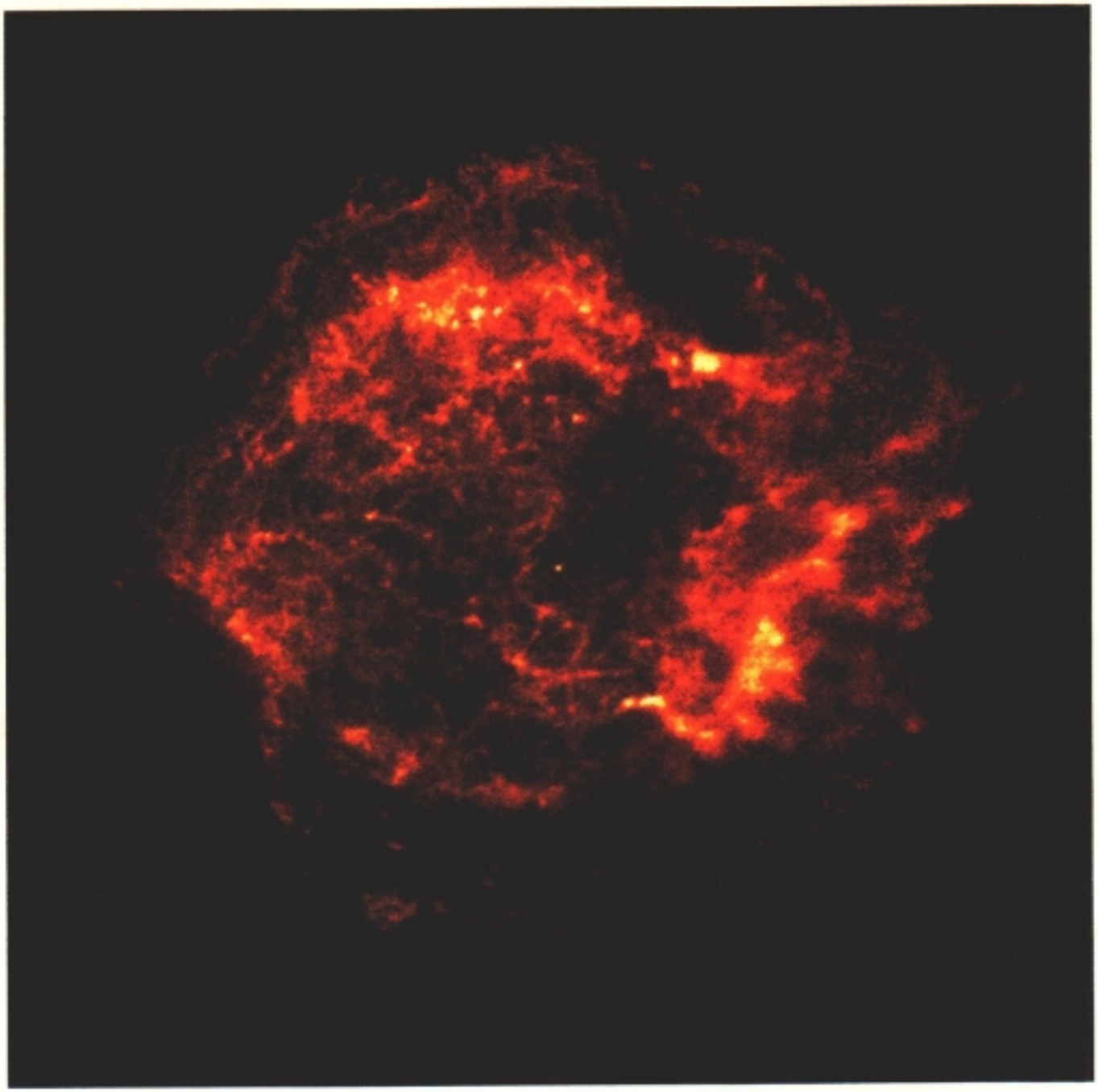

Spectroscopic Binaries

SB2
$n \sim 20$

	(E)	(L)		
WN :	~ 10	$- 60$	$\mathcal{M}_\odot$	$q(\text{WNL}) \simeq 1$
$\Downarrow$				
WC :	~ 5	$- 20$	$\mathcal{M}_\odot$	$q(\text{rest}) \ll 1$

<u>BUT</u>

are $\mathcal{M}_{WR}(\text{in binary}) = \mathcal{M}_{WR}(\text{single})$??

G. Münch 1950, ApJ. 112, 266

V444 Cyg (WN5+O6)

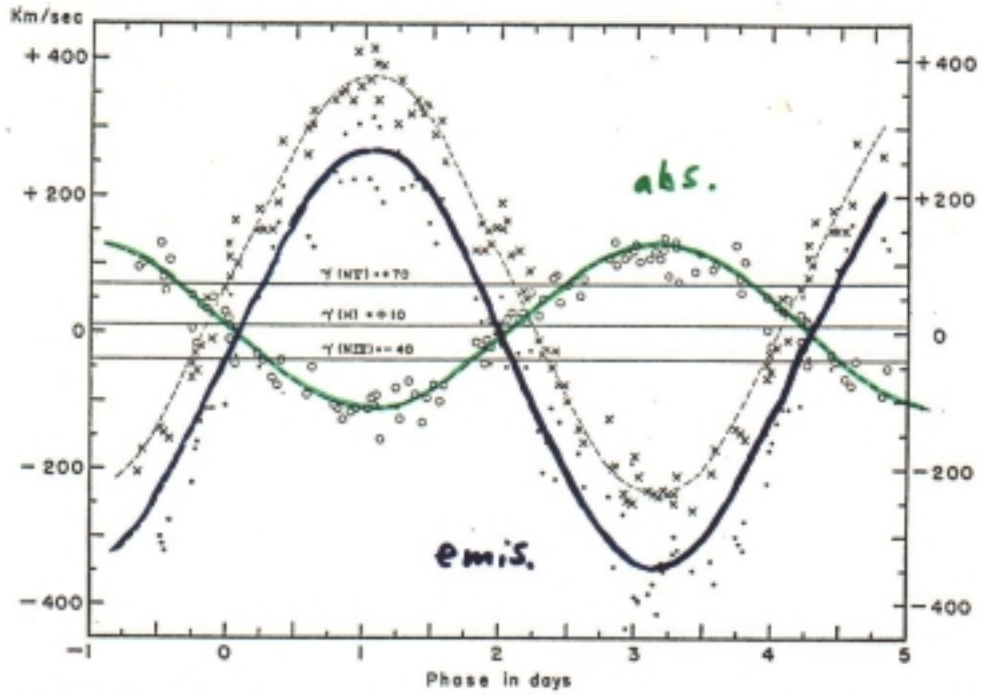

FIG. 2.—The radial-velocity-curves of HD 193576. The circles represent the average of the velocities derived from $H8$, $H9$, and $H10$. The crosses and dots represent the velocities given by the N V lines at λ 4603 and λ 4619 and by the N IV line at λ 4058, respectively.

P = 4.21 d.

TABLE 2

ELEMENTS OF THE SPECTROSCOPIC ORBITS

	O. C. Wilson	E. S. Keeping	Present Work
(Km/Sec)			
Emission γ	+ 56.4±4.4	N V: +55 N IV: + 8	N V: +70 N IV: −40
Emission K	308.6±6	301.5±3.9	305
Absorption γ	− 33.6±4.4	+ 32.8±1.5	+ 10
Absorption K	120.7±5.8	177.2±3.9	120
$m_0 \sin^3 i$ ($M_\odot$)	24.8	30.8	24.1
$m_w \sin^3 i$ ($M_\odot$)	9.74	17.3	9.5
$a_0 \sin i$ ($R_\odot$)	10.1	14.4	10.0
$a_w \sin i$ ($R_\odot$)	25.7	25.5	25.4
$(a_0+a_w) \sin i$	35.8	39.9	35.4

eclipses

⇒ $i = 78°$

$q = m_{WR}/m_O = 0.40$

orbit is b... line of ... by ... ... c... ... Ke... star ... WK ... by diffe... that the ... center of ma... km/sec to the ... the apparent ...

FIG. 3.—The ... (*empty circles*) an... apparent compon...

tions is often ... This distortion ... elongations. F... on the plate, d... ter tracing. He... is probably no...

The violet ... have also been ... is visible only ... λ 3889 edge ca... apparent comp... lines, given in ... the curve four... sorption edge ...

[11] *Ap. J.*, 100, ...

[12] *Op. cit.*, Fig... value which is le... of a possible intr...

Spectroscopic "Standard Model" (single WR)

Hamann, Hillier

→ radiation pressure driven winds, with:

- spherical symmetry
- homogeneity
- stationarity

and $v(r) = v_\infty (1 - R_*/r)^{\beta}$ ← $=1$

"β-law" assumed

(i.e. hydrodynamical problem not solved consistently)

→ parameters that specify the model:

$\dot{m}$, L, R_* ($\tau = 20$), v_∞, chem. comp.

(T_* follows from L, R_*)

+ more recently:

- clumping

rel. clump density

$$D \equiv \frac{\rho_{cl}}{\bar{\rho}_{wind}} \gtrsim 1$$

($\therefore$ filling factor $f = 1/D$)

Emission $\propto \rho^2 \Rightarrow \dot{m}$ reduced by factor $\sqrt{D}$

- line-blanketing (espec. Fe)

Results of Std. Model fits

$D \sim 4 \ldots 10$

$\Rightarrow \dot{m} \downarrow$ factor 2–3 cf. smooth wind

Wind momentum factor

$$\eta \equiv \frac{\dot{m} v_\infty}{L/c} \sim 1 \ldots 10$$

Abundances

WN : CNO cycle , $0 \leq X_H \lesssim 0.5$ $(\odot = 0.7)$

WC, WO : triple-α , $X_H = 0$

CMD →

$\dot{m}$ vs. L →

Hillier + Miller (1999 ApJ 519, 354)

HD 165763 = WR 111, WC5

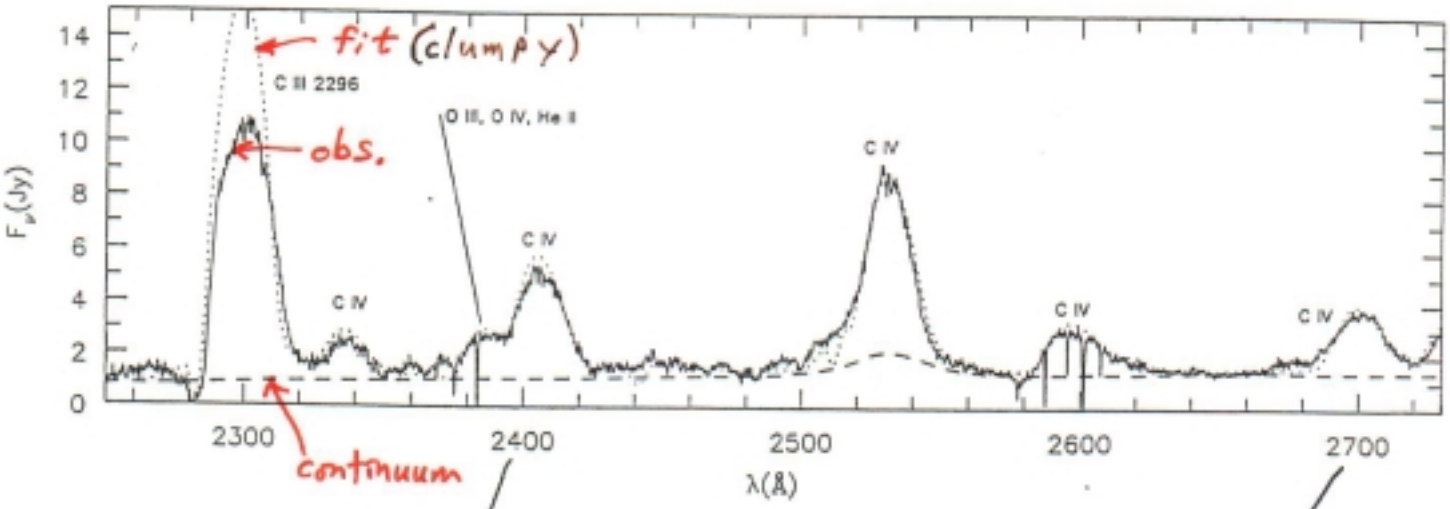

Models:

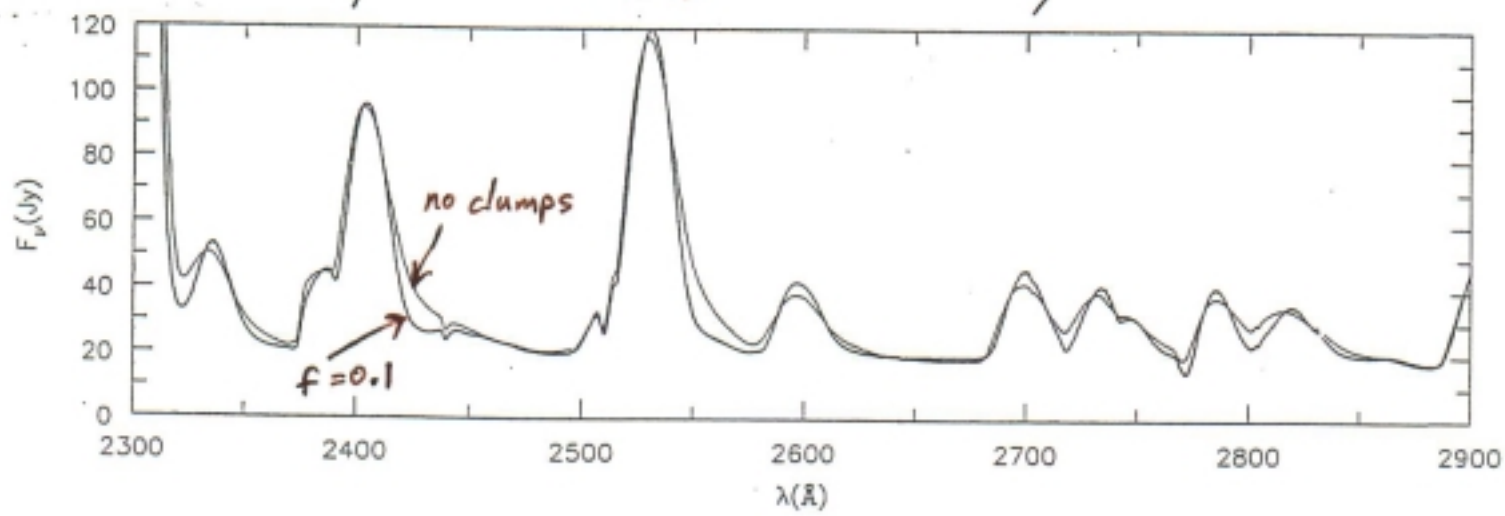

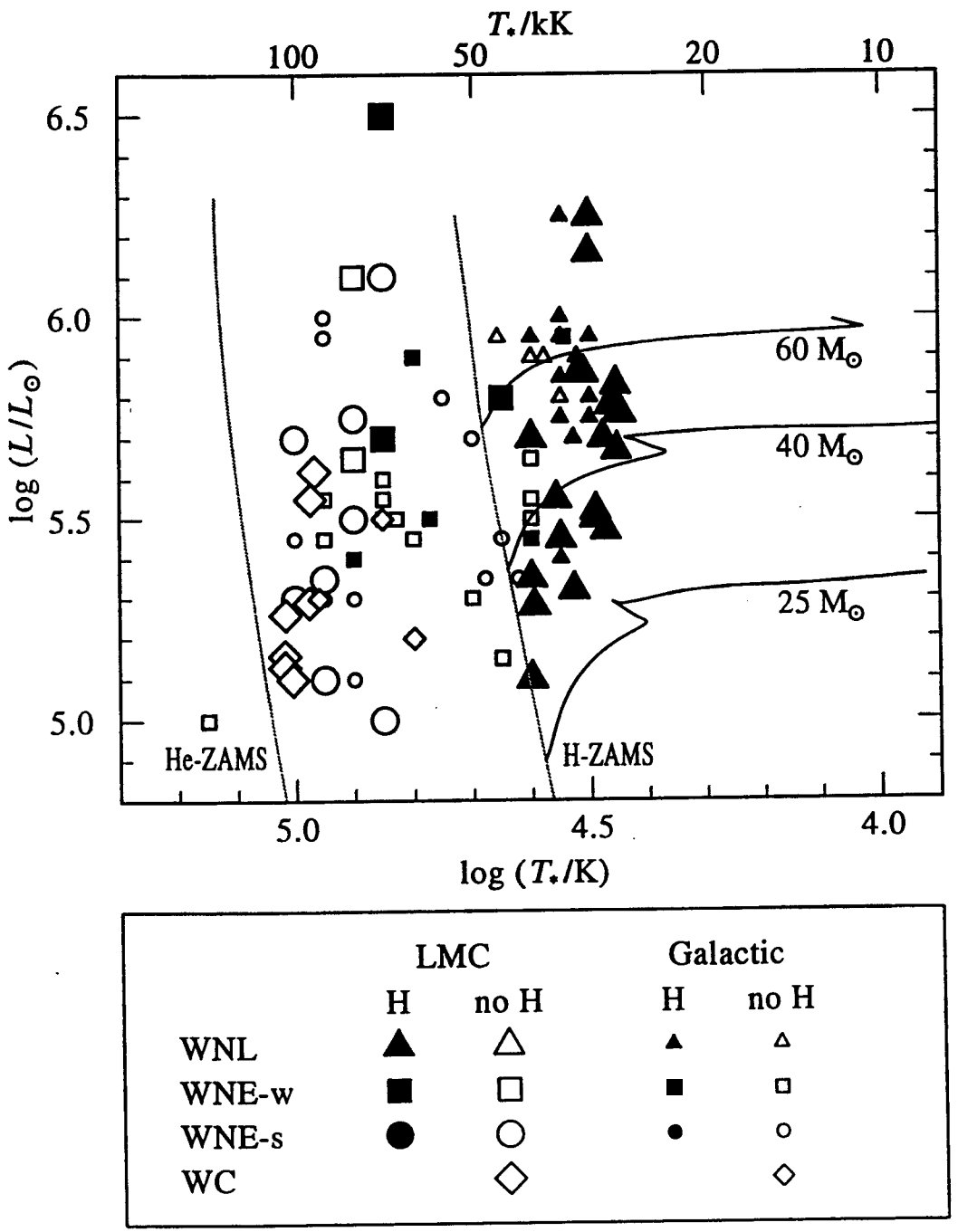
T*/kK
100
50
20
10
6.5
6.0
5.5
5.0
log (L/L⊙)
60 M⊙
40 M⊙
25 M⊙
He-ZAMS
H-ZAMS
5.0
4.5
4.0
log (T*/K)
LMC
Galactic
H
no H
H
no H
WNL
WNE-w
WNE-s
WC

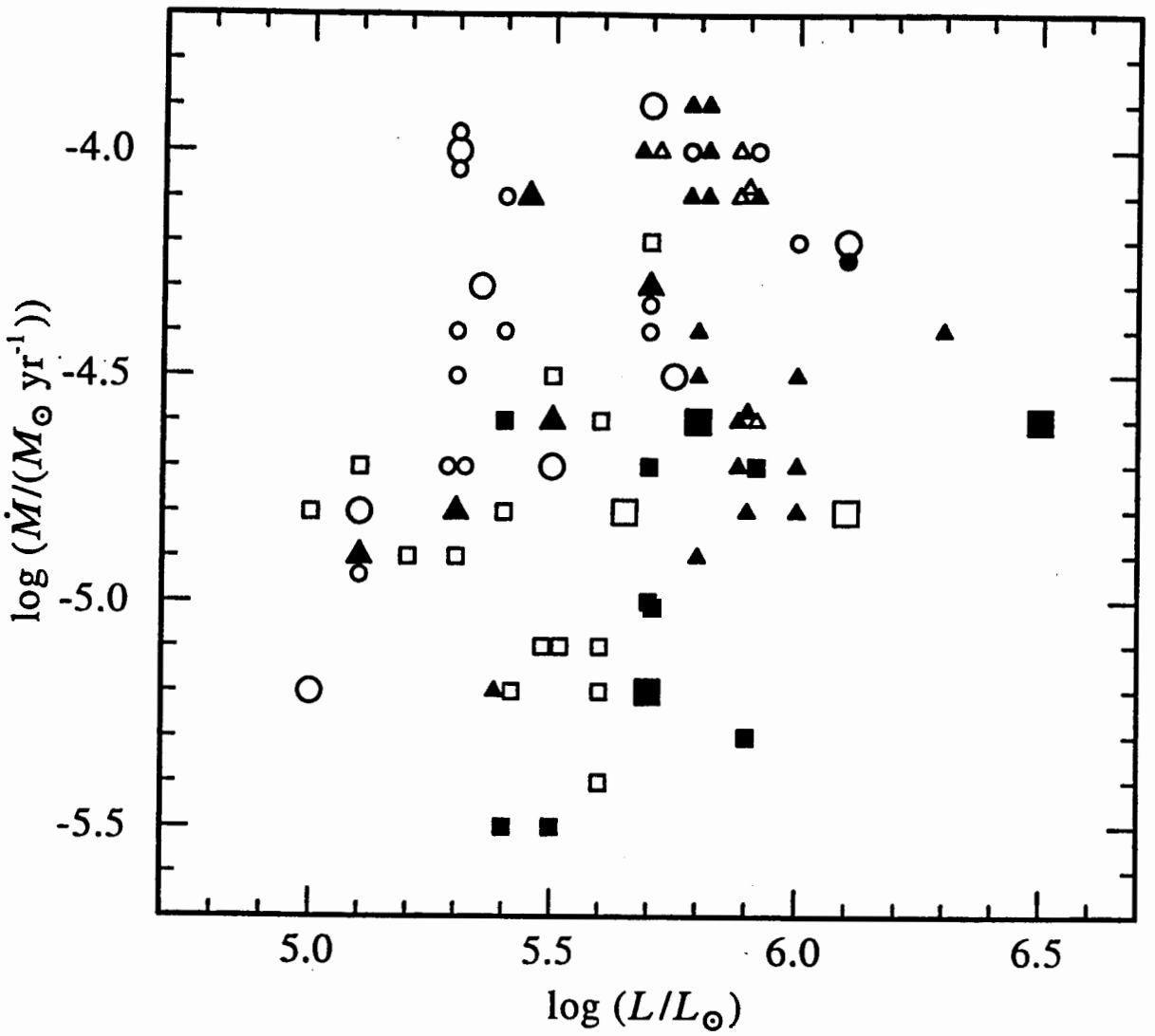
-4.0
-4.5
-5.0
-5.5
log ($\dot{M}$/($M_\odot$ yr^{-1}))
5.0
5.5
6.0
6.5
log ($L/L_\odot$)

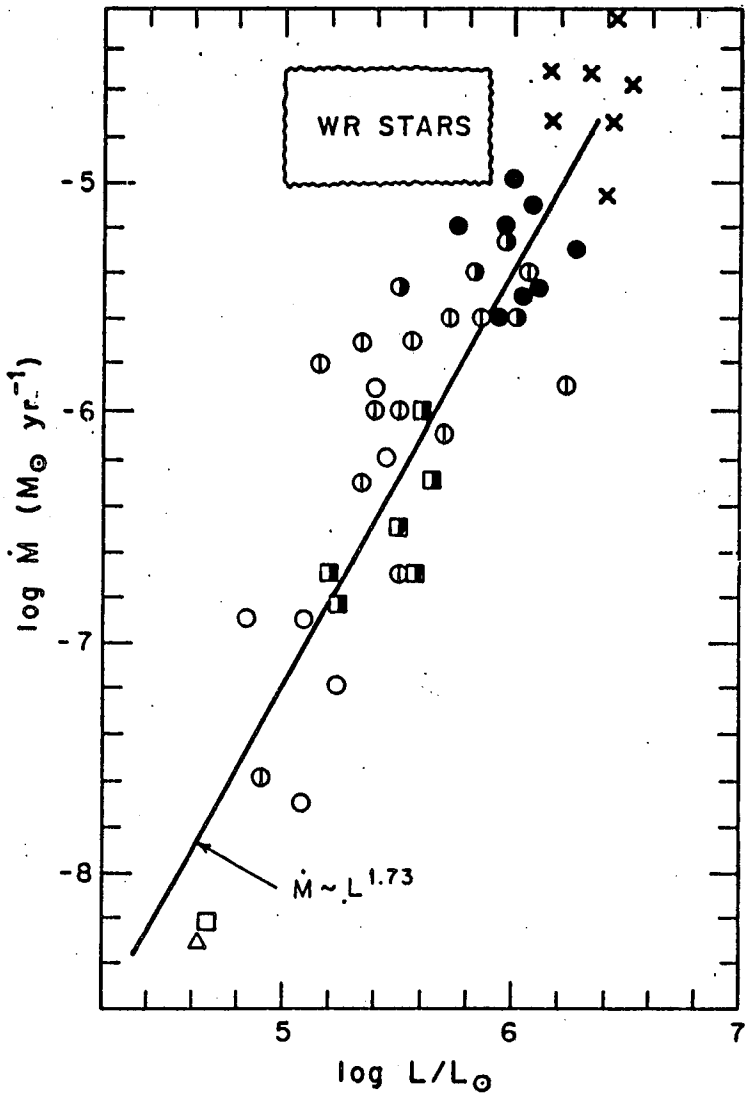

WR = epitome of hot stars with winds

Conti (1982 IAU Symp. 99 p.13)

WIND INTERACTIONS

WR!

$\boxed{\text{intra!}}$

Clumps $\Rightarrow$ manifestation of supersonic compressible turbulence.

$\downarrow$

dust formation is some WC winds?

(probably need extra compression of binary wind-wind collisions? $\rightarrow$ later)

St-Louis et al.
1987 ApJ 322, 870

HD 97152

WC7 + O5-7
P = 7.886 d

fit λ, 2λ

$\sigma_Q(O-C) = .016\ \%$

$\sigma_U(O-C) = .020\ \%$

$\sigma_{inst} = .015\ \%$

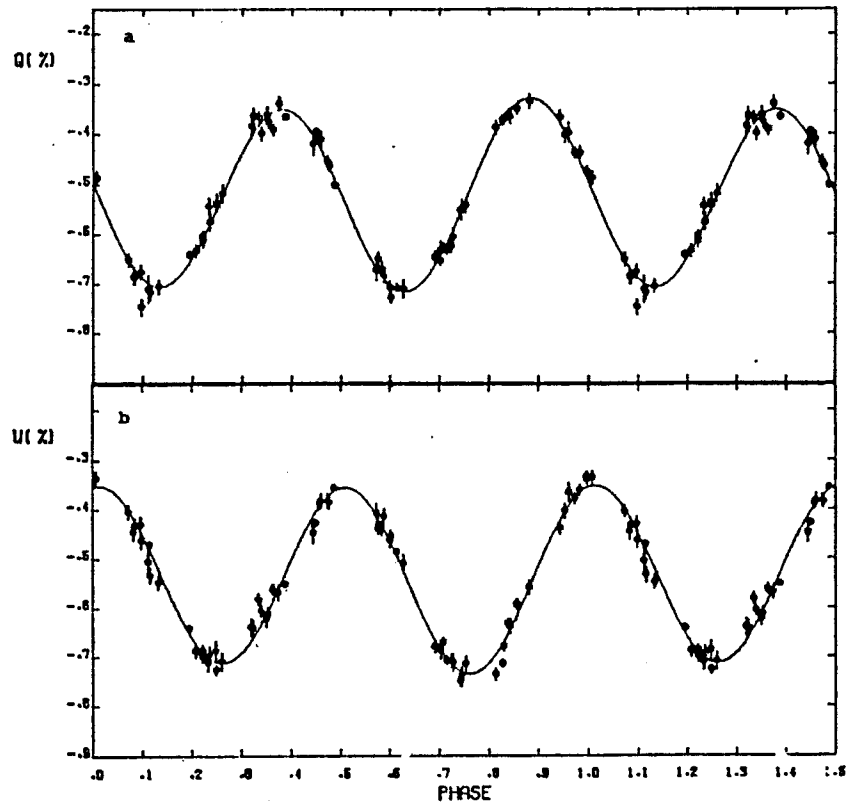

$i = 43.5^\circ \pm 5^\circ$

$$M_{WR} = \frac{3.6 \pm 0.3\ M_\odot}{\sin^3 i} = \underline{\underline{11}} \pm 3\ M_\odot$$

$$M_O = \frac{6.1 \pm 0.5\ M_\odot}{\sin^3 i} = \underline{\underline{18}} \pm 5\ M_\odot$$

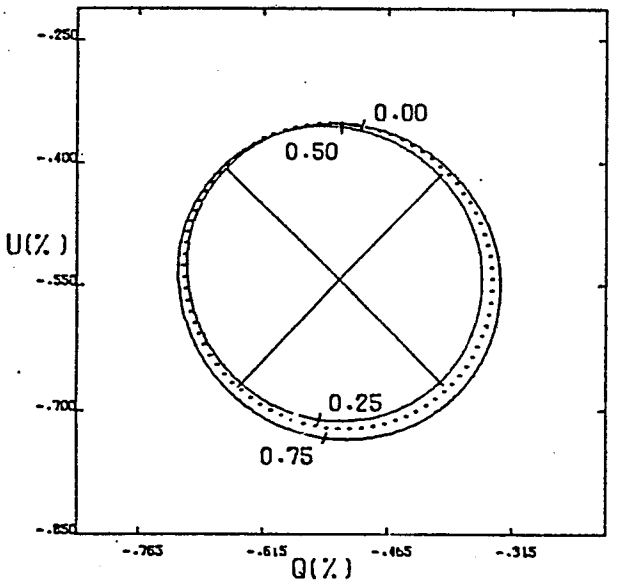

WR

HD 156385 WC7

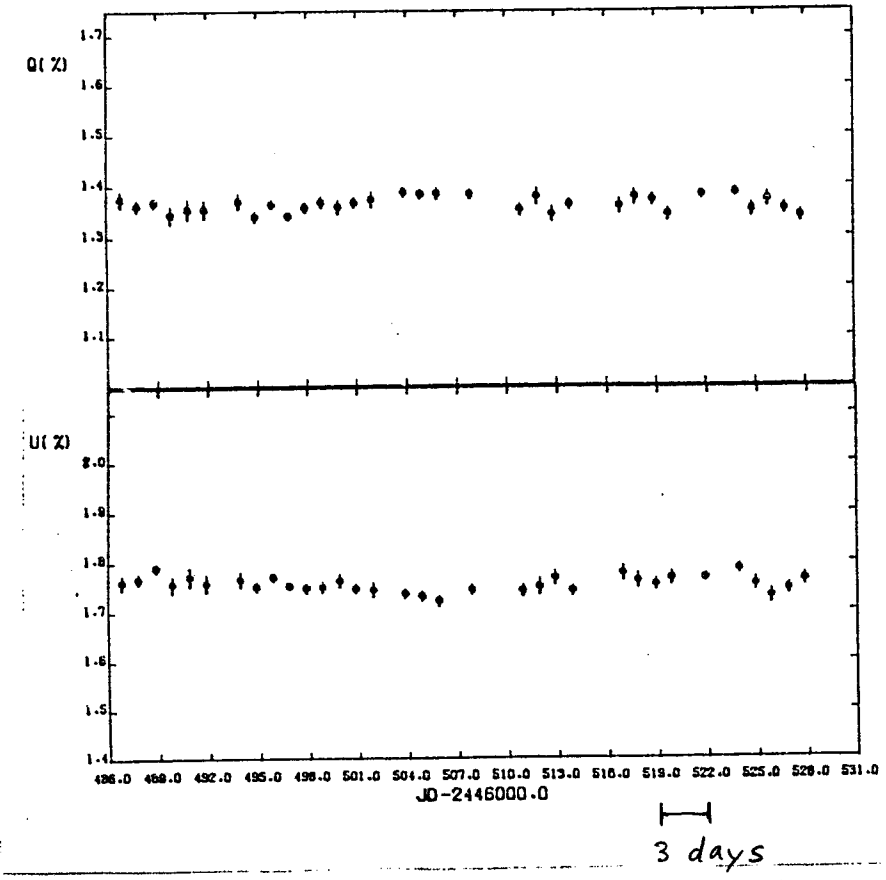

$\sigma_p(\text{inst}) \approx .015\ \%$

NB: even more constant than some polarized standards!

WR 111

HD 165763 WC5 $\sigma_p = 0.020$

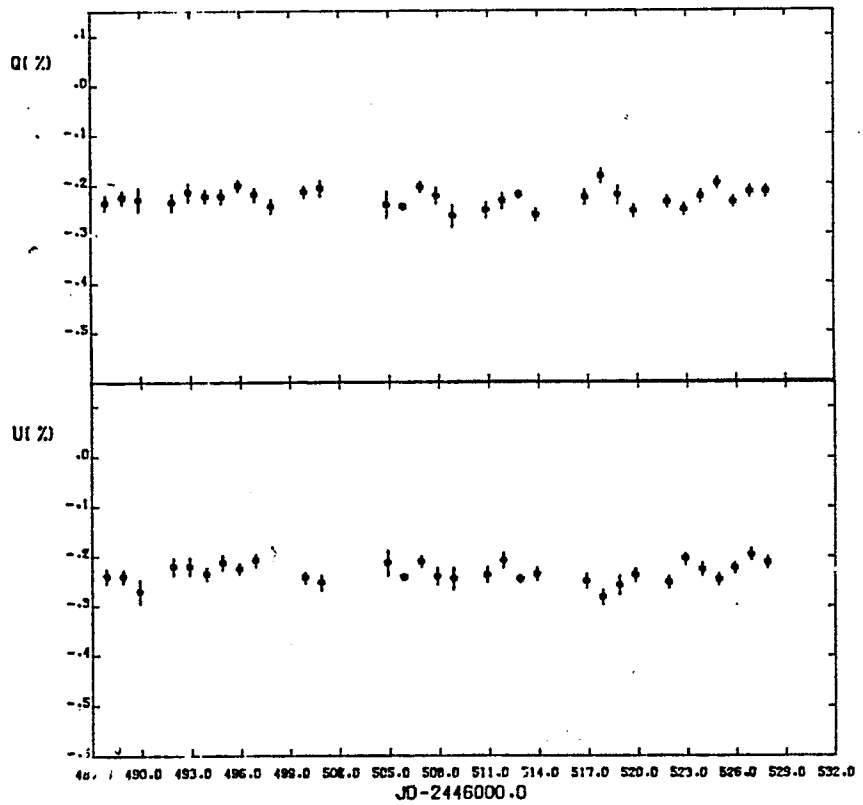

St-Louis et al. (1987)

WR 40

HD 96548

WN8

$\sigma_p = 0.155\ \%$

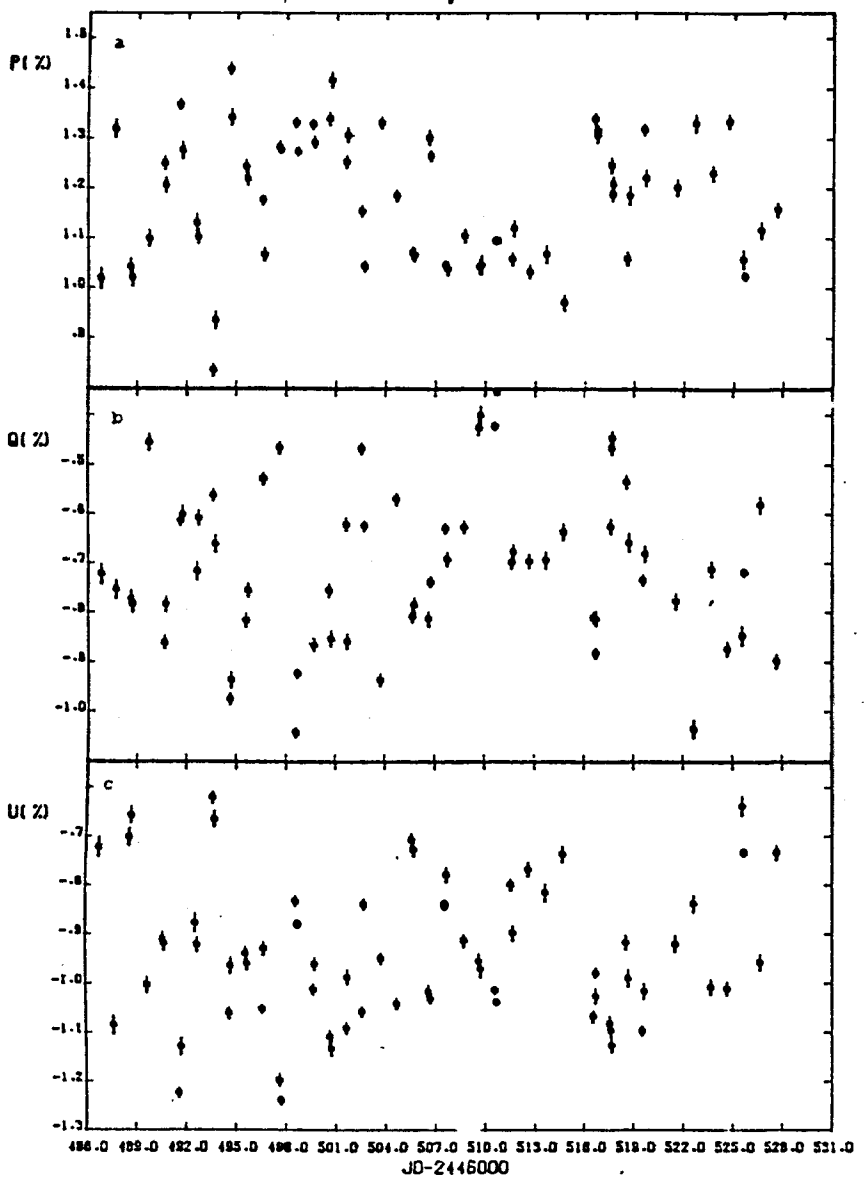

WR 40

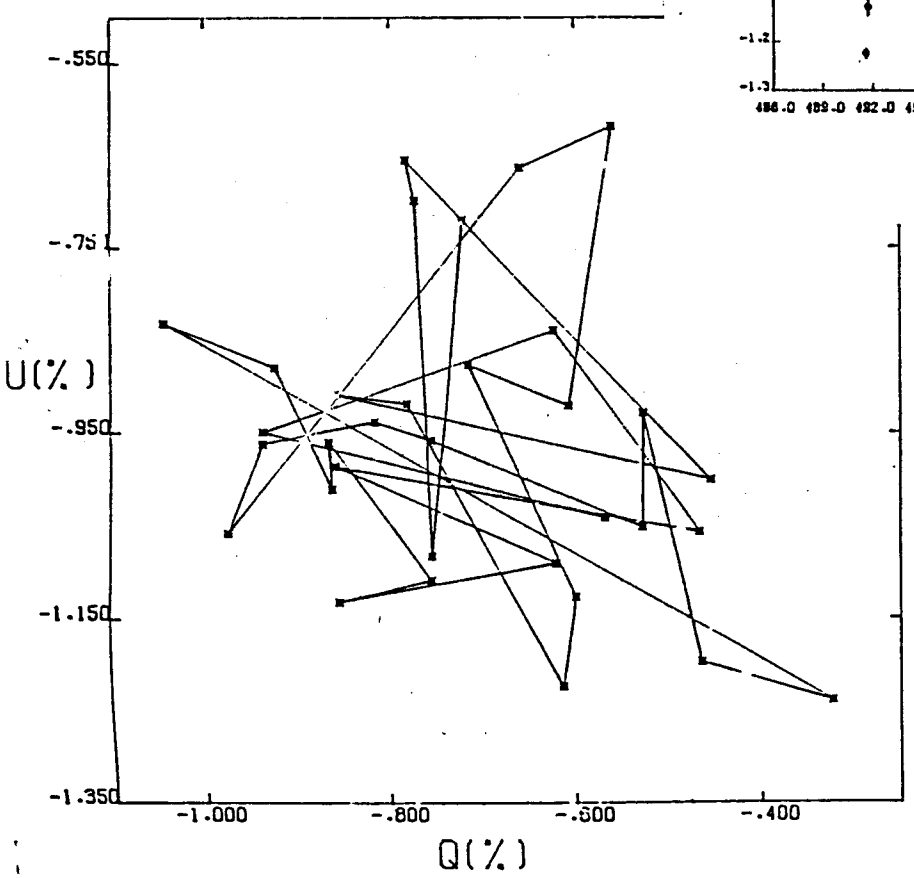

Drissen et al. (1987).

~like P Cyg (Hayes 1985) except time scale

WR 135

WC 8

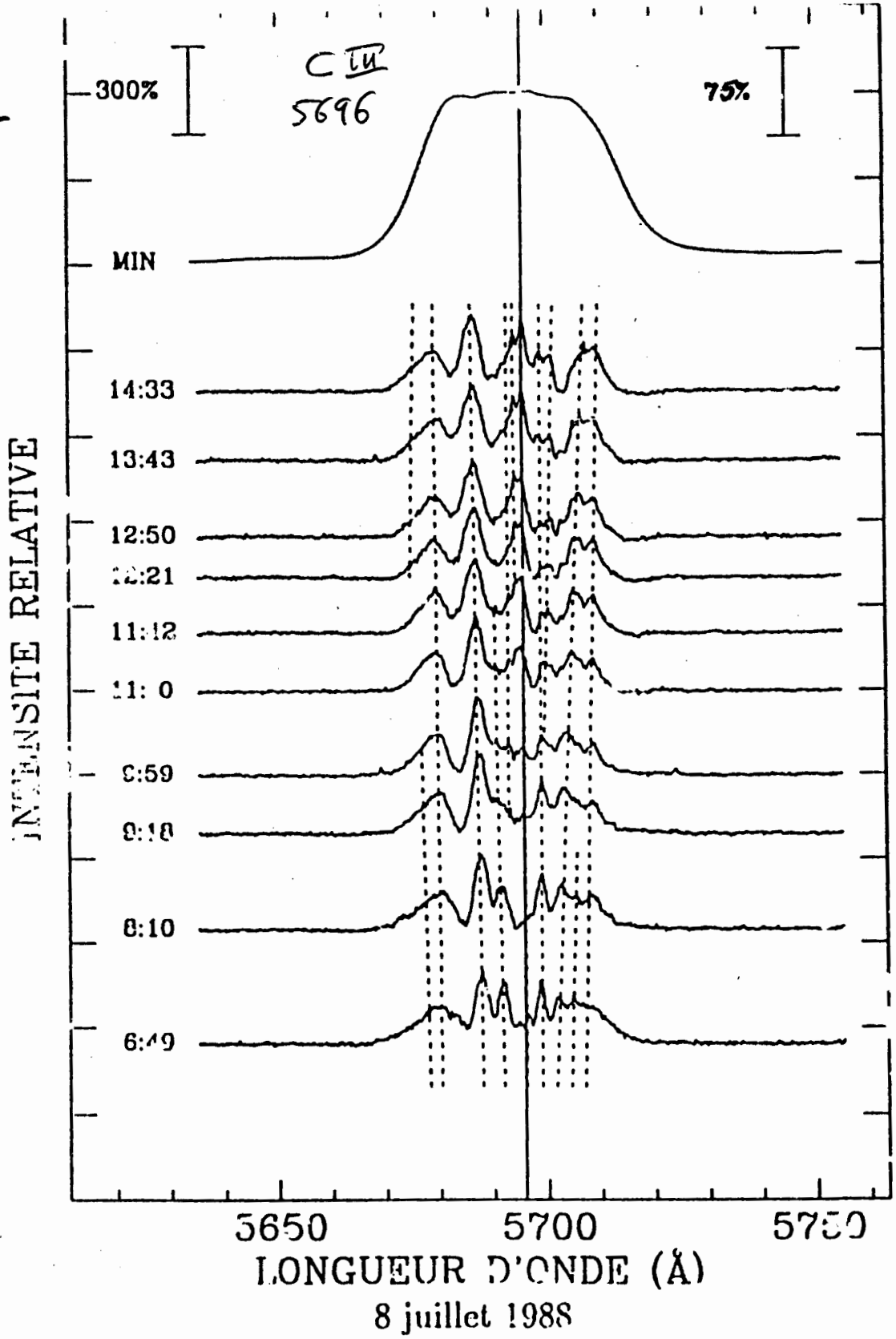

Fig. 1 Typical difference spectra (individual minus the smoothed minimum from four CFHT nights) as a function of UT for the WC8 star WR135 = HD192103. The difference spectra are blown up compared to the minimum by a factor 300/75 = 4. Dashed lines trace detected subpeaks from one spectrum to another.

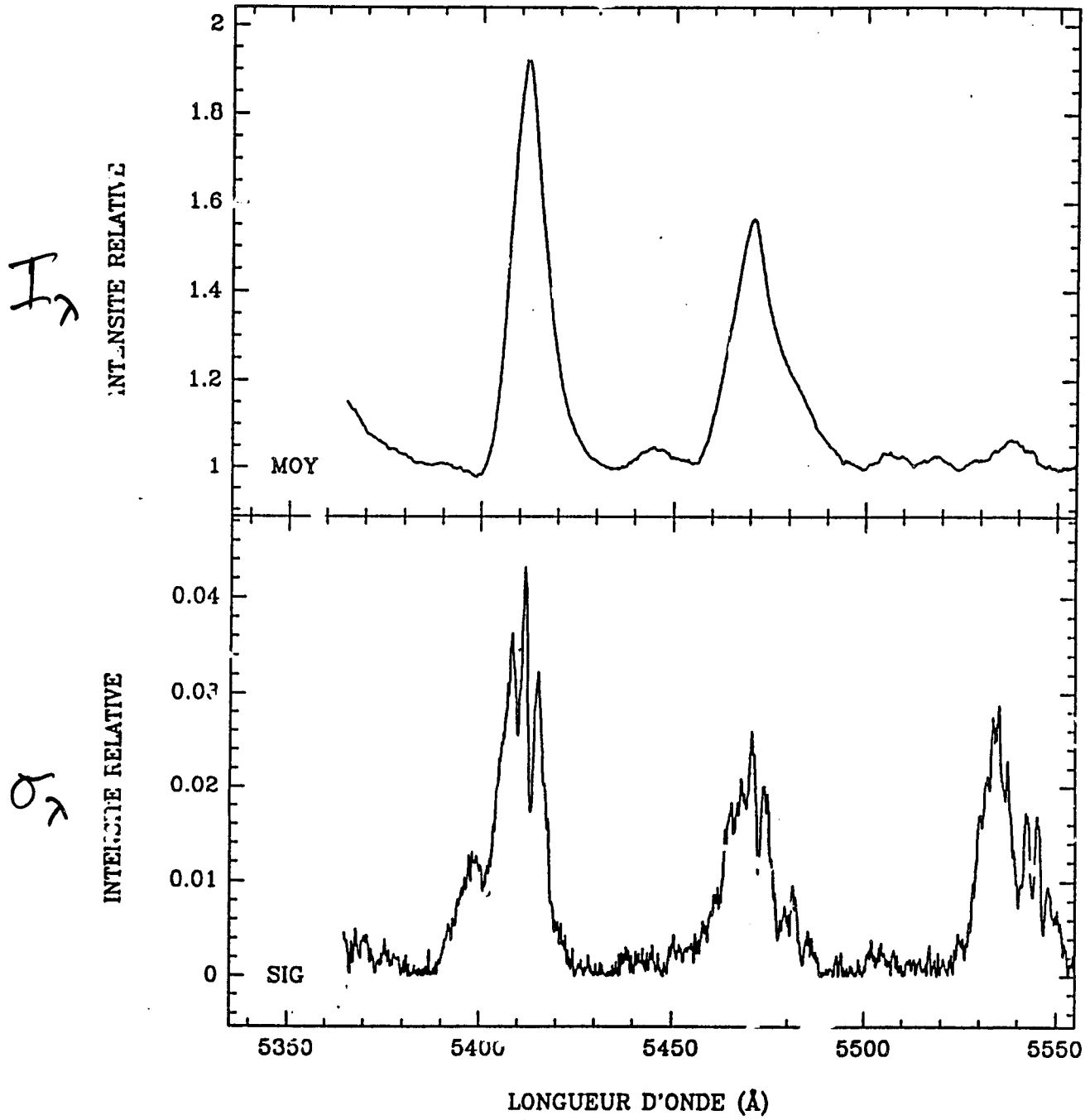

FIGURE 23e) WR103, HeII 5412 et CIV 5471.

WC9

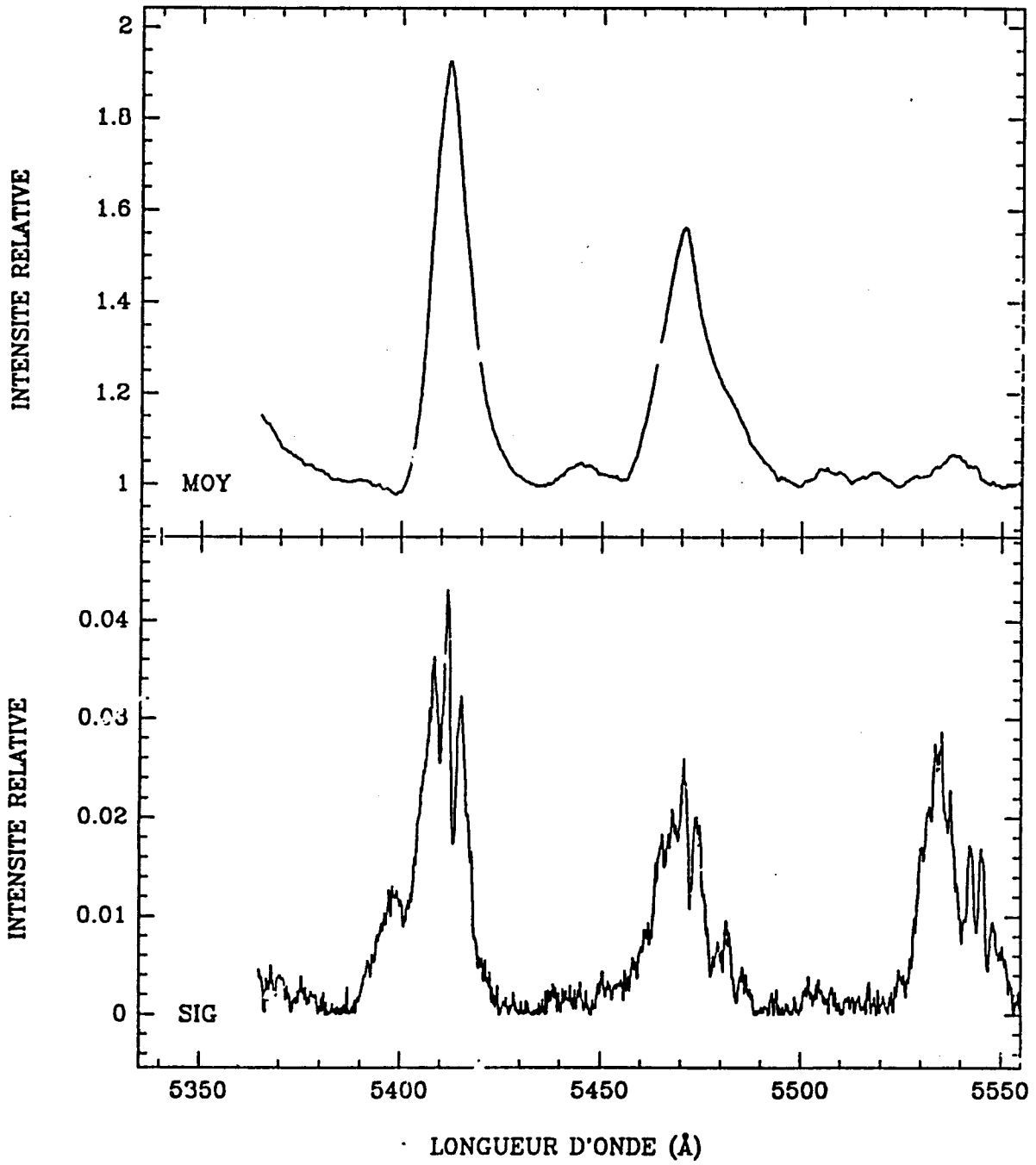

FIGURE 23e) WR103, HeI. 5412 et CIV 5471.

Lépine, Moffat, Henriksen
(1996, ApJ

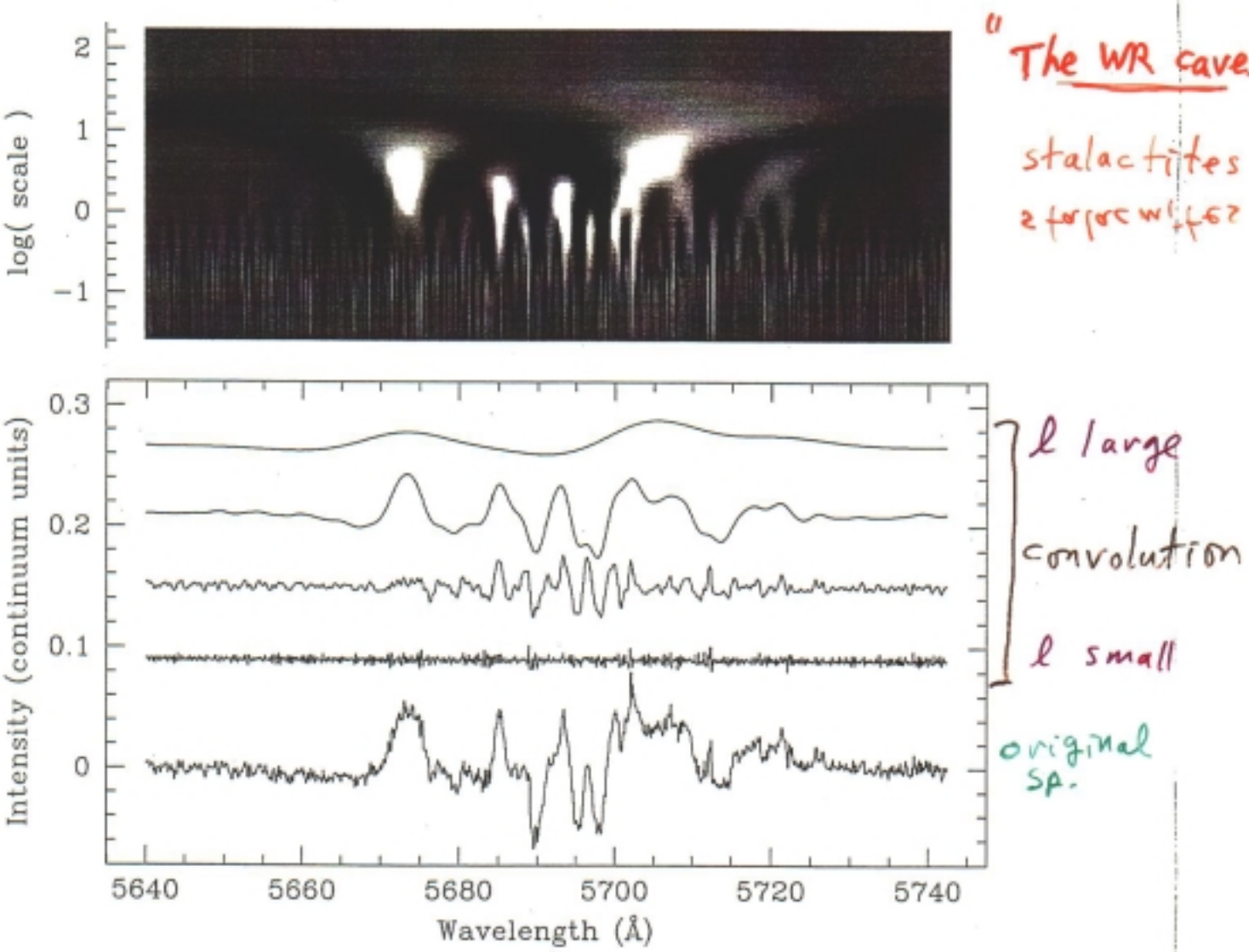

Fig. 1.— The top section shows the wavelet transform of a difference spectrum of the star WR137. The bottom section shows the same difference spectrum (bottom curve) decomposed into different scale components by using wavelet filtering. Upwards from the bottom curve are integrations of the wavelet transform over scale intervals (in Å) [a1,a2] = [0.02,0.13], [0.13,0.8], [0.8,5.0], and [5.0,32.0], respectively.

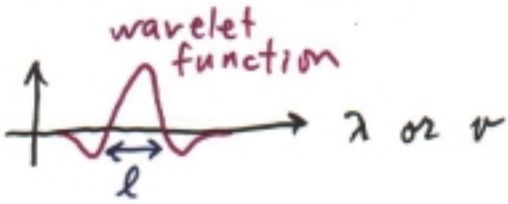

Convolution:

$$\frac{1}{\ell}(\text{wavelet}) \otimes [I(\lambda) - \bar{I}(\lambda)]$$

All structures detected on CIII 5696 Å line

WR 135, WC8

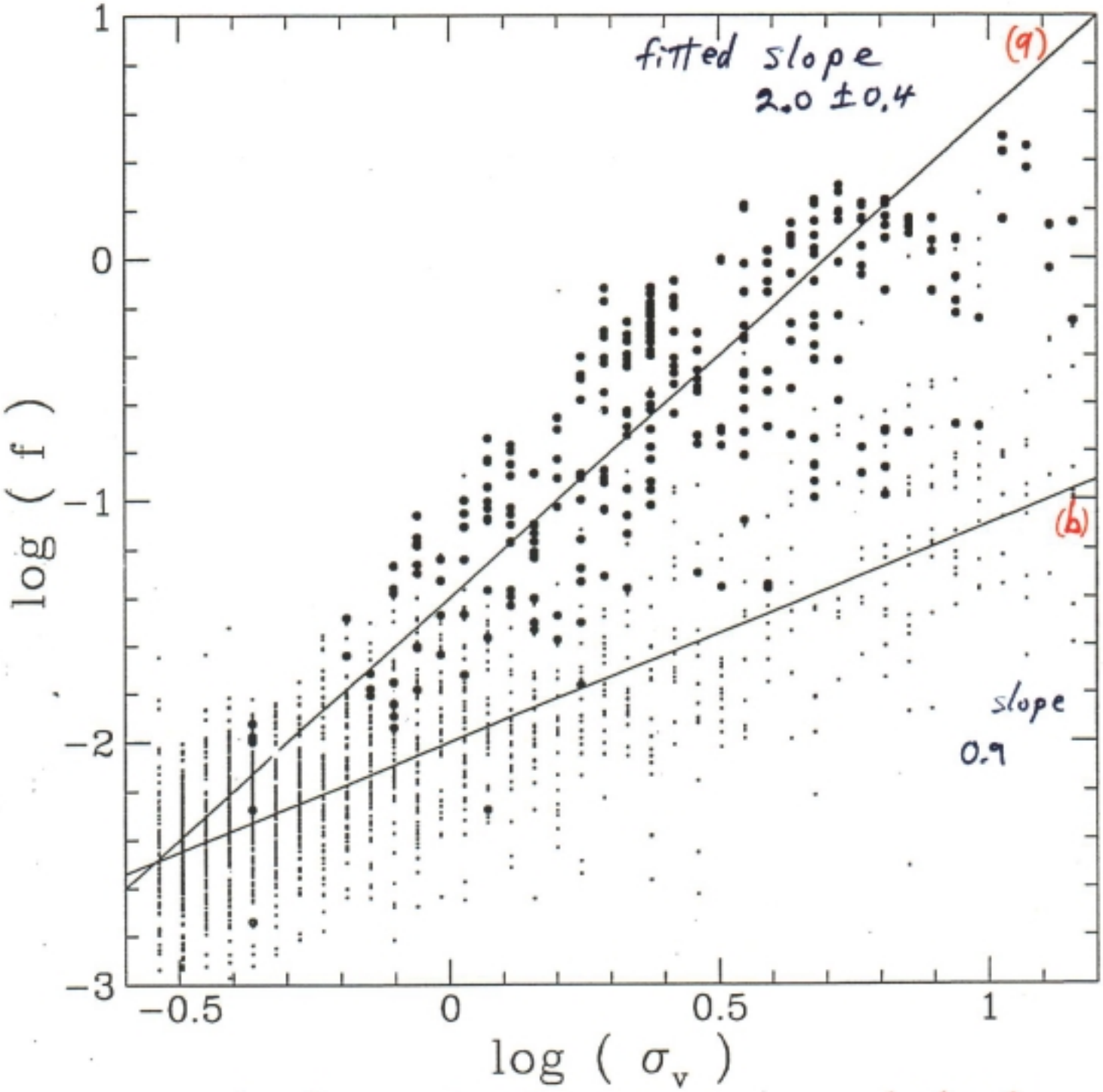

(a) intrinsic to star: appear on at least two successive spectra

(b) rest = noise

Log N vs. log f

intrinsic structures

C III 5696

WR 135, WC8

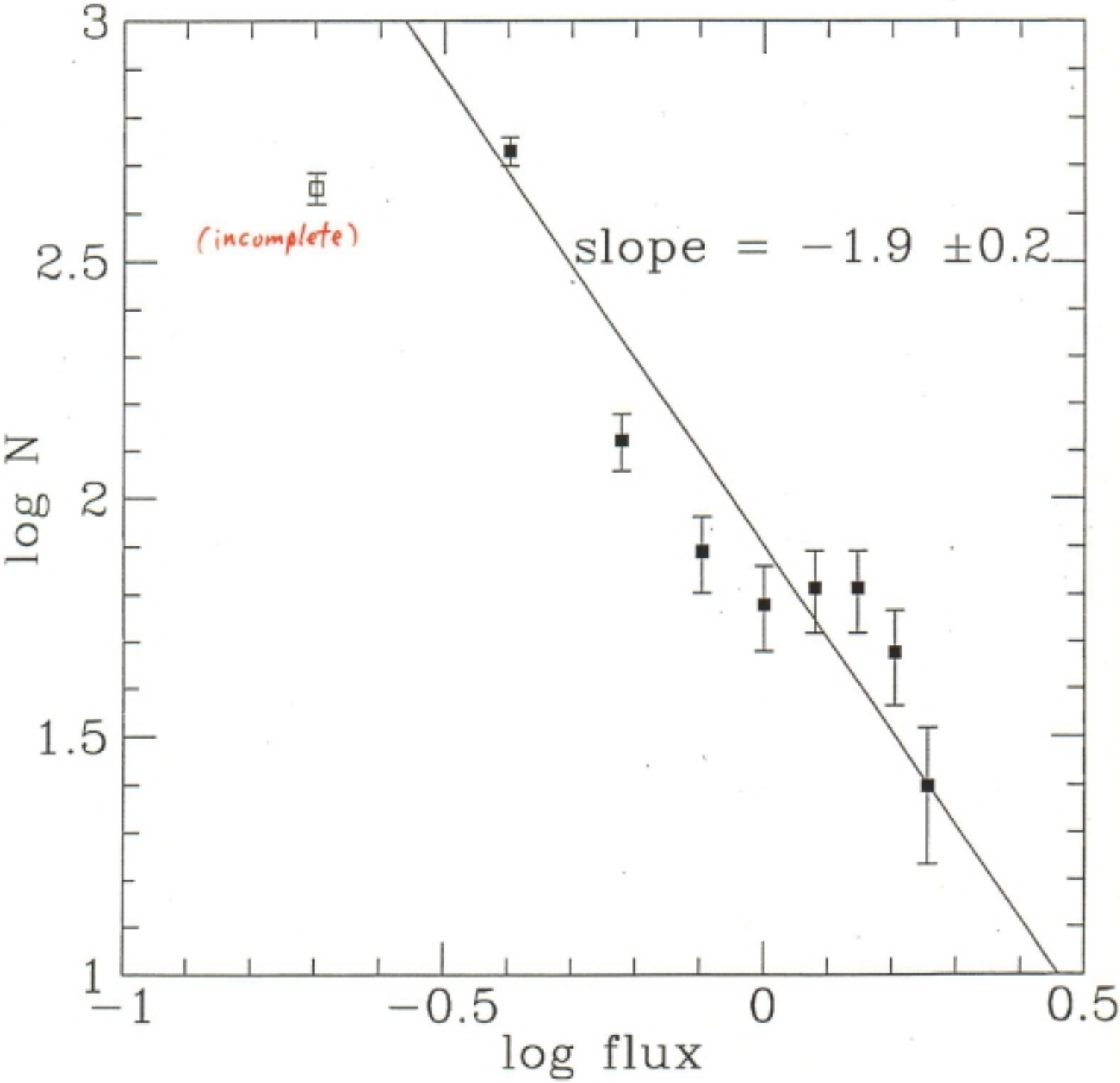

cf. WR 140, WC7 : slope = −2.2 ± 0.2

C III 5696

Scaling laws

Supersonic compressible turbulence (Larson)

(eg Henriksen 1990)

$$\left.\begin{aligned} \tau &\equiv \frac{\ell}{\sigma_v} \approx \frac{1}{\sqrt{G\rho}} \\ p &\equiv \rho \sigma_v^2 \approx \text{const.} \end{aligned}\right\} \quad \begin{aligned} \rho &\sim 1/\ell \\ \sigma_v &\sim \ell^{1/2} \end{aligned}$$

Hot stellar winds : observe f, σ_v

$$f \sim \rho^2 \ell^3 \quad (T \sim \text{const.})$$

$$\sim \ell \sim \sigma_v^2 \quad (\sim \text{as observed})$$

Mass spectrum

$$n(m)\, dm = N(f)\, df \sim f^{\alpha}\, df$$

$\therefore$ with $m \sim \rho \ell^3$

+ above $\Rightarrow$

$$m \sim \ell^2 \sim f^2$$

$$\Rightarrow n(m) \sim m^{\frac{\alpha-1}{2}}$$

$$\alpha \sim -2 \Rightarrow \frac{\alpha-1}{2} = -1.5$$

~ like GMC's

Falgarone, Phillips & Walker (1991, ApJ, 378, 186)

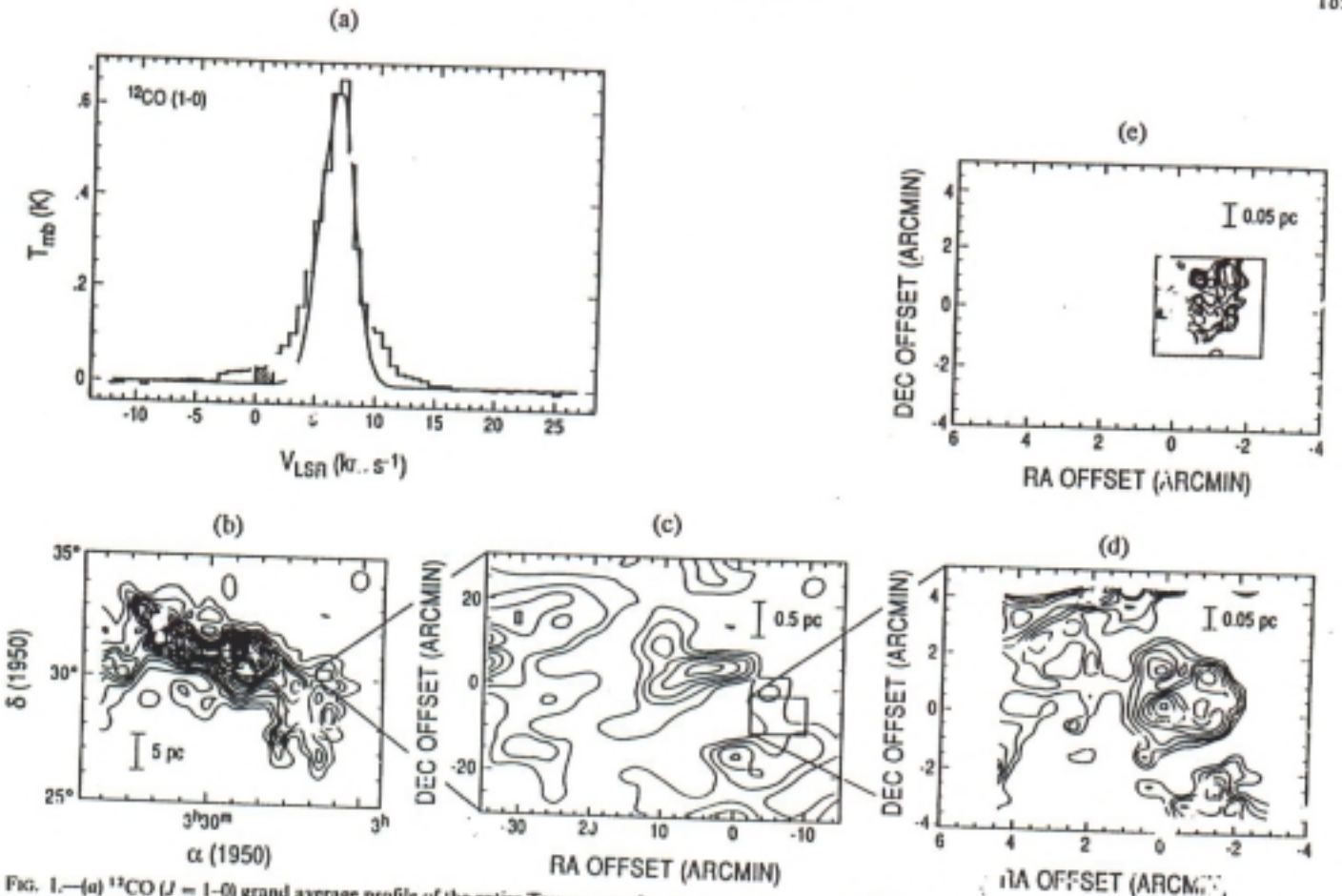

FIG. 1.—(a) ^{12}CO (J = 1–0) grand average profile of the entire Taurus complex mapped by Ungerechts & Thaddeus (1987). The velocity range of the small fields observed at high frequency and resolution is the hatched interval. (b) The field studied at high angular resolution, located on the appropriate fragment of the Ungerechts & Thaddeus velocity-integrated intensity map. First contour 0.5 K km s^{-1}, step 1.5 K km s^{-1}. (c) Velocity-integrated intensity of the ^{12}CO (J = 2–1) emission (CSO, HPBW = 30", sampling 5'). First contour, 2 K km s^{-1}, step 2 K km s^{-1}. The small boxes delineate the two areas (Taurus 1 and Taurus 2; see Tables 1 and 2) which have been observed with a sampling spacing of 30". Offsets are relative to the position α(1950) = 3^{h}07^{m}27^s.4, δ(1950) = 30°05'. (d) Velocity-integrated intensity of the ^{12}CO (J = 2–1) emission (CSO, HPBW = 30", sampling 30") within Taurus 1. First contour 1.8 km s^{-1}, step 0.3 K km s^{-1}. Offsets are relative to the position α(1950) = 3^{h}06^{m}54^s.9, δ(1950) = 29°58'. (e) Velocity-integrated intensity of the ^{12}CO (J = 3–2) emission (CSO, HPBW = 2'.2, sampling 18"). First contour 0.85 K km s^{-1}, step 0.2 K km s^{-1}. The origin is the same as in the previous map. The linear scales are computed for a distance to the cloud d = 200 pc.

J. Stutzki (1993 Rev. Mod. Astro. 6)

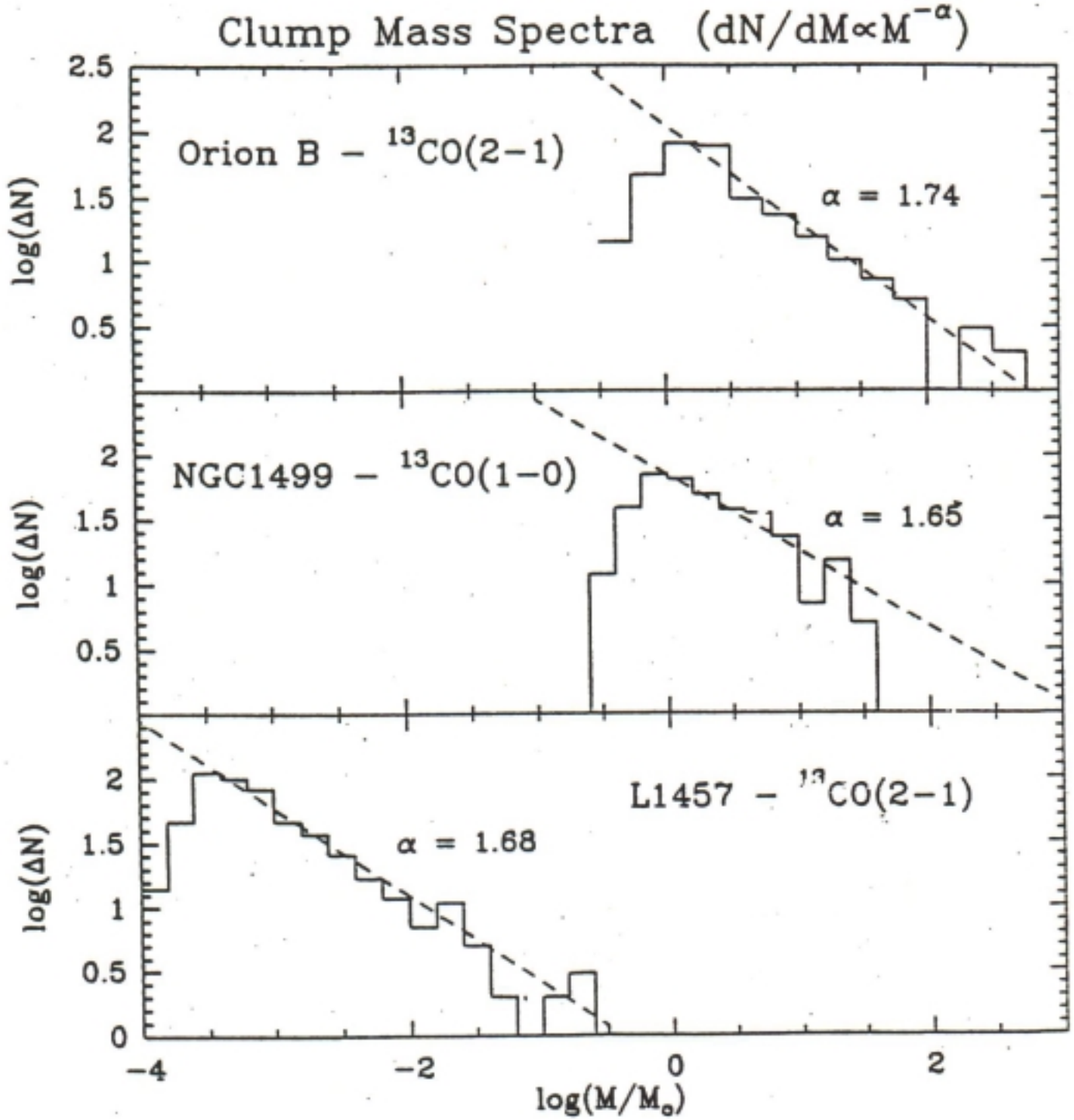

.... despite diff. range of physical conditions, sizes, masses covered, mass spectra follow the same power law.

ζ Pup O4 I(n) f

Eversberg, Lépine + Moffat (1998)

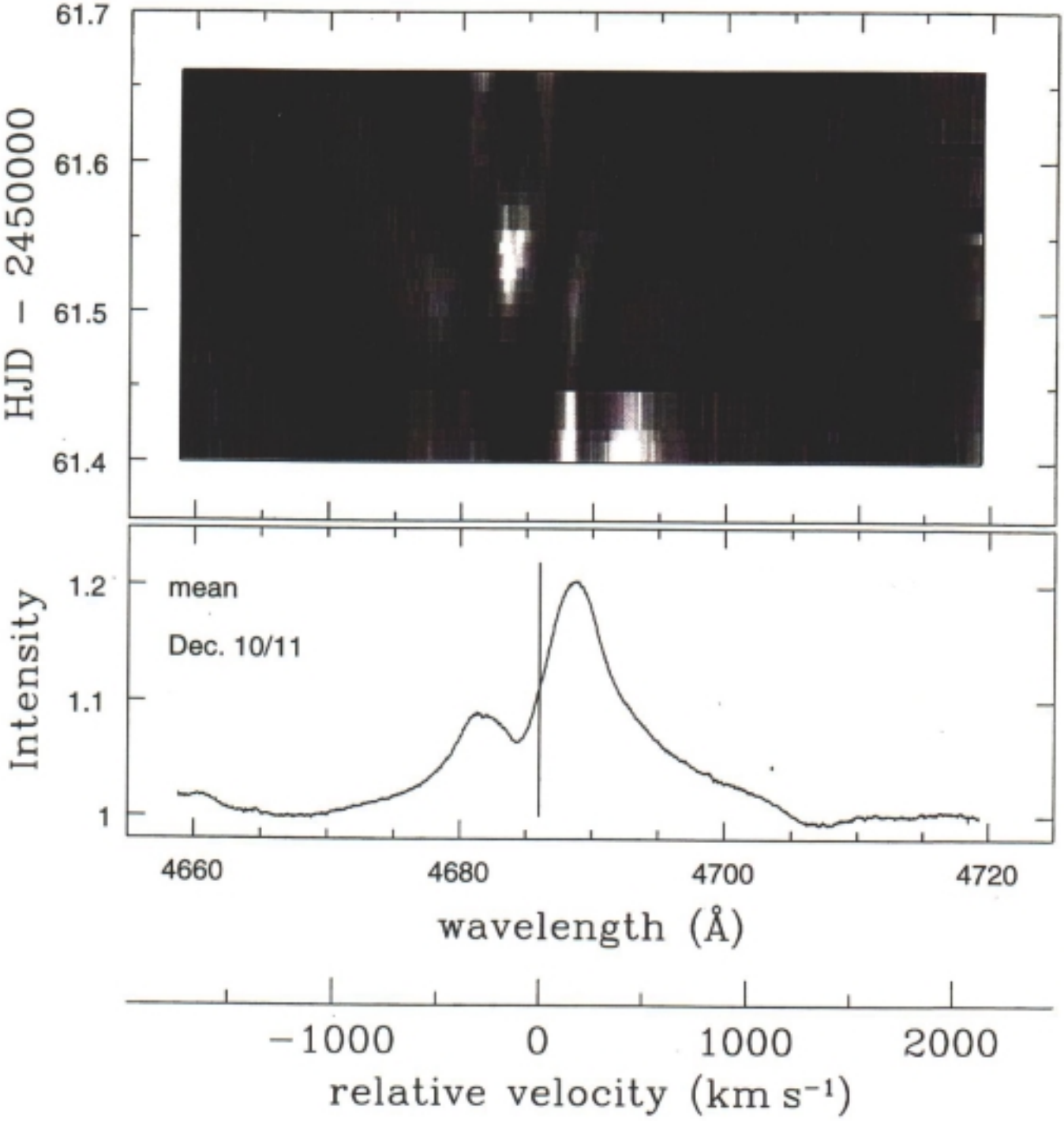

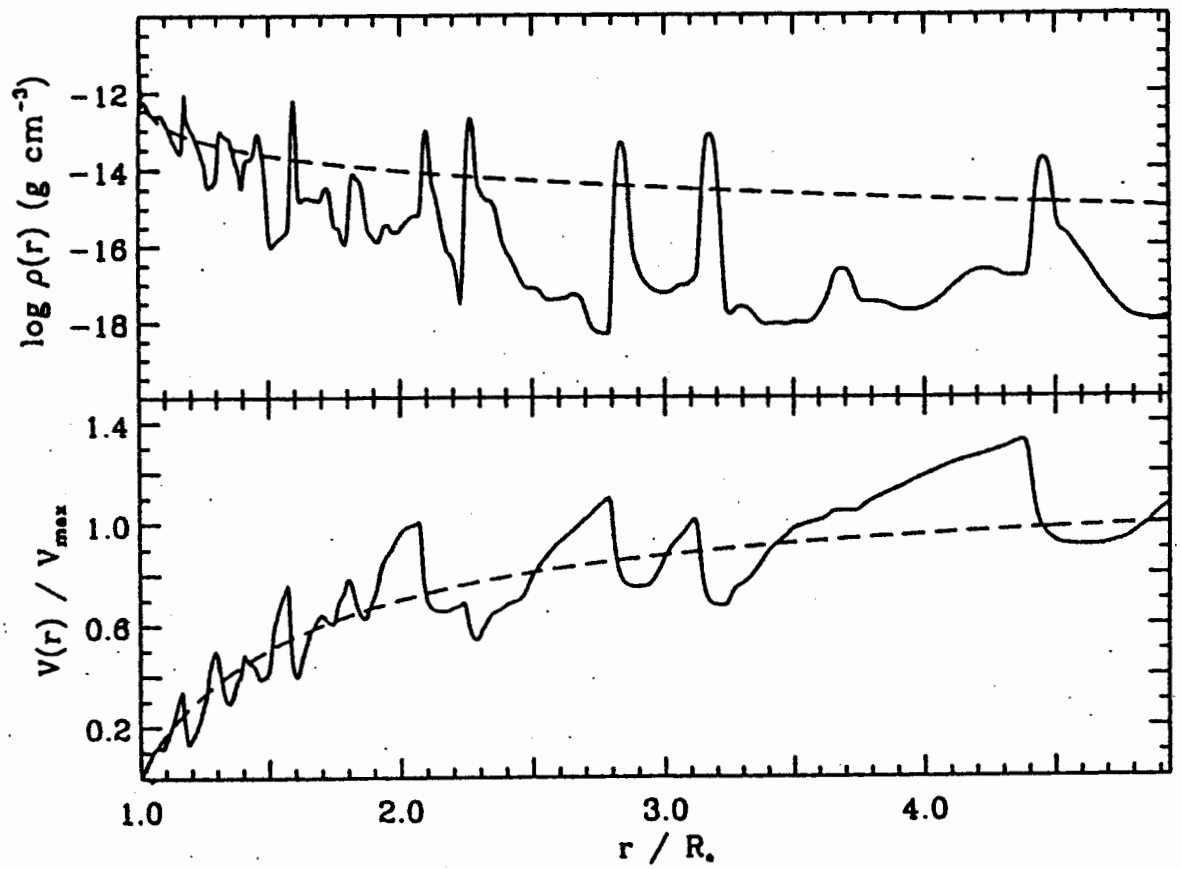

Figure 12: Density and velocity vs. radius in a dynamical structured wind at a fixed snapshot (for details, see text). (From Puls and Owocki, 1993.)

WIND INTERACTIONS

+ CSM / ISM

ISM (HI)

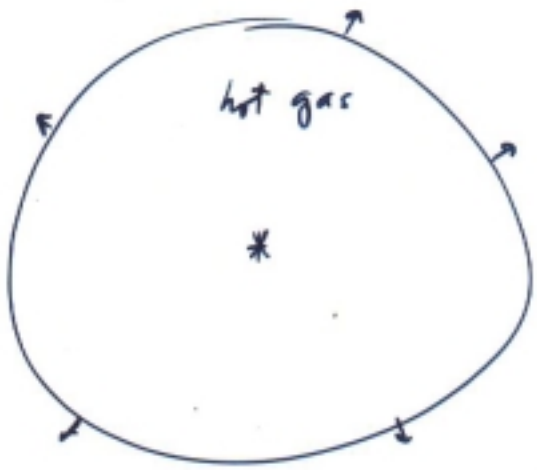

(1) O-star → fast wind

ϕ → ~100 pc

wind-blown bubbles common

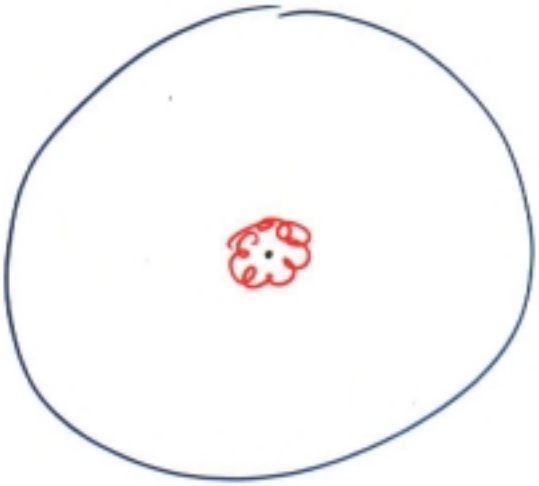

(2) LBV / RSG → slow, dense wind

ϕ → ~1 pc

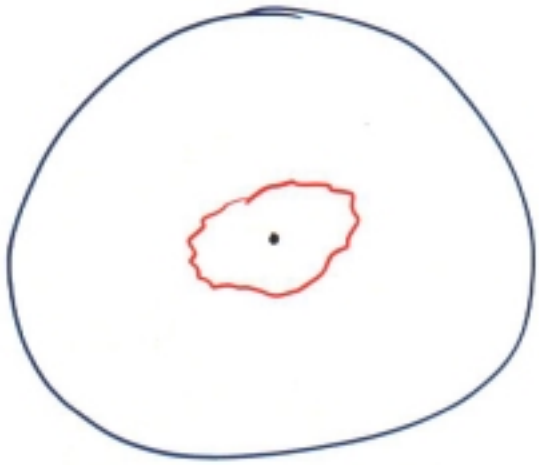

(3) WR → fast wind

ϕ → sev. pc

ectra were
ed by using
ration was

ise ratio of
rs to give a
t necessary
n s^{-1}) and to
f the slit in
resent data
ide a useful
the spatial
n 3.3 below.
correspond-
WHM=14–
duced data.
ements with

ne profiles of
m. Increasing
n in Plate 1. In
lit. It is worth
combine high
Fabry–Perot
rs, were taken
of the present

complex, with
we have fitted

RCW 58

WR ring nebula

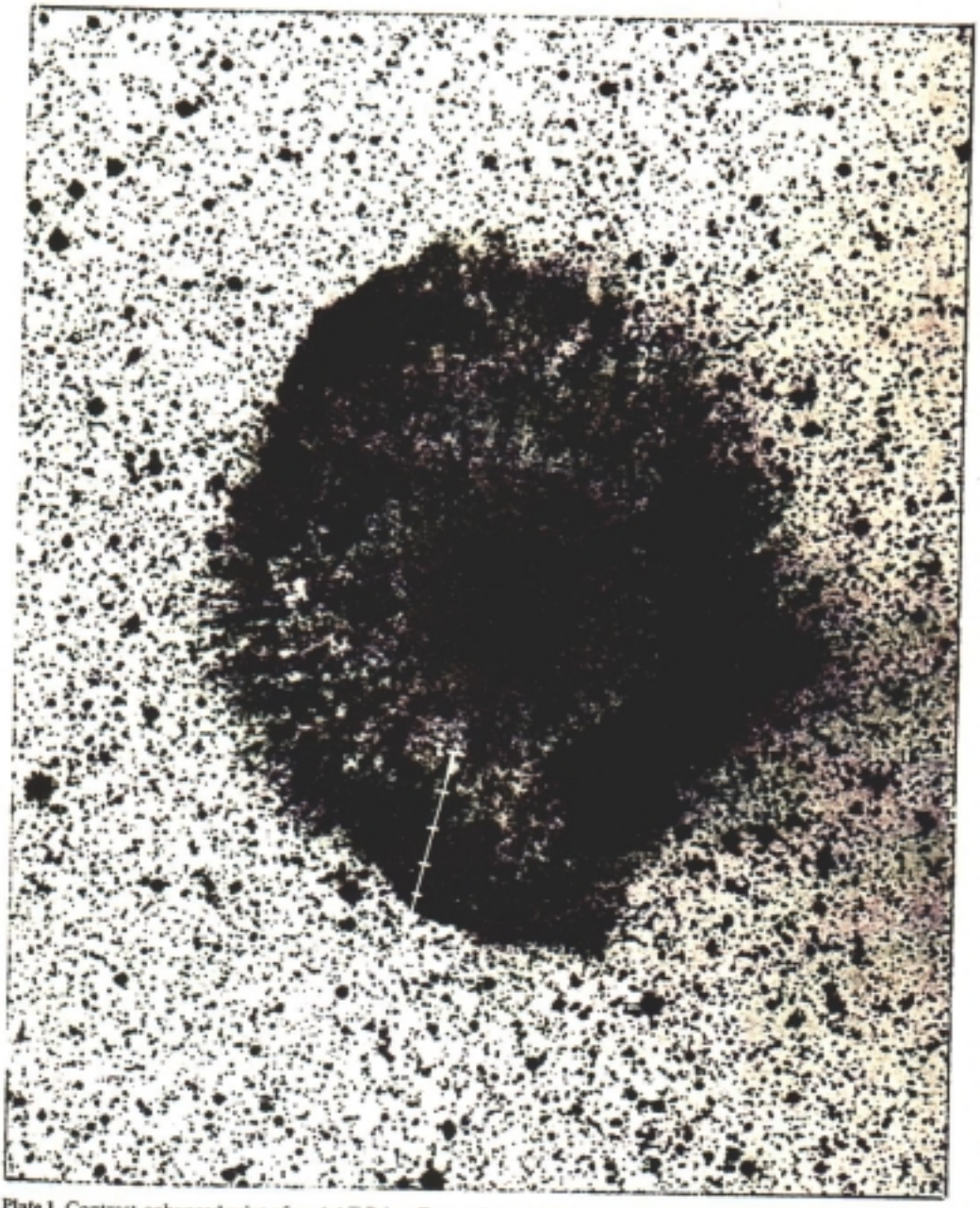

Plate 1. Contrast-enhanced print of an AAT Prime Focus plate of RCW 58, obtained on Kodak IIIa-F emulsion with RG 630 filter giving a passband from ~6300 to ~7000 Å. The exposure time was 80 min., the seeing ~2 arcsec FWHM. North is to the top and east to the left; the scale is shown by the 2 arcmin long bar at the bottom left-hand corner. Also indicated is the position of the spectrograph slit used to acquire the data presented in this paper. The slit is 2.9 arcmin long, centred at 1950 coordinates RA=11^{h}04^{m}25^s.5 and Dec=−65°17′40″, with position angle Φ=167°. The numbers from 1 to 120 refer to spatial increments on the detector. (Photo kindly supplied by D. Malin, AAO.)

Central star
WR40, WN8

[facing page 628]

L.J. Smith, M. Pettini, J.E. Dyson, T.W. Hartquist
1988, MN 234, 625.

Grosdidier, Moffat, Joncas + Acker (1998, ApJ 506, L127)

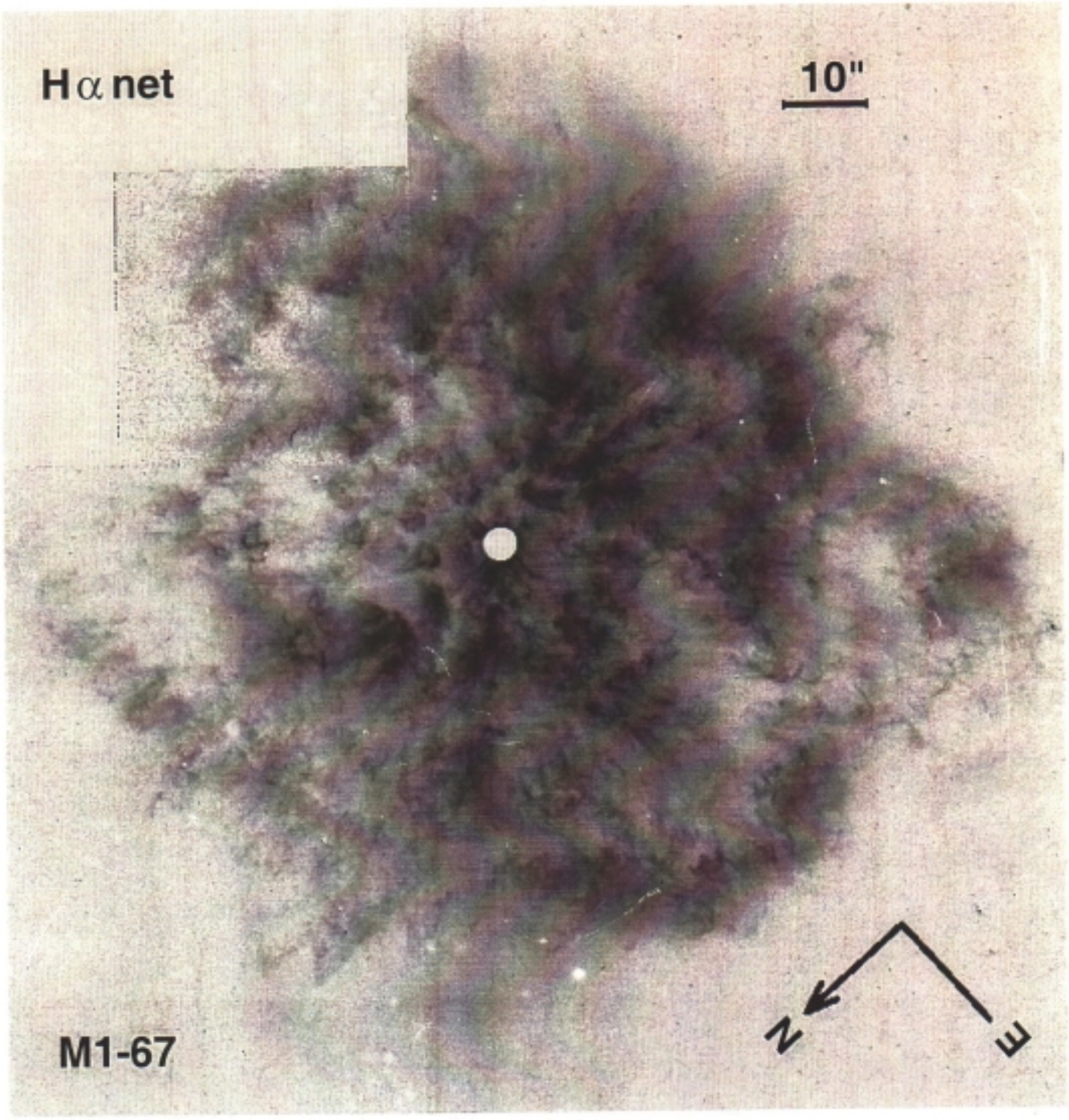

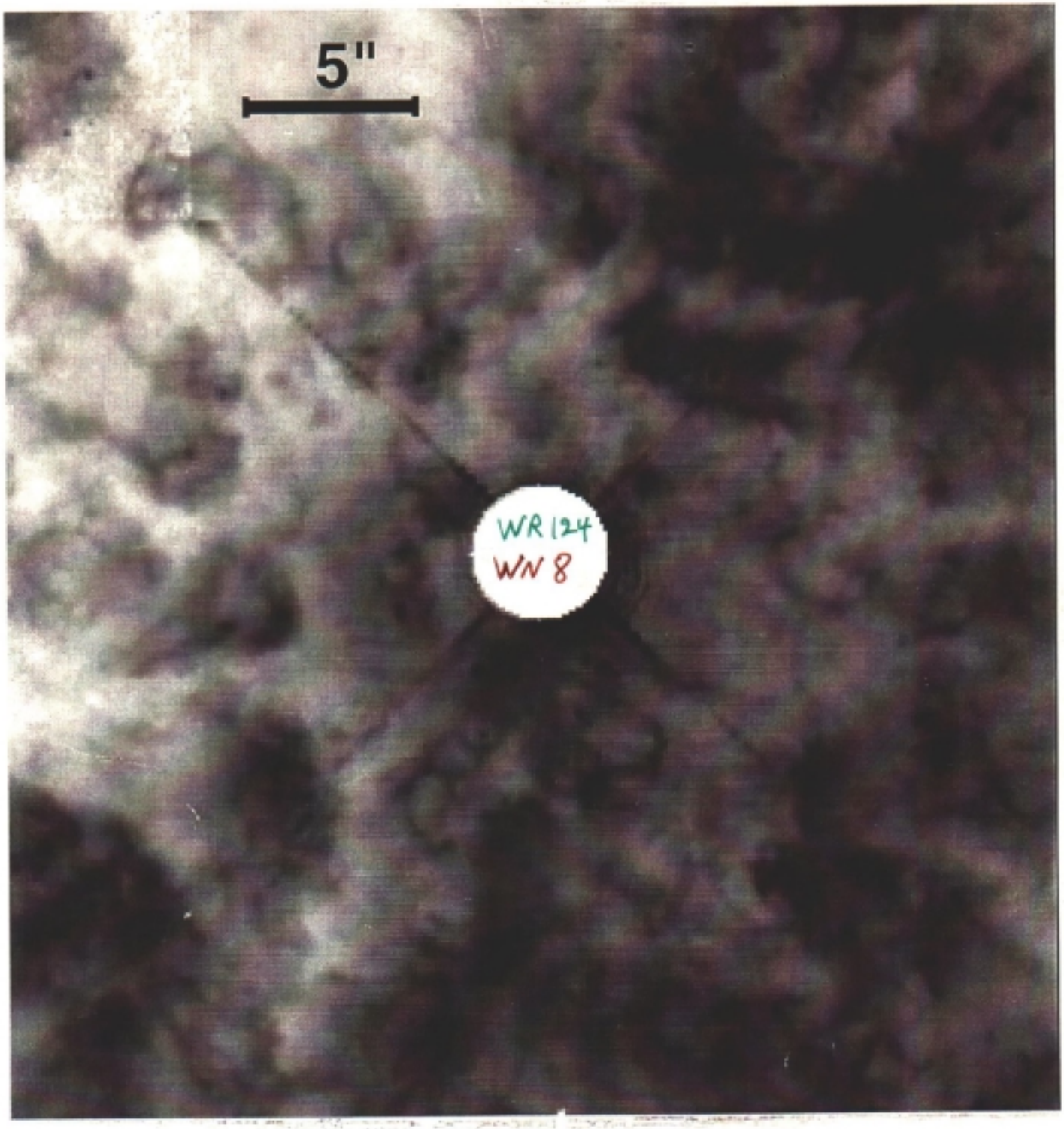
5"
WR 124
WN 8

Grosdidier et al. (1999)

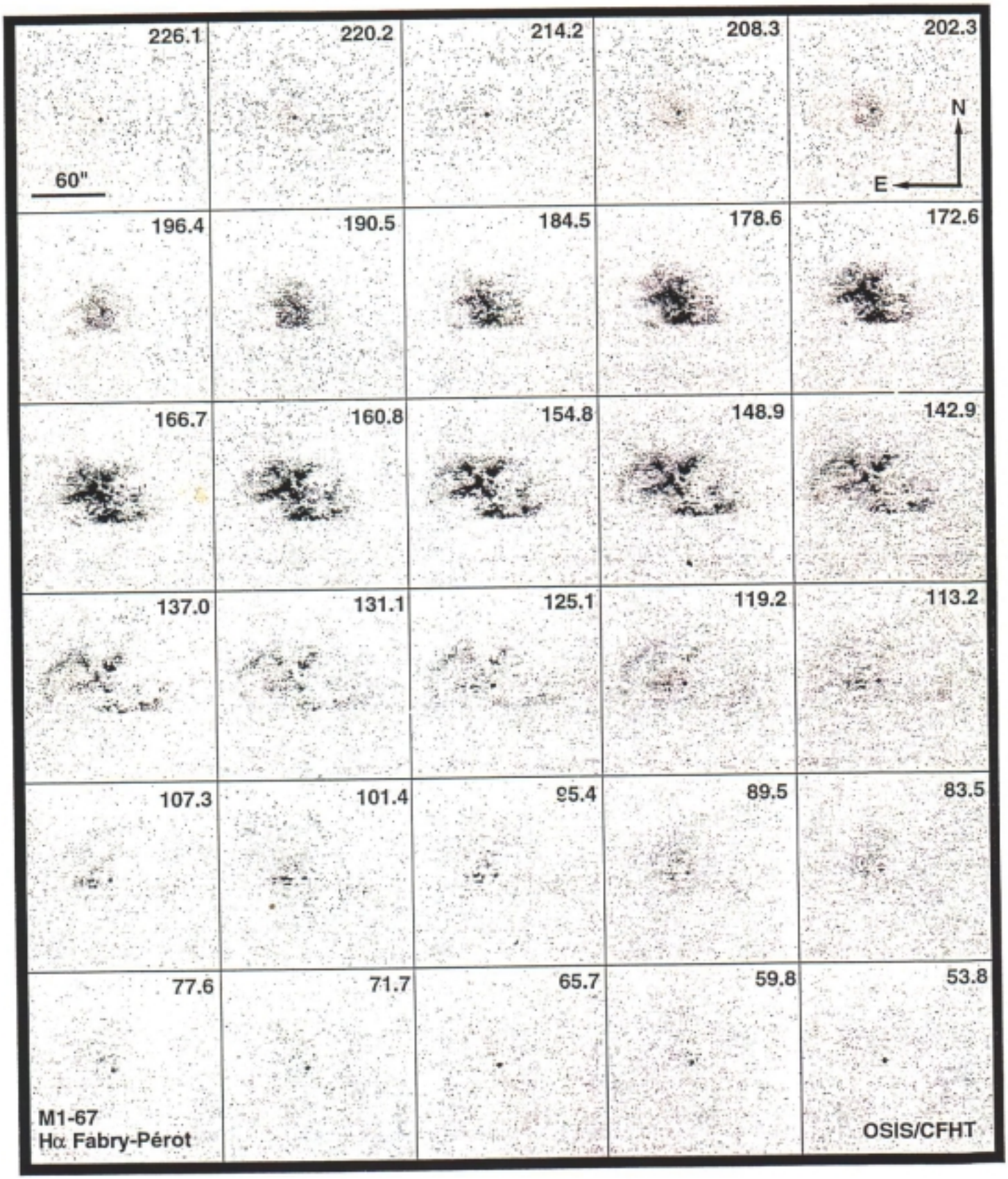

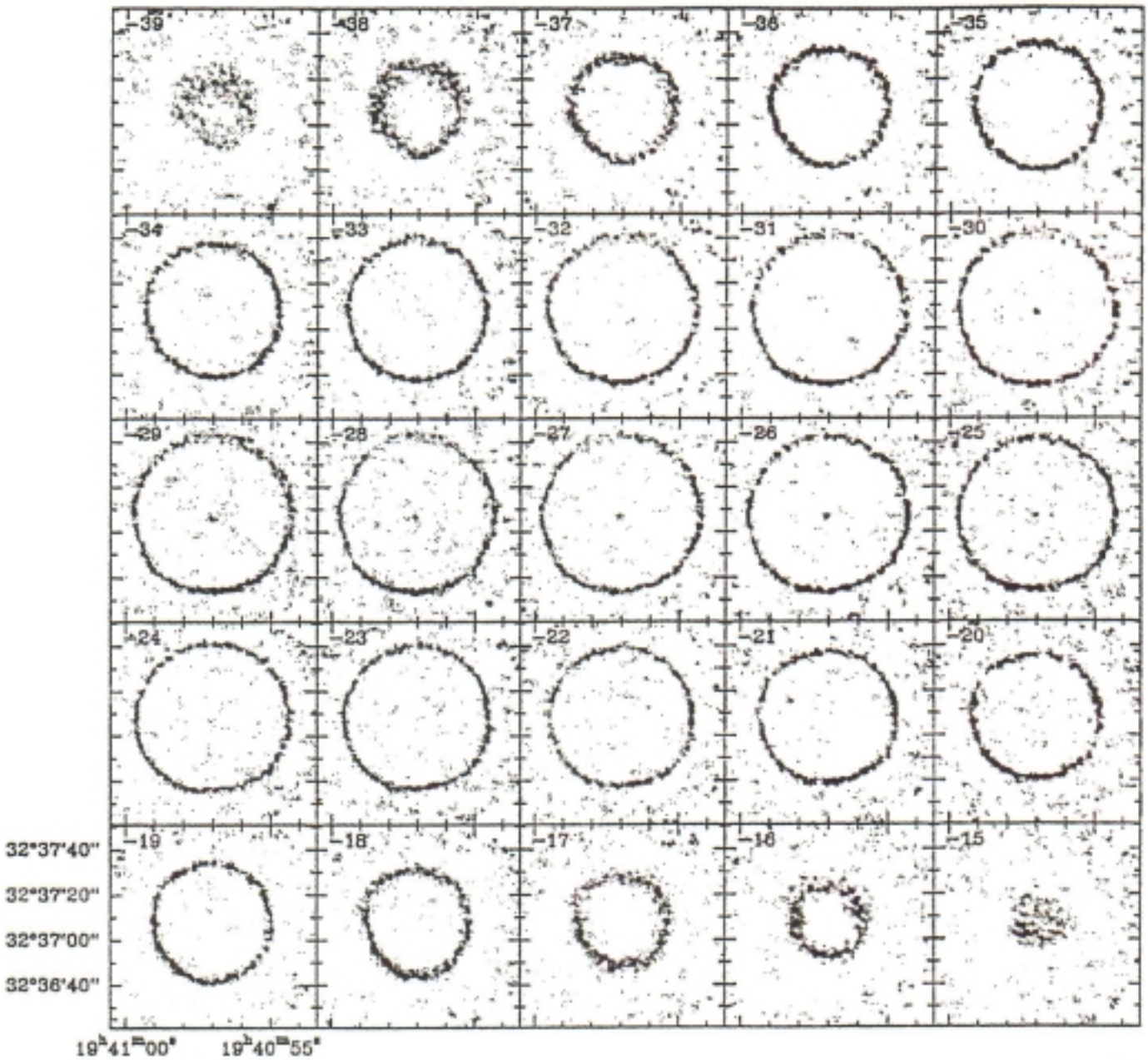

Figure 6. Molecules in a Circumstellar Envelope.
The carbon-rich envelope ejected by the star TT Cygni, mapped in CO(1–0) with the IRAM interferometer with a 3″ beam. The maps show velocity channels, indicated by the labels in the upper left of each box, in $\mathrm{km\,s^{-1}}$. (Lucas & Guélin 1998; Olofsson et al. 1998).

1996 A&A 305, 229

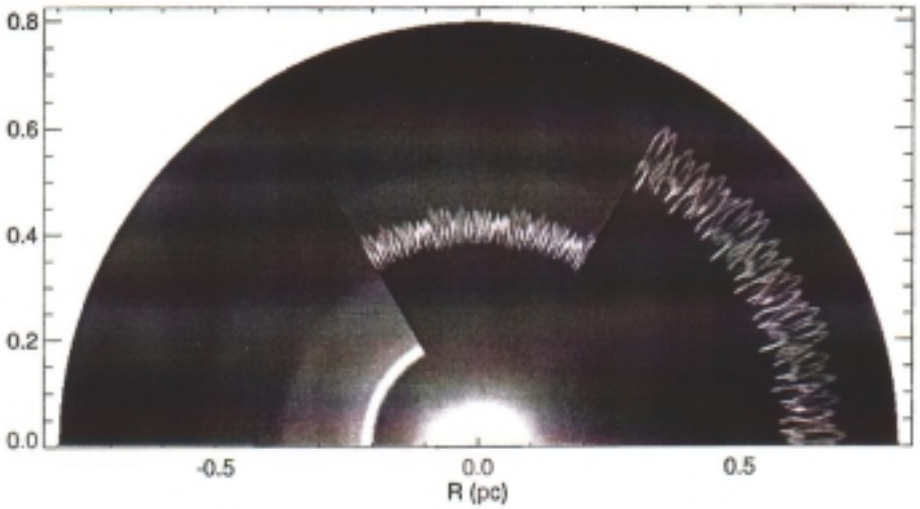

LBV stage

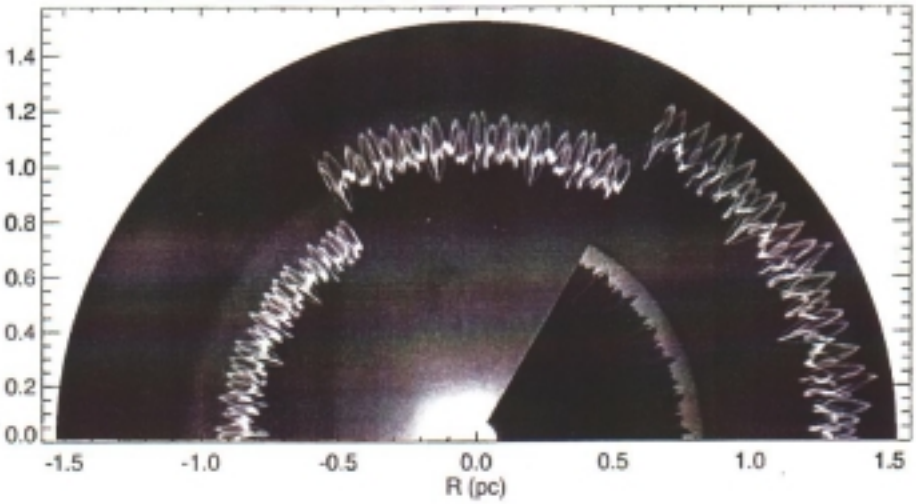

late LBV → transition to WR

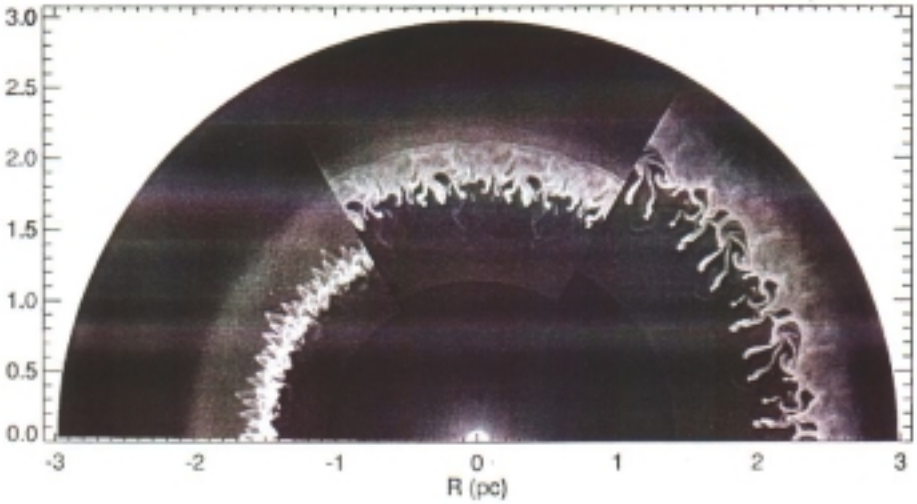

Fig. 10a–c. Logarithm of the circumstellar gas density (in g cm^{-3}) during the LBV and early WR phase, computed on a 3 pc grid with twice the numerical resolution of the run shown in Fig. 9. Note that each 60° slice is now composed of three identical 20° slices. The time difference between consecutive frames is 900 yr. The gray scale minima and maxima given correspond to the density extrema in each frame. Numerical resolution limits the density maxima, so they should be taken as lower limits. **a** During the LBV stage (t = 3.357 10^6 yr). The gray scale goes from max=-20.2 (white) to min=-23.2 (black). Only the inner 0.75 pc are shown. **b** The late LBV and transition to the WR stage (t = 3.3597 10^6 yr). The gray scale goes from max=-20.8 (white) to min=-24.3 (black). Only the inner 1.5 pc are shown. **c** The early WR stage (t = 3.3624 10^6 yr). The gray scale goes from max=-20.8 (white) to min=-26.3 (black)

early WR

WIND INTERACTIONS

binaries

- Non-thermal radio
- IR (dust)
- optical emission-line excess
- X-rays

White + Becker (1995 ApJ 451, 352)

WC7 + O4-5 I

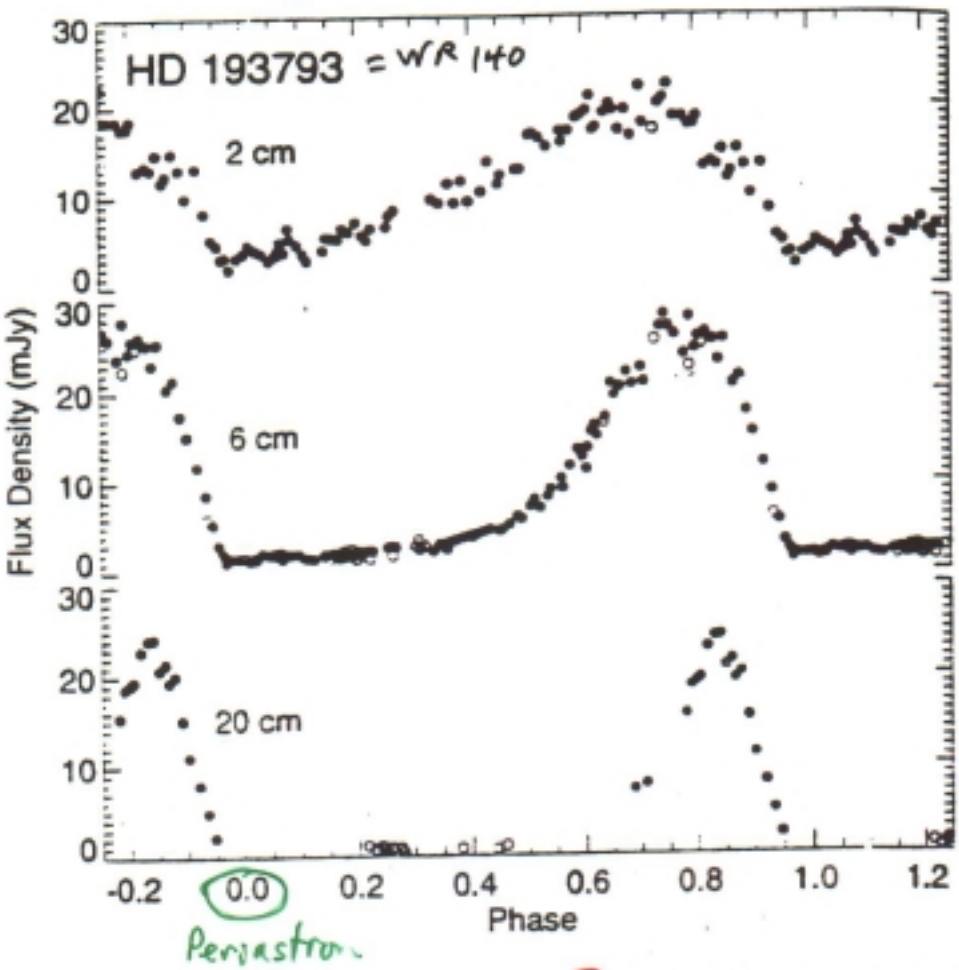

P = 7.9 yr, e = 0.85

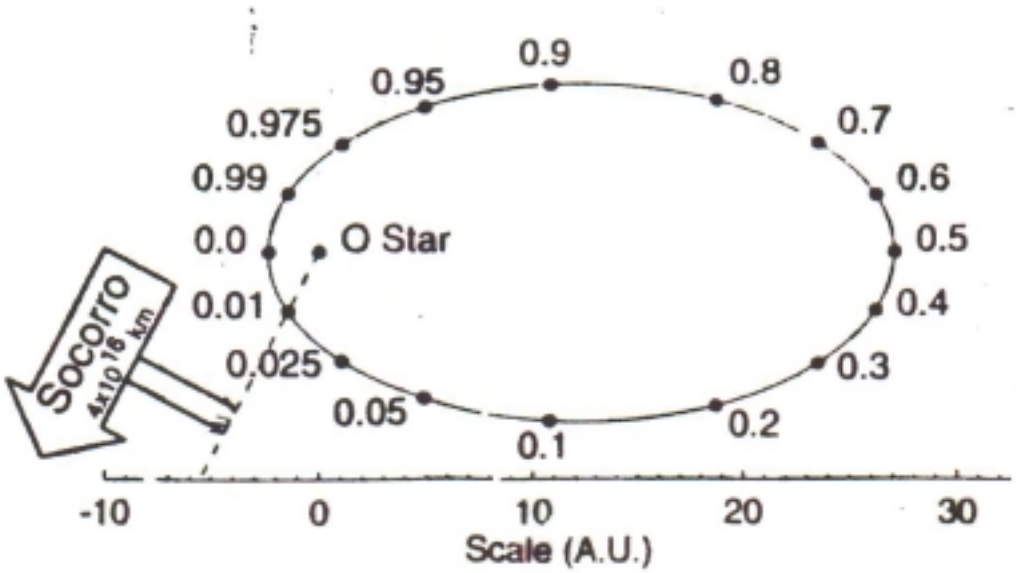

WR 147

$d = 630$ pc (Churchwell et al. 92)

$\dot{m} = 4 \times 10^{-5}\ M_\odot\ a^{-1}$

MERLIN

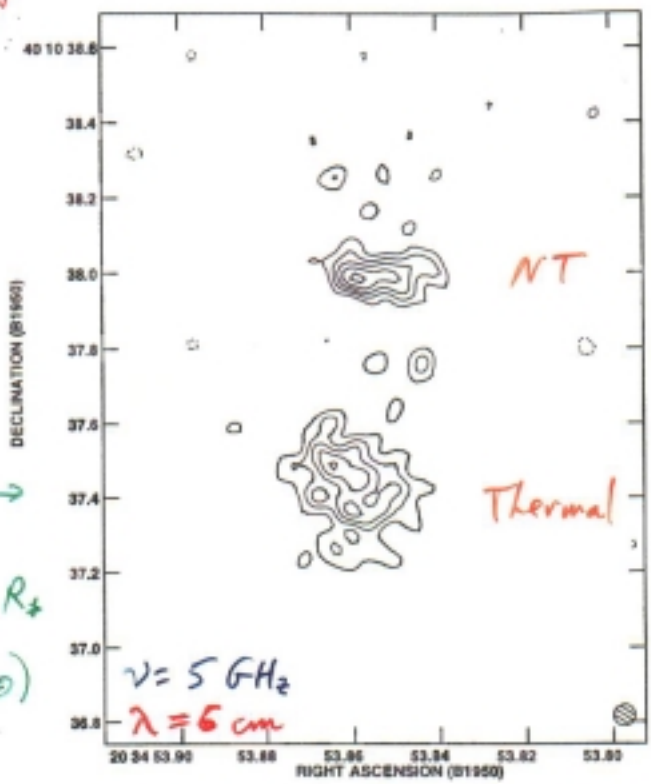

$r \sim 0''.2$

$\simeq 2500\ R_*$

$(R_* \sim 10 R_\odot)$

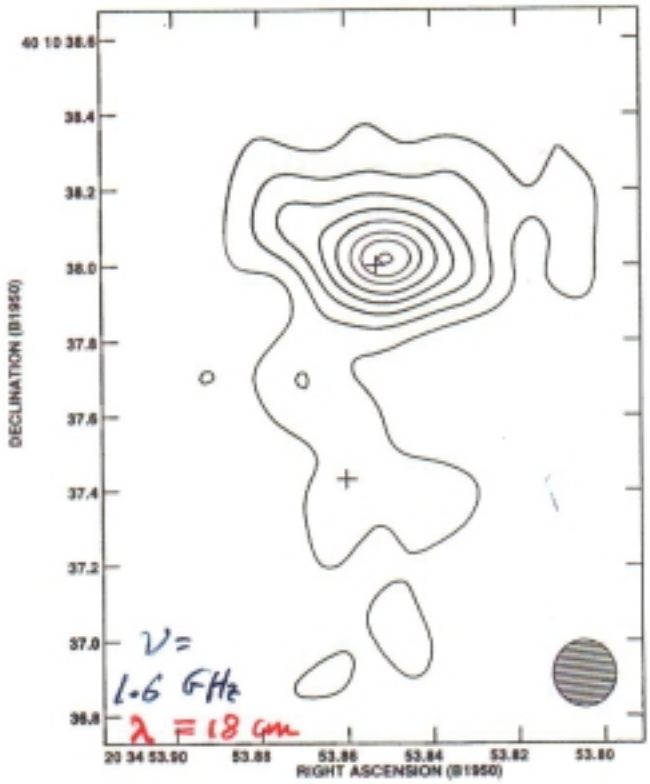

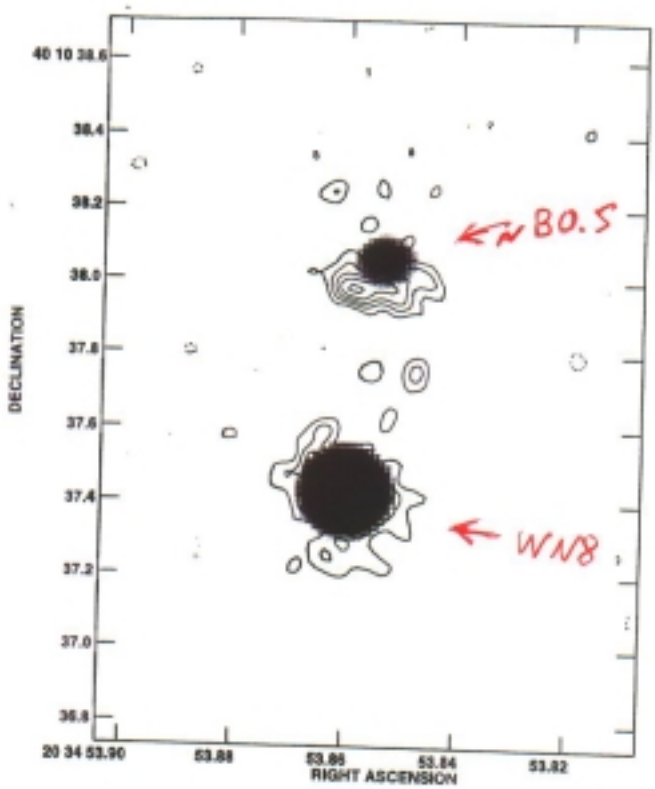

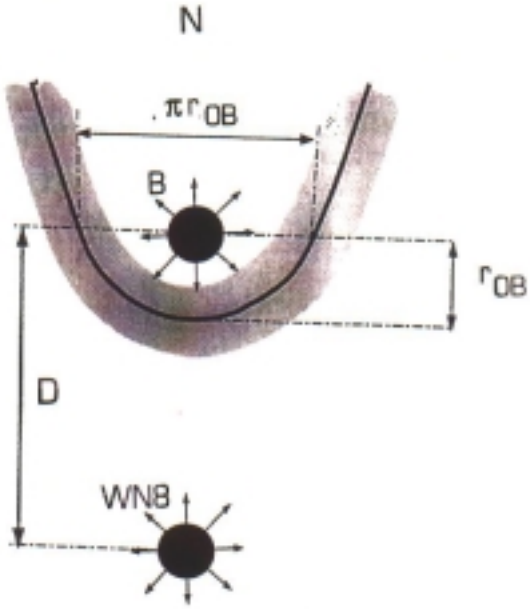

Williams et al. (1997)

MERLIN

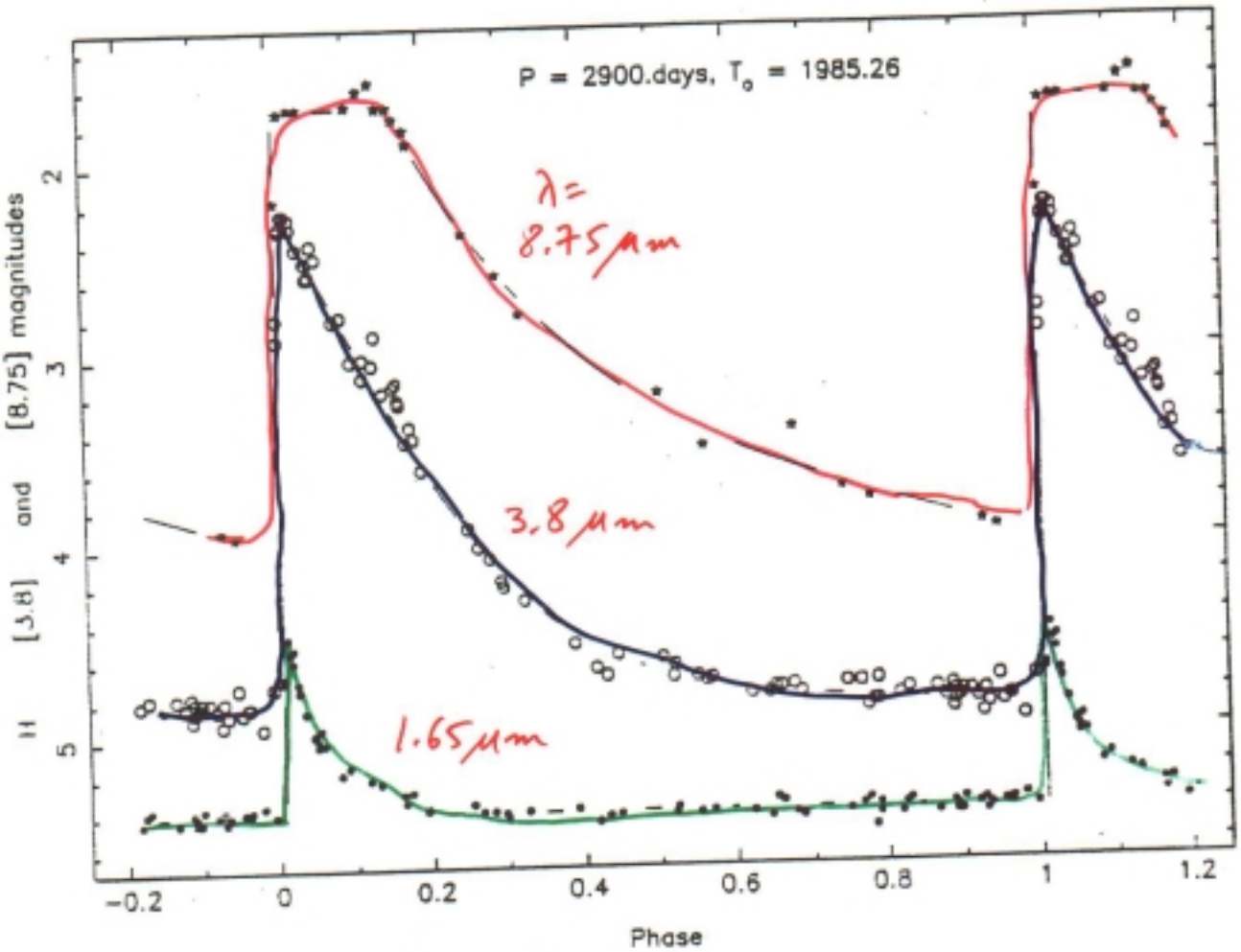

= HD193793

Fig. 3. Photometry of WR140 at 8.75μm(*), 3.8μm(o) and H (1.65μm, •) phased to tl photometric period and time of periastron passsage in W90.

→ rapid dust formation at periastron, then slow cooling

1995 A+A 298, 549

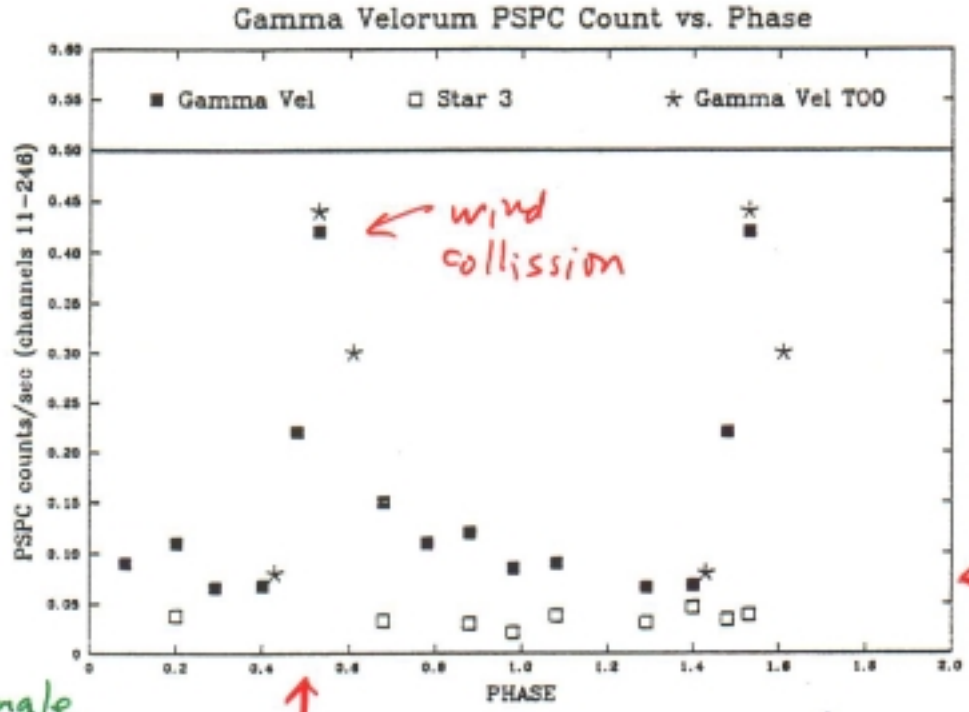

0.1–2.5 keV

Cone angle $2\theta \sim 50°$

O-star in front

$P = 78^d.5$

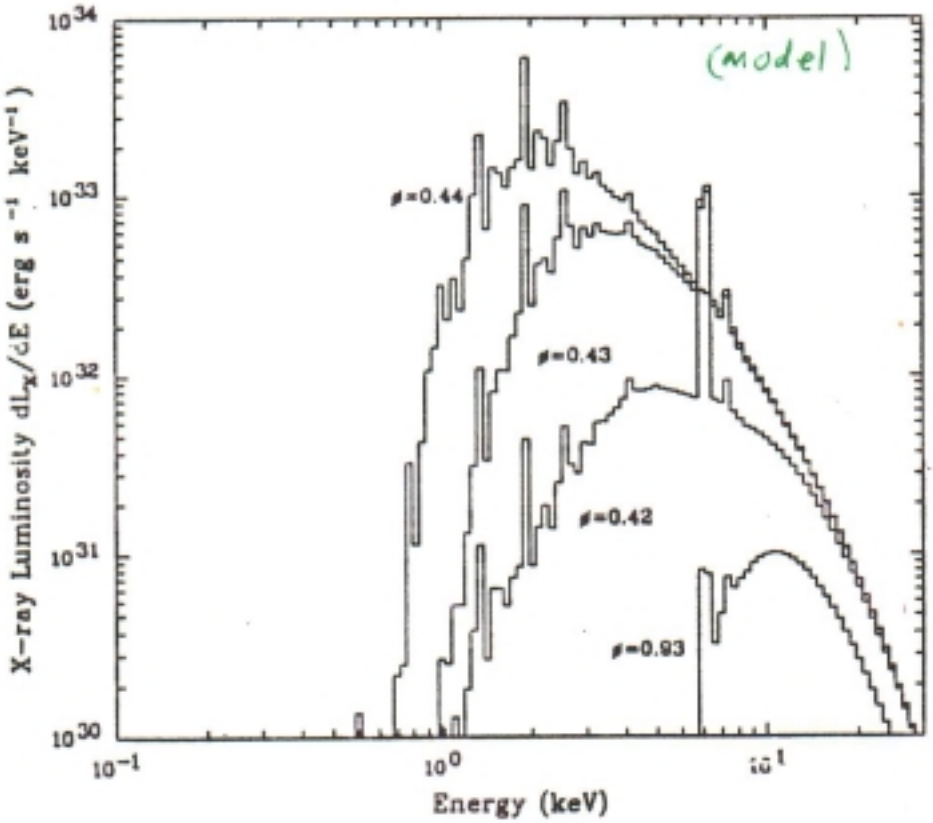

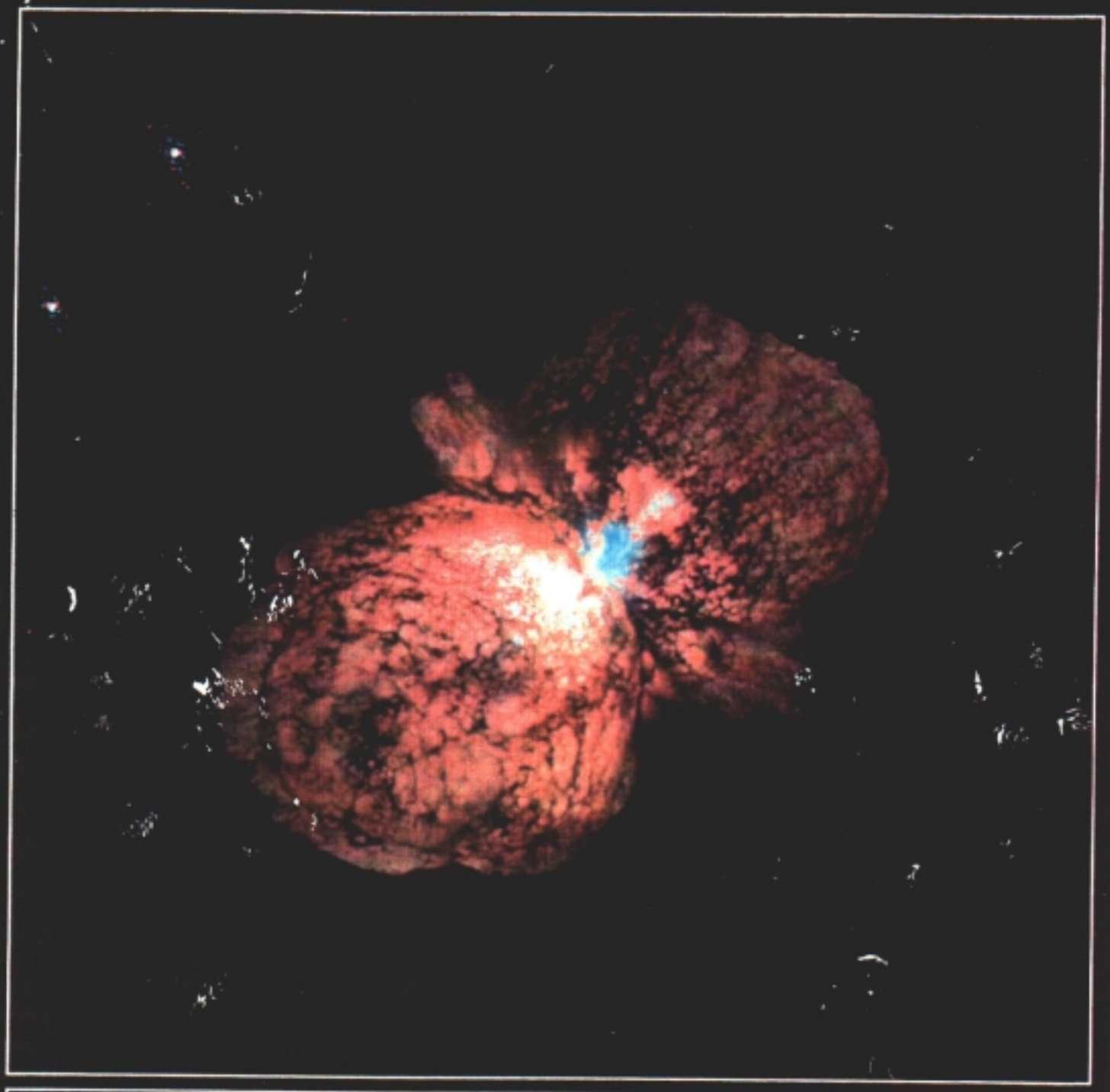

Eta Carinae

Hubble Space Telescope • WFPC2

PRC96-23a • ST ScI OPO • June 6, 1996 • J. Morse (U. CO) and NASA

Chandra η Car

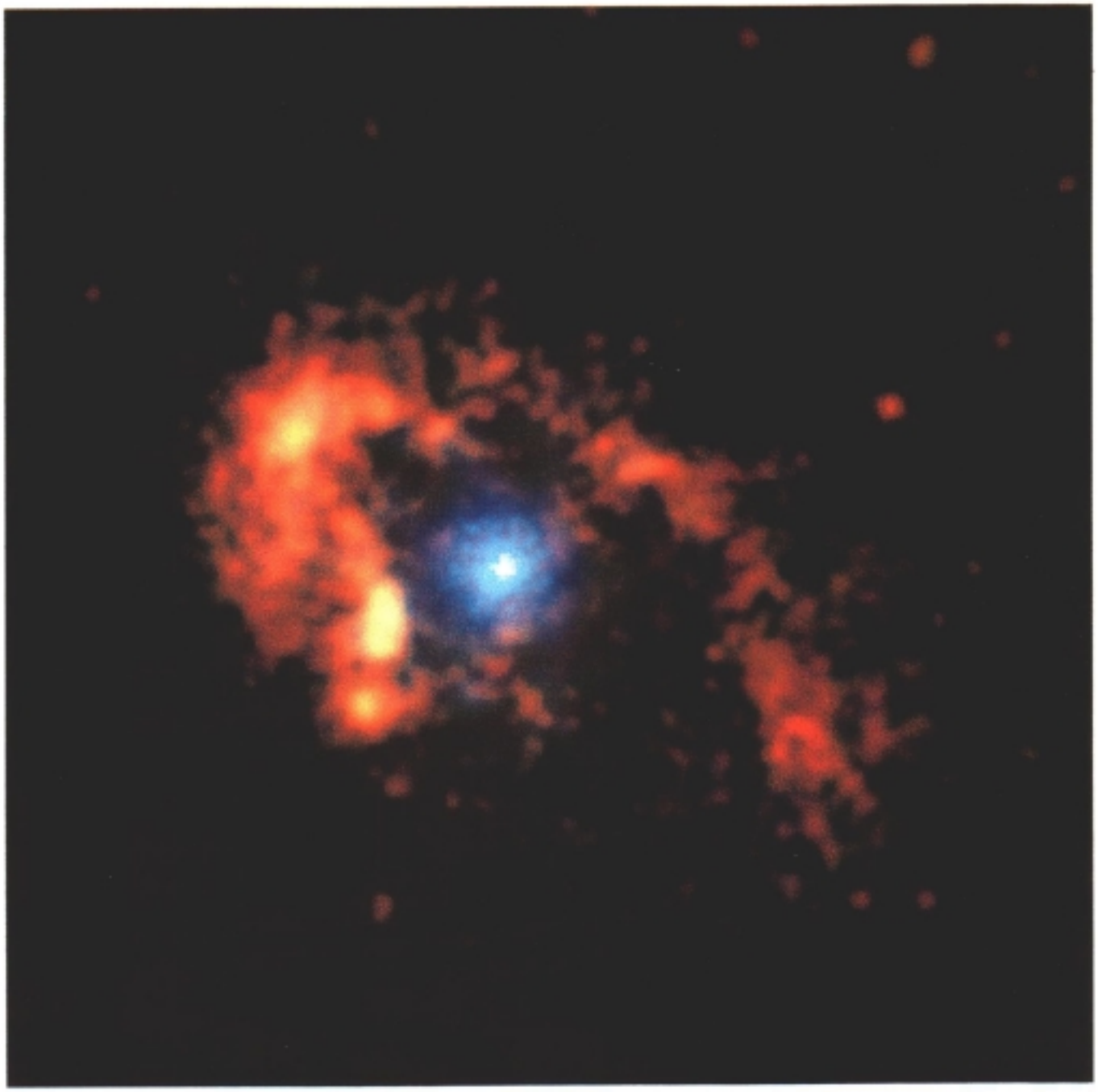

Stevens, Blondin, Pollock 1992 ApJ 386, 265

2D hydro simulation
(V444 Cyg, P = 4.2 d)

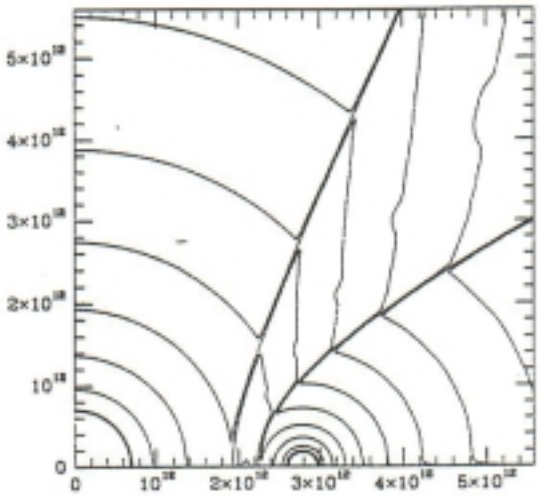

FIG. 11.—V444 Cyg simulation assuming adiabatic winds. Density contour lines are spaced by a factor of 2. The axes are labeled in units of centimeters, with the binary separation $D = 2.8 \times 10^{13}$ cm. The cooling in this model has been arbitrarily set to zero, and consequently the winds are adiabatic. The parameters for this model are $\dot{M}_{WR} = 1.4 \times 10^{-5}\ M_\odot\ yr^{-1}$, $v_{WR} = 2000$ km s^{-1}, $\dot{M}_O = 10^{-6}\ M_\odot\ yr^{-1}$, and $v_O = 2000$ km s^{-1}. No strong instabilities are seen. The surface of each star, as assumed in the simulation, is drawn with a heavy solid line. As mentioned in the text, this does not necessarily represent a realistic stellar radius.

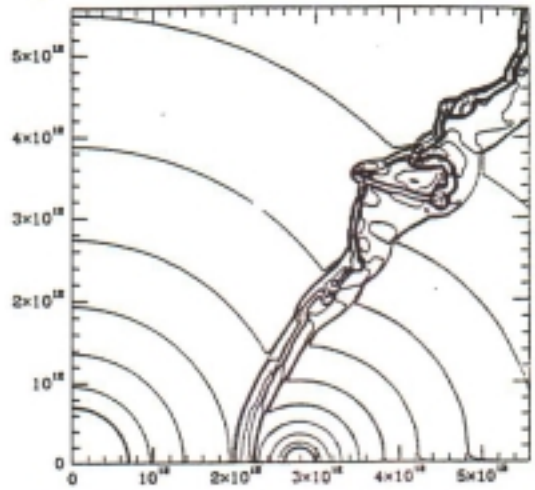

FIG. 12.—V444 Cyg simulation with cooling self-consistently included. The parameters used are the same as for Fig. 11. The cooling time scale is shorter than the flow time scale, and the postshock gas cools to some extent. The cooling is stronger in the W-R wind than in the O star wind (corresponding to a smaller value of χ). Note that the flow is strongly unstable.

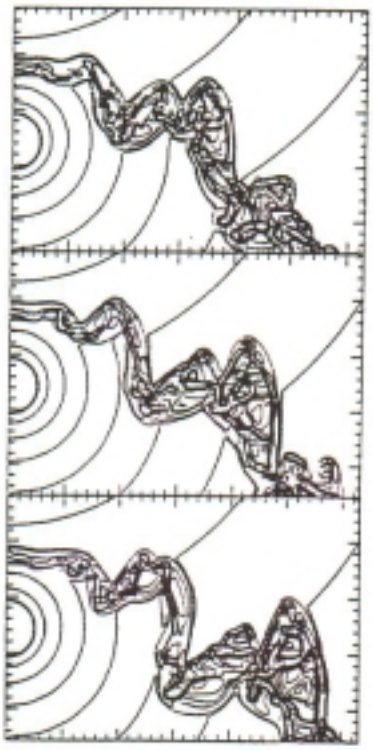

FIG. 15.—Time sequence of models for V444 Cyg, showing the growth and evolution of the instabilities in the shocked region. The three plots are separated by 1 hr between frames. The density contours are spaced by a factor of 2.

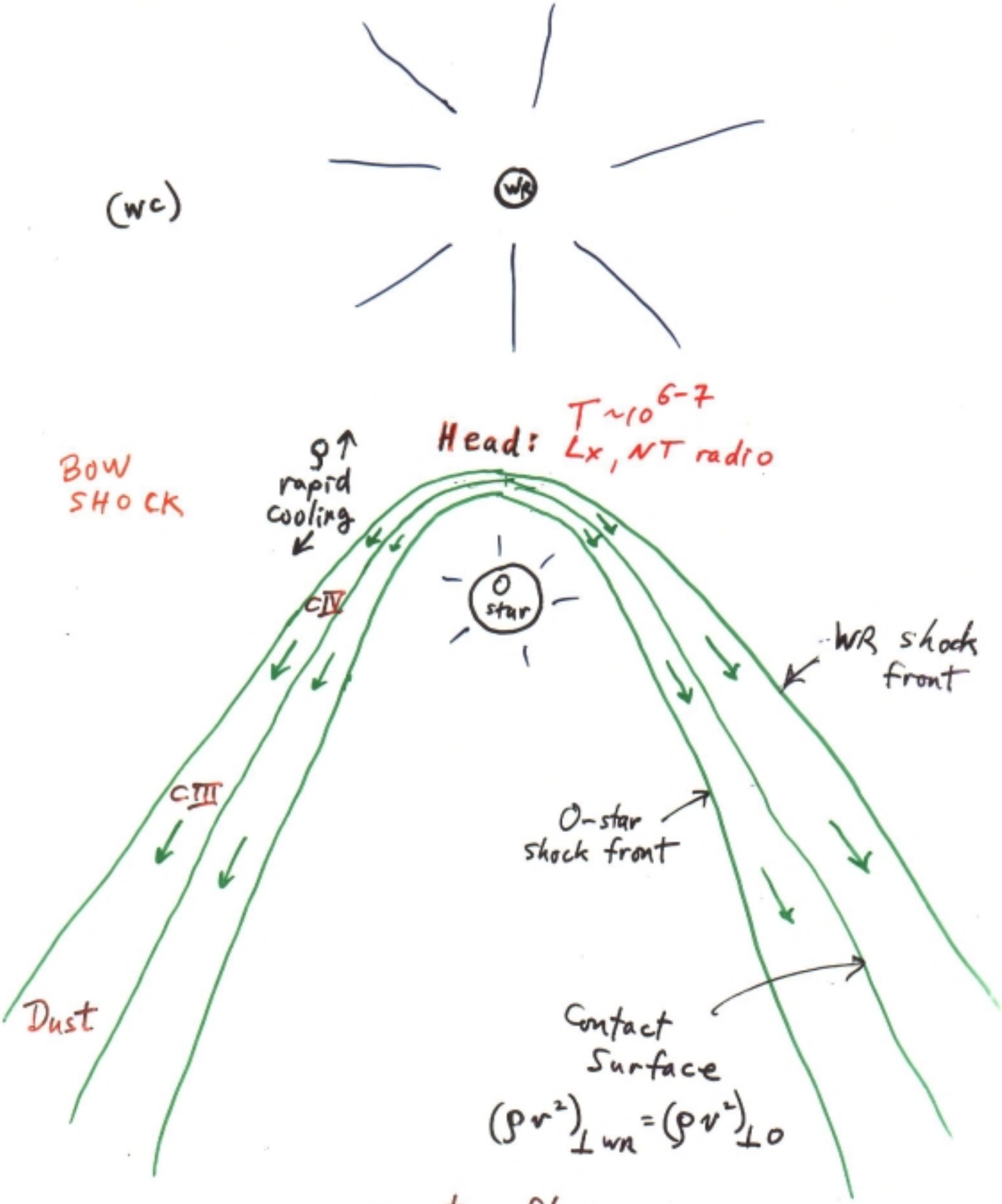

momentum flux

$$\rho v^2 = \frac{\dot{m} v}{4\pi r^2}$$

Usov (1995)

$$\theta \simeq 120^\circ \left(1 - \eta^{2/5}/4\right) \eta^{1/3}$$

$\Delta\theta \lesssim \theta$ (adiabatic)

$\sim$ small (effic. cooling)

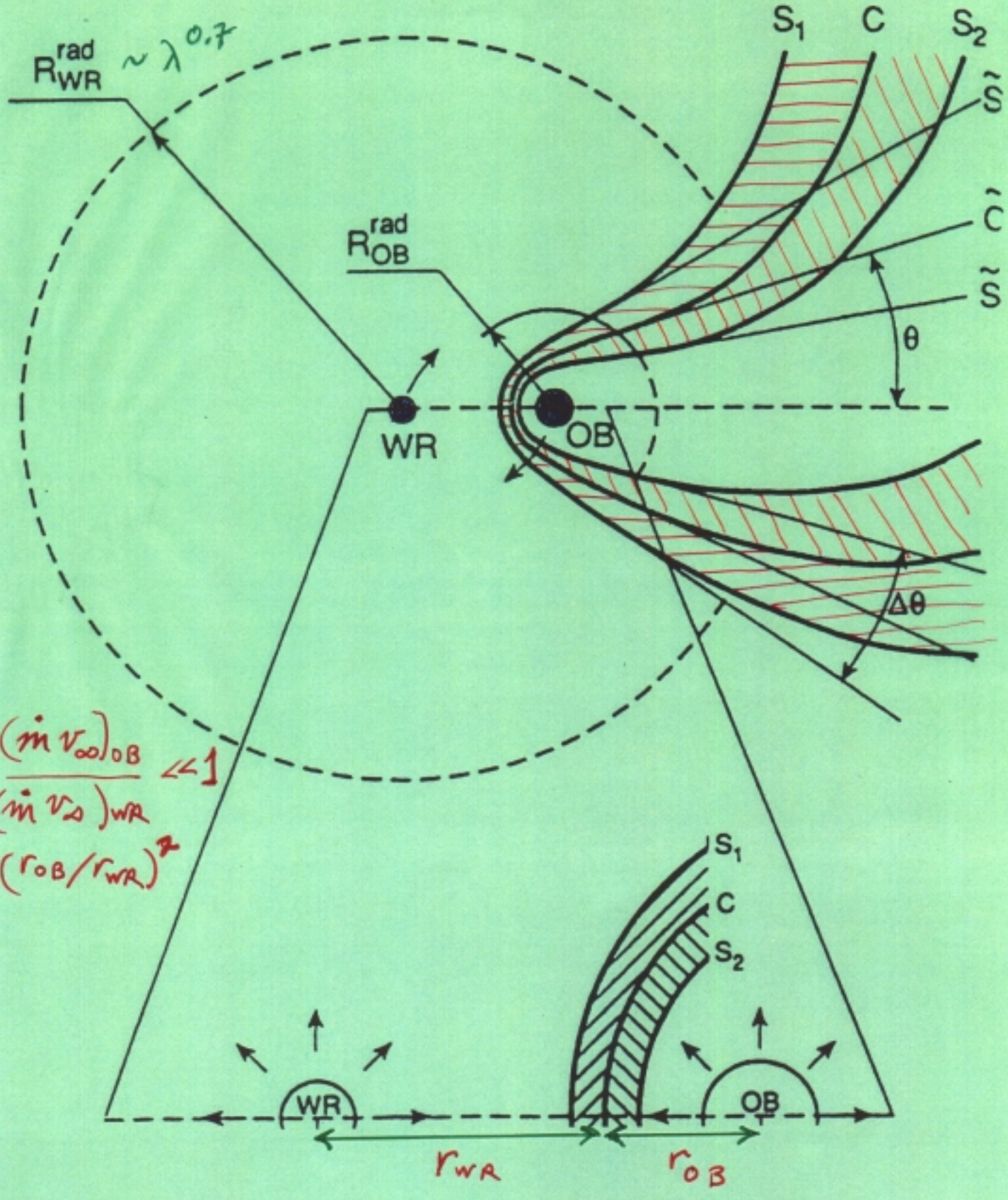

$$\eta \equiv \frac{(\dot{m} v_\infty)_{OB}}{(\dot{m} v_\infty)_{WR}} \ll 1$$

$$= (r_{OB}/r_{WR})^2$$

V444 Cygni WN5+O6 P = 4.2 d.

He I 4471, Bow shock features ('cleaned' from the O star absorption)

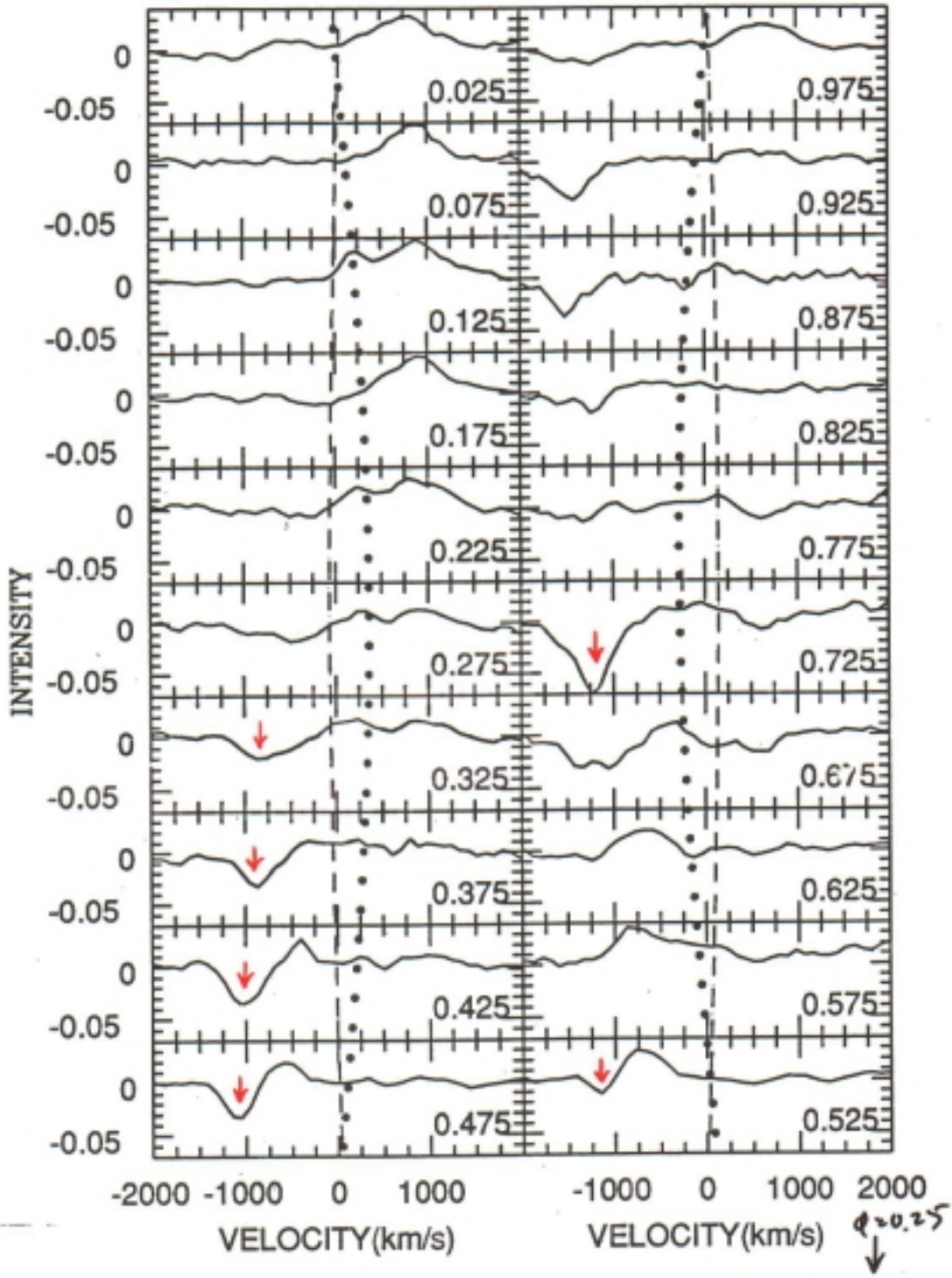

$2\beta \approx (0.7-0.5)\,360^\circ$
$\approx 70^\circ$

 (Ye. Ba. et al. 1994)

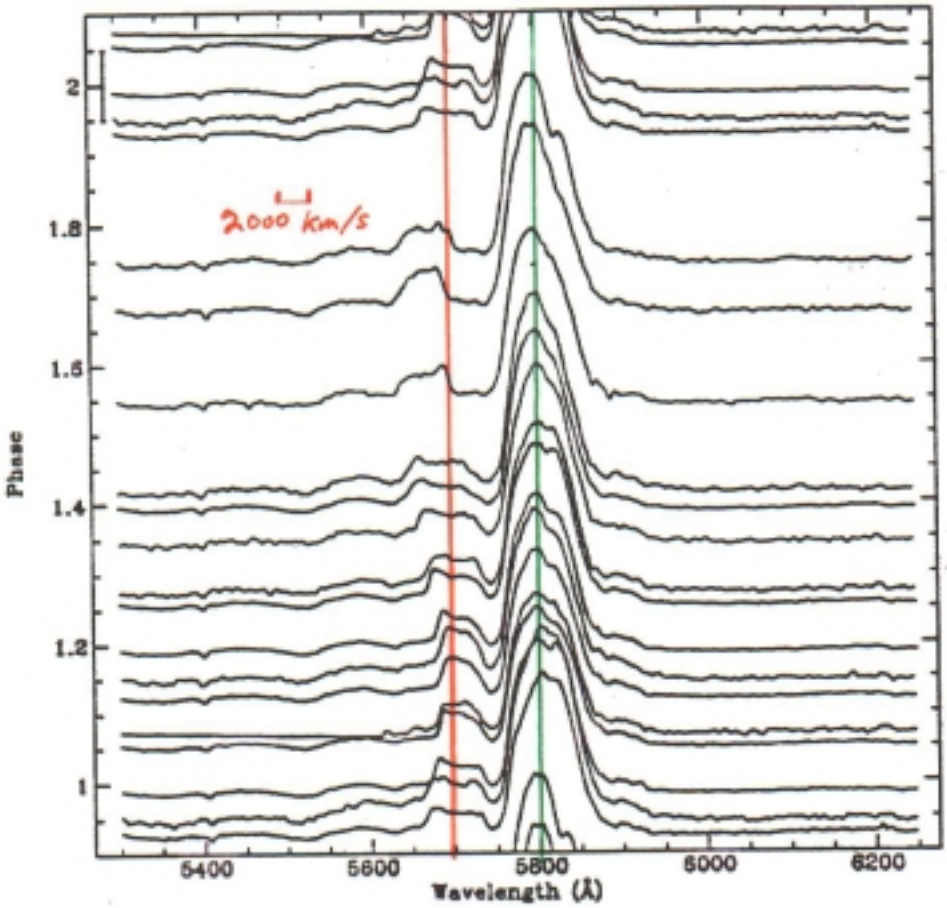

Fig. 1. Montage of spectra for B22. Error bar indicates continuum level.

↳ WC ~~6~~ 4 + O5-6 V-III , P = 14.926 d

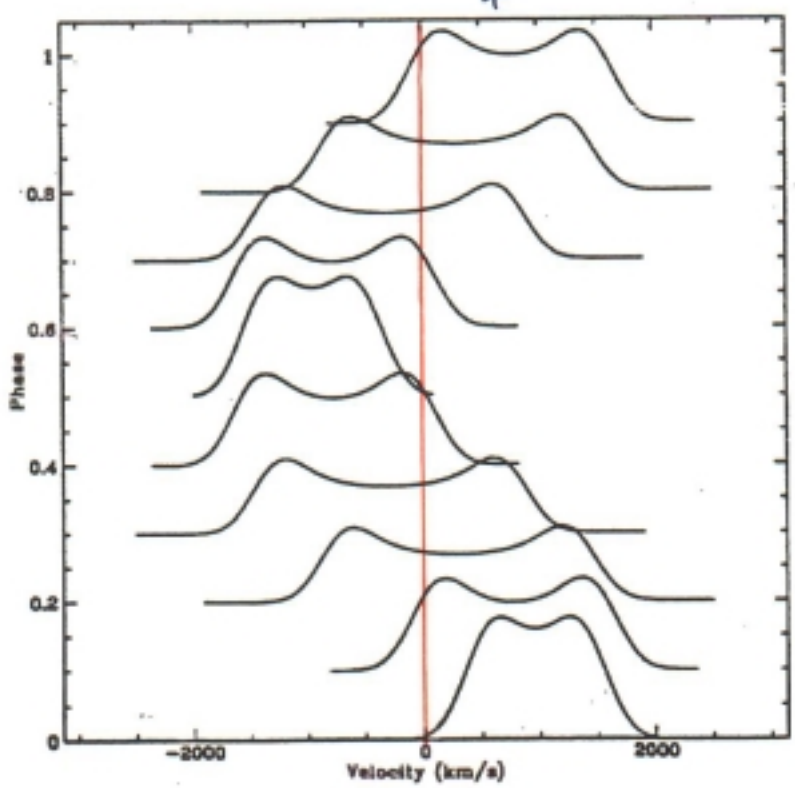

Lührs' model:
$i \approx 63°$
$\beta = 47°$
$V \approx 1570$ km/s

Fig. 2. Calculated profiles for a Lührs model of B22.

Optically thin, uniform, expanding RING
(or thin disk)

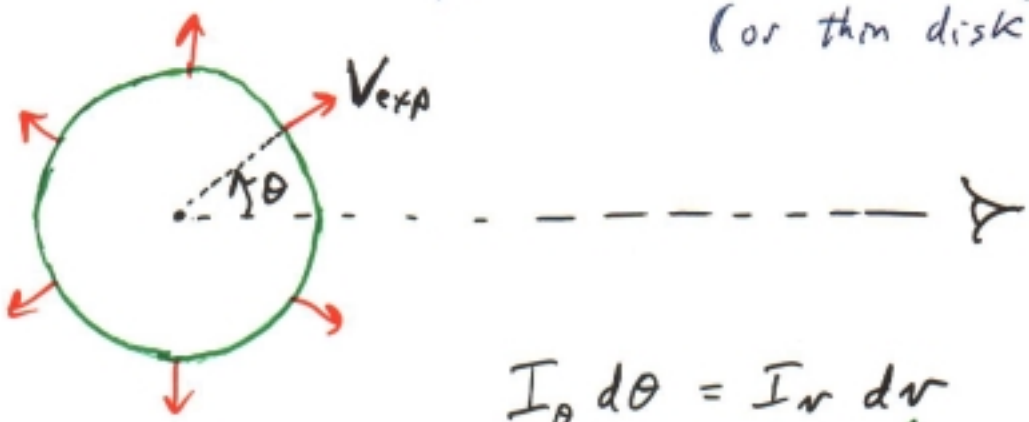

$$I_\theta \, d\theta = I_v \, dv$$

const.

Doppler-Fizeau vel. $= \frac{\Delta\lambda}{\lambda_0} c$

$$v = -V_{exp} \cos\theta \quad \Rightarrow \quad dv = V_{exp} \sin\theta \, d\theta$$

Line profile $$I_v = I_\theta \frac{dv}{d\theta} = \frac{I_\theta}{V_{exp} \sin\theta} = \frac{I_\theta / V_{exp}}{\sqrt{1-(v/V_{exp})^2}}$$

.... cf. opt. thin, uniform, rotating RING:

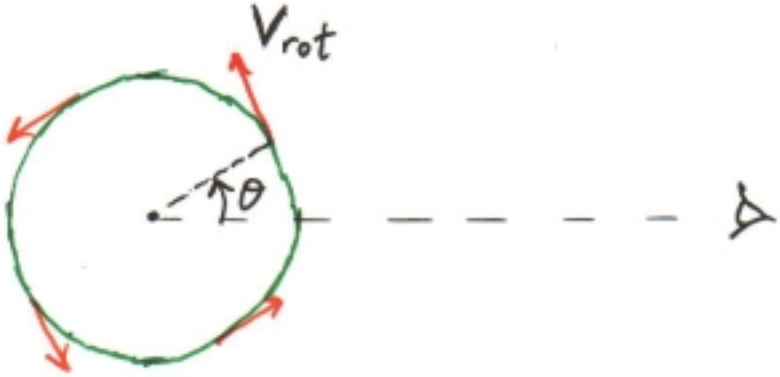

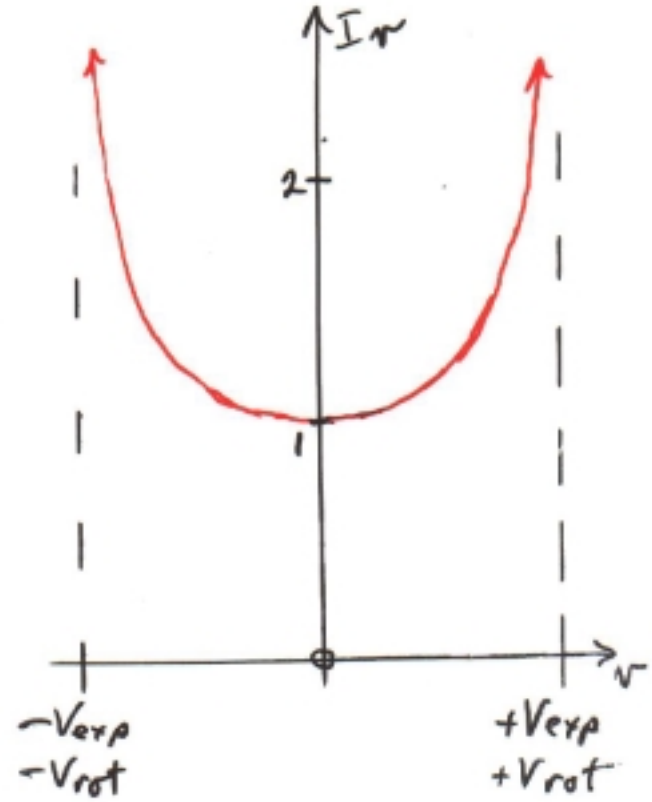

$$v = V_{rot} \sin\theta$$

$$\Rightarrow dv = V_{rot} \cos\theta \, d\theta$$

Line profile $$I_v = \frac{I_\theta / V_{rot}}{\sqrt{1-(v/V_{rot})^2}}$$

same form

Wind Collision – Geometric model

$e = 0$ (Lührs 1991, 1997)

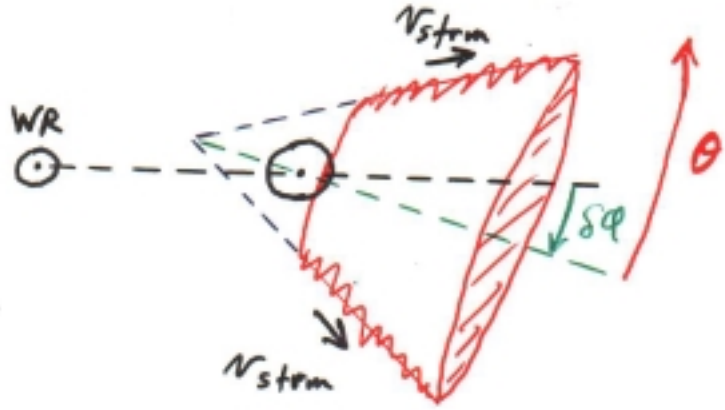

line emission from uniform, opt. thin, thin cone:

$$I_\nu \, d\nu = \frac{I}{2\pi} \frac{d\nu}{\sqrt{v_*^2 - (\nu - \bar{\nu})^2}}$$

for $\quad -v_* \leq (\nu - \bar{\nu}) \leq v_*$

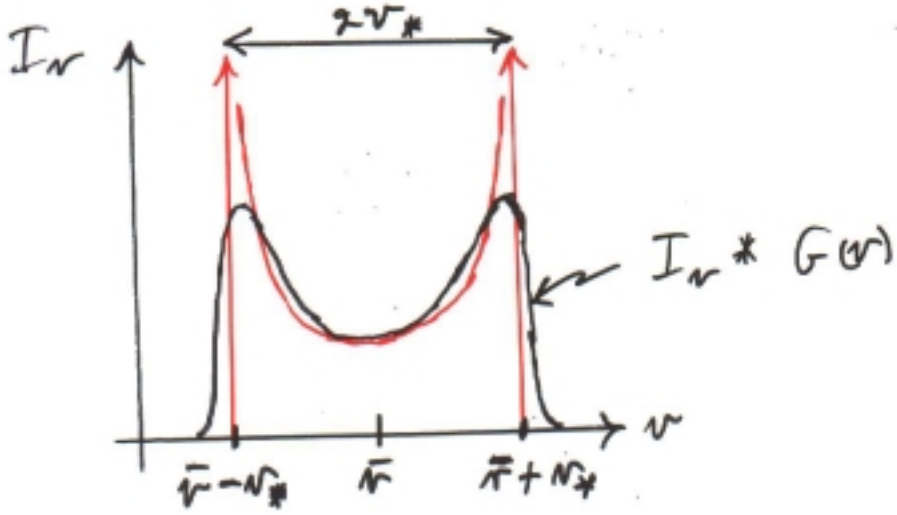

width: $2v_* = 2 v_{strm} \sin\theta \sqrt{1 - \sin^2 i \cos^2(\varphi - \delta\varphi)} > 0$

$\rightarrow$ minimum at $\varphi = \delta\varphi, 180° + \delta\varphi$

mean RV: $\bar{v} = v_{strm} \cos\theta \sin i \cos(\varphi - \delta\varphi)$

cf. WR orbit: $v_{orb}(WR) = V_0 + K_{WR} \sin\varphi$ $\rightarrow$ 90° phase-shift for $\delta\varphi = 0$

(WR in front at $\varphi = 0$)

Adiabatic
($\Delta\theta \approx \theta$)

Lührs' model

Bartzakos 98

$\bar{\theta}$ =

90°

"sheet"

45°

20°

"pencil"

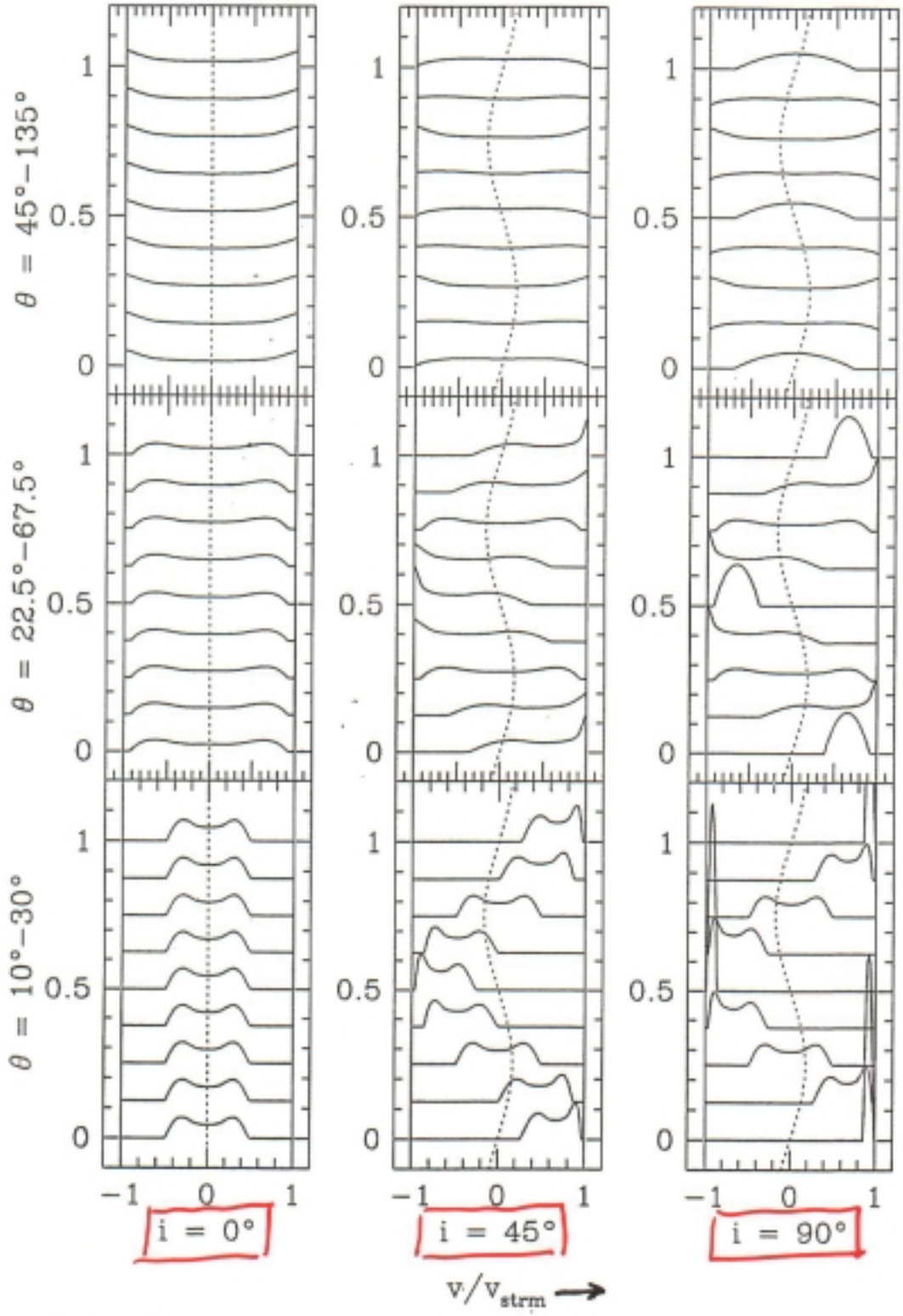

orbit face-on

edge-on

Williams (1995)

Incidence of heated dust as a function of subtype

Type	Persistent	Episodic	None (?)
WC9	WR59 65 69 73 76 80 95 96 103 104 106 112 117 118 119 121	WR70 98a	WR81 88 92
WC8	53 113	48a	11 60 77 101 135
WC7	none	125 137 140	42 50 56 57 64 68 79 86 90 93
WC4	none	19	incomplete

○ dust spirals

Tuthill et al. (1999)

WR 104

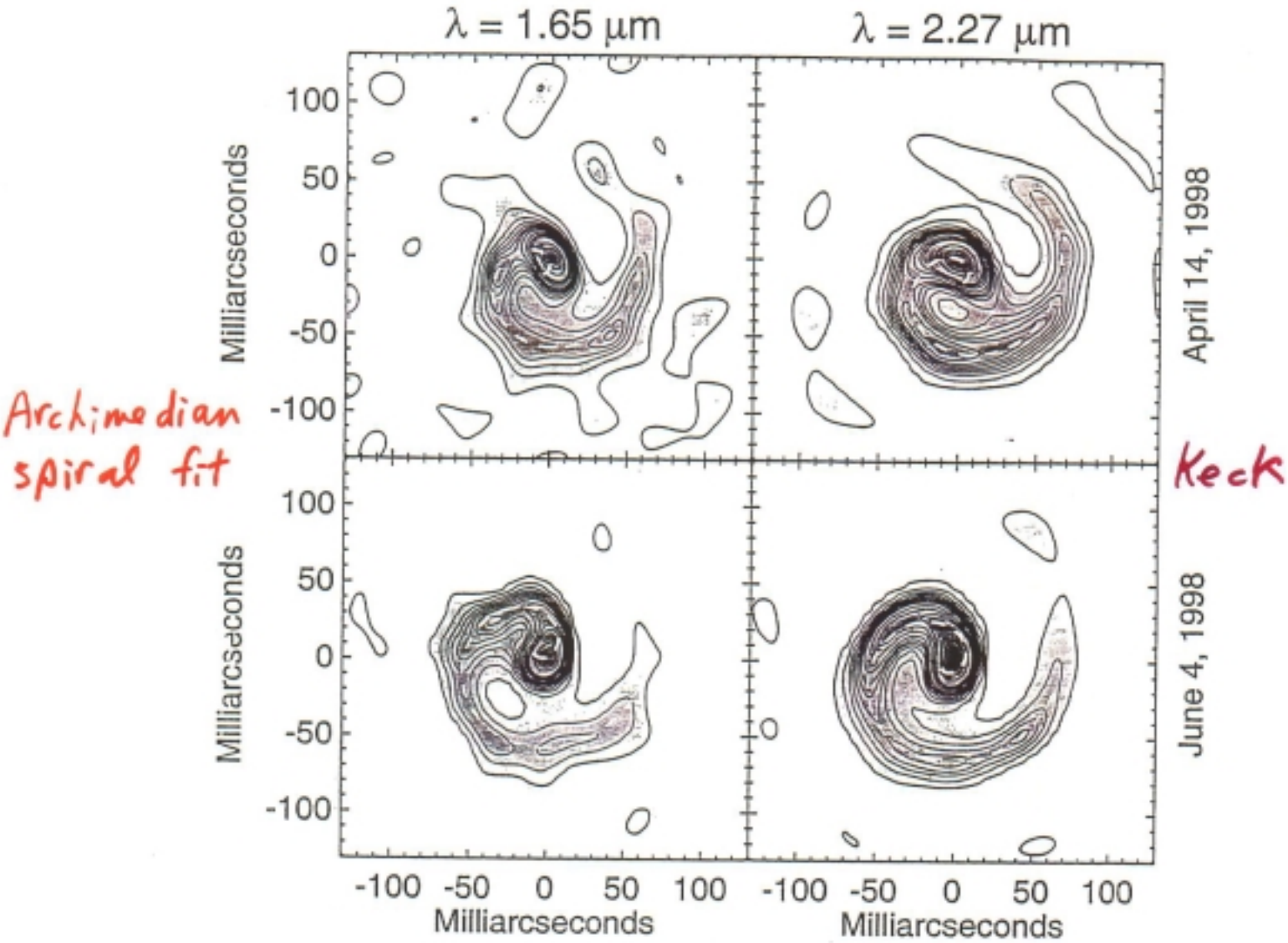

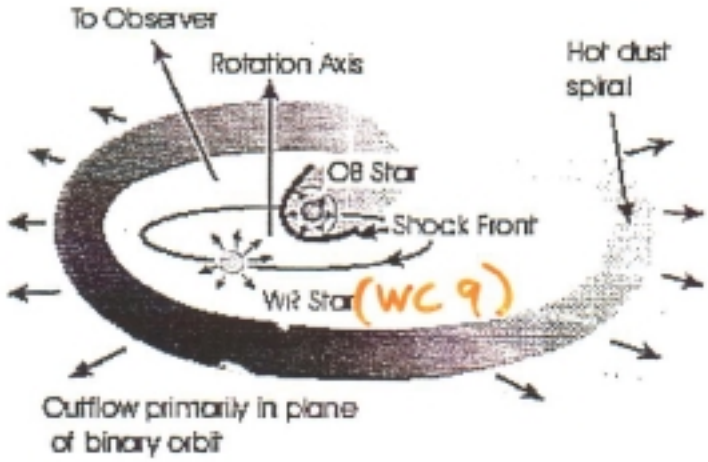

Figure 2: Schematic diagram of the WR 104 binary system. The illustration shows the WR star, the OB companion, wind-wind collision front, and the resultant dust outflow plume (not to scale). The spiral shape is a consequence of material being swept radially outwards by the WR wind from a rotating dust nucleation zone associated with the shock front where the stellar winds collide.

WR 137 WC7 + O, P = 13 yr

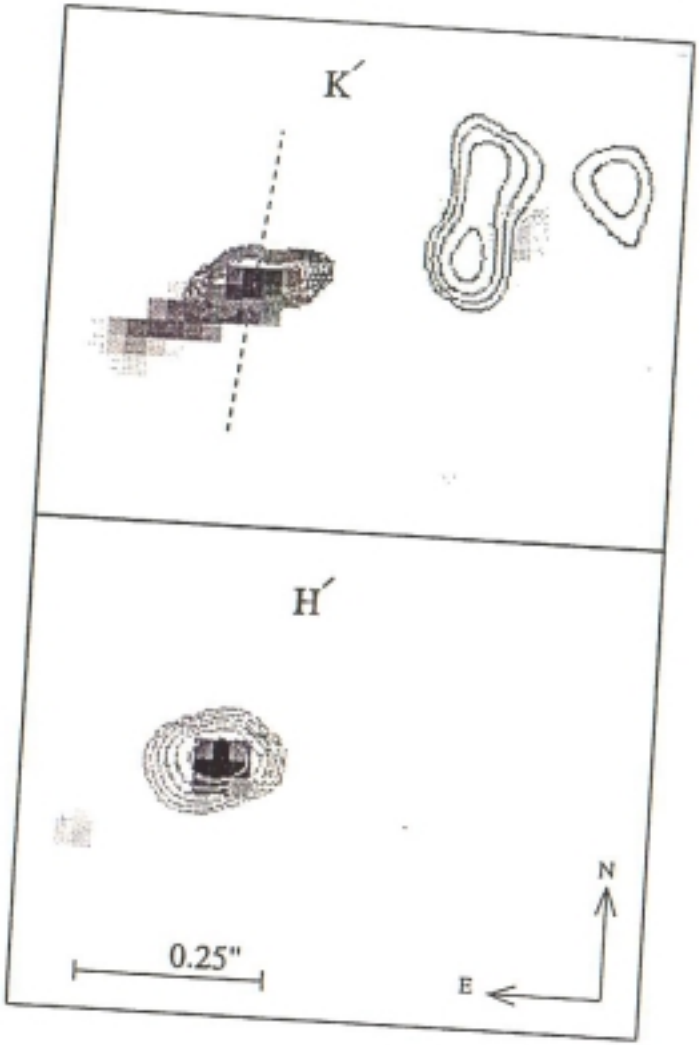

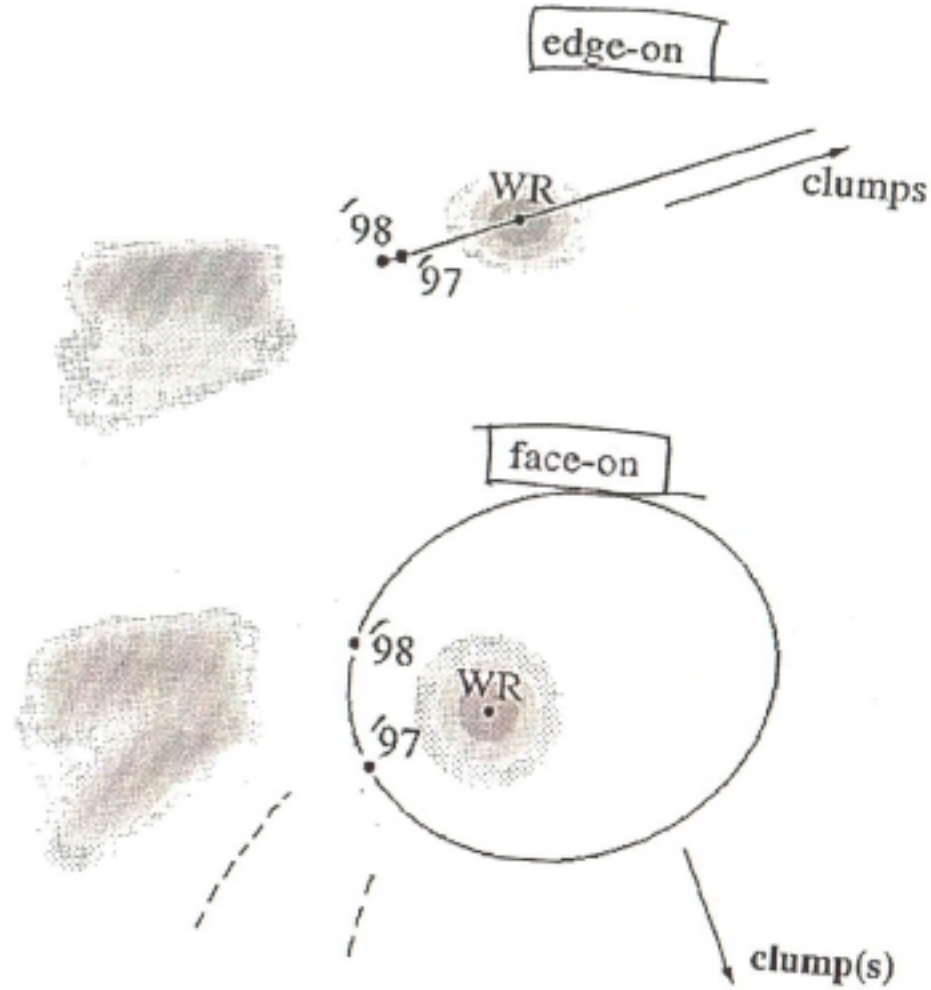

Marchenko et al. (1999)

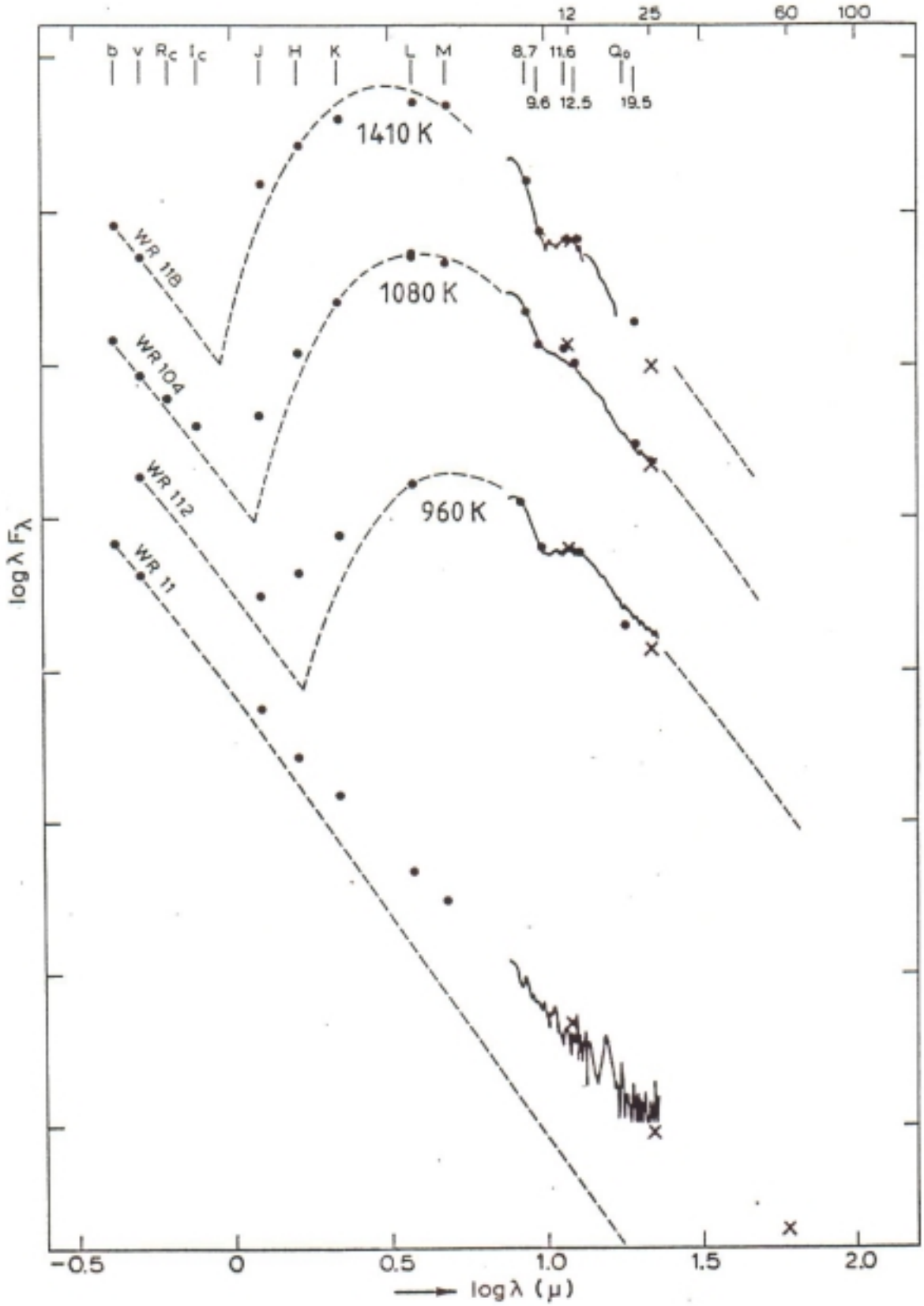
12
25
60
100
b
v
R_c
I_c
J
H
K
L
M
8.7
11.6
Q_0
9.6
12.5
19.5
1410 K
1080 K
960 K
WR 118
WR 104
WR 112
WR 11
log λ F_λ
-0.5
0
0.5
1.0
1.5
2.0
log λ (μ)

Dust formation in WR stars

(Le Teuff 2001)

- WC only ⇒ amorphous C-dust
- for WCL: (1) episodic at periastron (WR + OB)
  (2) permanent
- for WCE: (1) only

Single WCL Model

$R_* \sim 10\, R_\odot$
$T_* \sim 30\,000$ K
$T_{eff} \sim 20\,000$ K

$\dot{m} \sim 3 \cdot 10^{-5}\, m_\odot/yr$
$= 4\pi r^2 \rho v$ ← const.

$\Rightarrow \rho \sim \frac{1}{r^2}$

dust appears

~700 R_*

1-5% of C

2 processes: (a) nucleation (gas → solid)
(b) growth (accretion of solids)

<u>Nucleation</u>
- not observed directly
- requires high density

$\rho(\text{clumps}) \rightarrow 200\, \bar{\rho}$
not enough

⇒ Single WC cannot form dust unaided

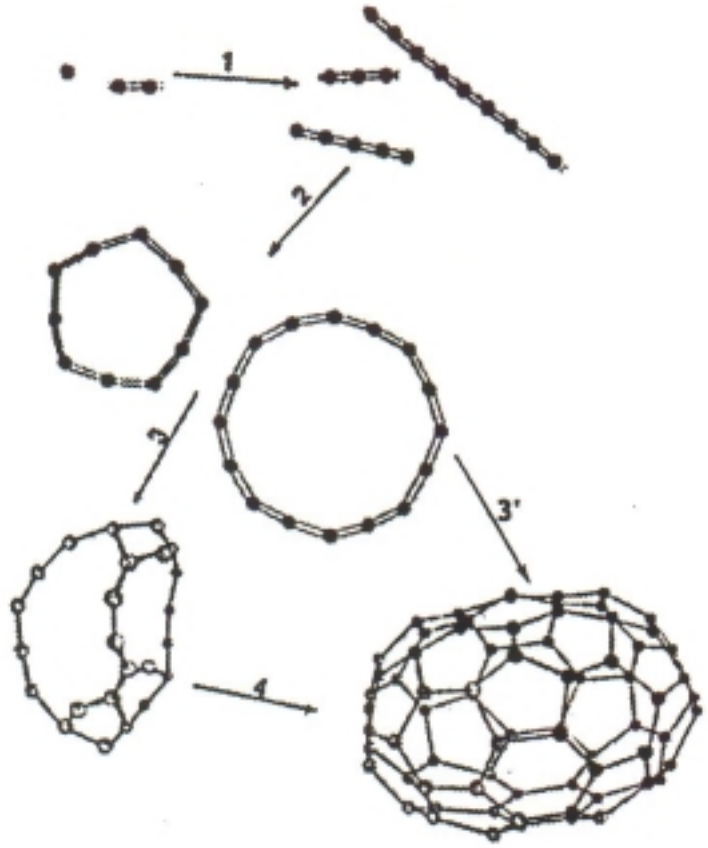
1
2
3
3'
4

Binary WC + OB

- additional compression via wind-wind collision
- + mixing with H-rich matter from OB companion

If all WR "dustars" = binary

⇒ episodic = long-P, $e \neq 0$

permanent = short-P, $e \simeq 0$

BUT
- only 52% of dustars are identified as binaries
- only 36% of WC + OB form dust

⇒ Colliding-wind binaries not the only way (?)

CONCLUSIONS

WR Stars are important!

- all massive stars ($m_i \gtrsim 25\, m_\odot = f_1(Z)$)
  $\longrightarrow$ WR phase
- stable stars with strongest known winds
- see nuclear products from core < SN
- energize + enrich ISM (ions, dust)
- age-dating starbursts ($4-7\, Myr \simeq f_2(Z)$)

OUTSTANDING PROBLEMS

- Why $\dot{m}(WR) \sim 10 \times \dot{m}(O)$?

  What initiates + drives $\dot{m}$ (WR)

  P_{rad} vs. pulsations

- Role of rotation

  $\dot{m} = \dot{m}(m_i, t, x, y, z, \Omega(t), \vec{B}, \ldots)$

- What is detailed structure of WR winds?

  shape, inhomogeneity

- Role of binaries in evolution
- Single-star evolution still uncertain

  convection, $\dot{m}$, Ω, ...

- Link to BHs and SN Ib/c

Ideally need direct resolution

eg. need $\sim 10\,\mu$ arcsec to see $1\,R_\odot$ in closest WR (γ Vel, $d \simeq 300$ pc)